Resonance hairpin probe for electronegative plasma diagnostics

Nishant Sirse

PhD

2013

Resonance hairpin probe for electronegative plasma diagnostics

A thesis for the degree of

DOCTOR OF PHILOSOPHY

Presented to
The school of physical sciences
Dublin City University

By
Nishant Sirse

Research Supervisors:

Dr. Shantanu Karkari
and
Prof. Miles Turner

External Examiner: Prof. Nicholas St. J. Braithwaite
Internal Examiner: Prof. John Costello

2013

Declaration

I hereby certify that this material which I now submit for assessment on the programme of study leading to the award of PhD is entirely my own work, that I have exercised reasonable care to ensure that the work is original, and does not to the best of my knowledge breach any law of copyright, and has not been taken from the work of others save and to the extent that such work has been cited and acknowledged within the text of this work.

Signed:

ID No.: 58103791

Date: 16/01/2013

This thesis is dedicated to my mother for her unconditional love, support and encouragement.

Abstract

The practical applications of resonance hairpin probe for characterizing electronegative plasma is investigated. In particular the hairpin probe was operated in a time-resolved mode for measuring the electron density evolution during pulsed laser photodetachment of negative ions in an oxygen inductively coupled plasma (ICP) discharge. From the temporal evolution of the electron density, the negative ion temperature is determined from the characteristic diffusion time of negative ions in the photodetached channel. This is compared with an independent method based on the temporal evolution of the plasma potential during photodetachment measured by a floating emissive probe. Temporal evolution of negative oxygen ions in a pulsed dc magnetron discharge is also obtained using pulsed photodetachment and a time-resolved hairpin probe. The results are found to be in reasonably good agreement with those measured from Langmuir probe assisted photodetachment.

Two important applications addressed in this thesis are the use of steady state and pulse biased hairpin probes. For overcoming the limitations arising because of the finite sheath width around the resonator pins, the hairpin was systematically biased at strong negative dc potentials ($e\varphi >> kT_e$) with respect to the plasma. A plot of resonance frequency verses probe bias is shown to provide a unique value for the electron density. Comparison of the sheath corrected electron density based on the step front sheath model and that obtained with a planar Child-Langmuir sheath approximation, were found to be in good agreement at higher densities (above $1x10^{16}$ m^{-3}), however small deviations were observed at lower densities (below $3x10^{15}$ m^{-3}) due to deviation from a planar sheath assumption. Finally, qualitative measurement of negative ion parameters is performed by pulse biasing the hairpin probe. Comparison of the temporal evolution of the electron density before and post application of a negative pulse bias allows one to obtain both the negative ion density, negative ion temperature, as well as the positive ion density. The relative measurements of the negative ion parameters using this technique are found to be in reasonably good agreement with the hairpin probe assisted laser photodetachment however the absolute measurements are underestimated by a factor of 10. The discrepancy in the measured absolute negative ion parameters and the limitations behind this technique are discussed.

Acknowledgements

I would like to express my gratitude to all those who contributed to completion of this thesis. First of all I would like to acknowledge my supervisors Dr. Shantanu Karkari and Professor Miles Turner for giving me opportunity to be a research postgraduate student at the National Centre for Plasma Science and Technology (NCPST), Dublin City University, Ireland. I especially want to thanks Dr. Shantanu Karkari for his availability, time to time discussions, planning of work activities and writing papers, constructive comments and ideas which kept me motivated over the years of my postgraduate study. I would also like to appreciate for his extra efforts during the second half of my PhD in which he already started his new job in India, but agreed to remain my supervisor. I also want to thanks Prof. Miles Turner for his valuable comments on plasma sheaths.

The research performed in this thesis would not have been possible without the people who helped me during the experimental work. Therefore I would like to give my gratitude to Dr. Jim Conway who worked with me during laser photodetachment experiment, Dr. Cezar Gaman and Mr. Everaldo Gaspar to provide and make me learn about LabVIEW programmes. I would like to thanks to Mr. James Lalor, Mr. Pat Wogan, Mr. Des Lavelle, Mr. Conor Murphy and Mr. Ray Murphy for providing technical support. I am also grateful to the administrative team in the NCPST and school of physical science, namely Samantha, Sarah, Sheila, Trish, Claire and Lisa and my colleagues Sean, Nina, Huw, Samir, Zhenning, David and Muhammad. I would also like to thank Trevor for helping in proofreading the thesis.

I wish to thank Dr. Jean Paul Booth and Dr. Sophie Bouchoule for inviting me to LPP, Ecole Polytechnique, France and LPN, CNRS, France and for providing financial assistance during my visit. Also to Prof. James Bradley for his financial support to invite me to the University of Liverpool, UK and giving me opportunity to work in magnetron sputtering plasma source and providing Langmuir probe data.

I would like to thank my friends and colleagues Mubarak, Gurusharan and Sarveshwar for their continuous support during my PhD. Their family members Deepa, Sanju and Arundhati (wife of shantanu) for inviting me on different occasions and being like family during my stay in Ireland. I wish to give my love to their kids Bhavya, Richa, Riya and Rhony for making me smile. I would also like to thanks Yasmina for her support and helping in starting a new life in France, the phase when I was writing my thesis along with a new position.

I would like to thanks my family, my parents, Baby and Narayan, my wife, Rupal and my sisters, Varsha and Ritu for their unconditional love, sacrifice and care. I love them so much, and I would not have made it this far without them. And last, but by no means least, my newborn daughter, Vrishti to come in our family with blessings.

The financial support of the Association EURATOM fusion DCU is gratefully acknowledged.

Nishant Sirse

Contents

List of figures

Chapter1

Introduction

Plasma assisted technologies have established themselves in all areas of industry, with new applications constantly evolving. Foremost among these industries is the electronic industry where plasma processing is indispensible for manufacturing very large-scale integrated microelectronic circuits. Besides plasma processing is an important technology used in wide range of applications such as the aerospace, automotive, steel, biomedical and toxic waste management industries (figure 1.1).

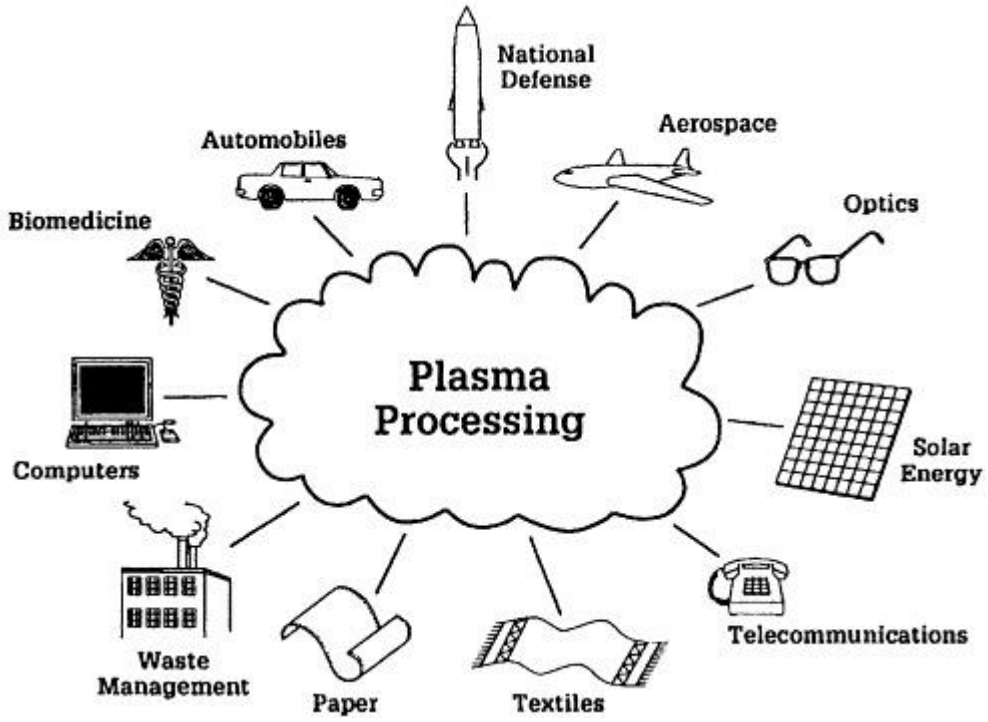

Figure 1.1: Application of plasma processing in several industries.

Electronic industries are fuelled by the semiconductor industry in which billions of transistors are accumulated in very small areas (~few mm^2) using plasma processing to make a microelectronic integrated circuit or a chip. It is roughly estimated that about 30% of the equipment used in semiconductor chip manufacturing is plasma based. Etching and deposition are two main processes to make integrated circuit. Etching involves removal of material from the surface whereas deposition means the formation of thin layers on a substrate. To make an integrated circuit, first submicron electronic

devices such as transistors, capacitors, etc are etched onto a silicon wafer which is followed by the deposition of thin layers of dielectric materials such as silicon dioxide or silicon nitride for insulation. The crucial parameter in the etching process is anisotropy, which means that the etch rate should be directional. To achieve this, positive ions from the plasma are accelerated in the direction perpendicular to the substrate by sheath potential. This process is known as Ion-Enhanced etching. However a common problem that exists in Ion-Enhanced etching is charge build up which leads to non directional etching when high aspect ratios are desired. A solution to this problem is neutral beam etching in which mainly neutral active species (radicals) are directed towards substrate [Samukawa 2006]. Electronegative plasmas are one of the most efficient sources for producing neutral beam.

The etching process described above is chemical etching, not physical etching. This means: a chemical reaction takes place between the solid atoms (from the substrate to be etched) and reactive species from the plasma. Molecular gases containing fluorine or chlorine are found to be the most effective in producing reactive species in the plasma. In fact in most of the plasma processing applications, electronegative gases such as Cl_2, SF_6, CF_4, C_4F_8, $Ar+O_2$ etc are used. For example Cl_2 based discharges are found to be a good source of etchant for platinum and aluminium [Flamm 1990]. The active chlorine atoms are produced in the plasma by electron impact dissociation of chlorine molecule according to the reaction $e + Cl_2 \rightarrow e + 2Cl$. Along with the formation of reactive species the electronegative gases also produces negative ions mainly through dissociative attachment. The role of negative ions in plasmas is important as their presence in the discharge can modify the Bohm speed that in turn affects the positive ion flux at the substrate. With an abundance of negative ions the electron population may reduce significantly in the plasma. On the other hand, the effective temperature of the plasma may increase as low energy electrons are lost via attachments with neutrals to form negative ions. The discharge impedance also increases with the increase of negative ions.

For neutral beam heating in fusion devices the hydrogen plasmas are the primary requirement for the production of MeV range neutral beams for plasma heating in ITER like machines [Boilson 2005]. The neutral beams are formed via charge exchange collisions between the negative hydrogen ions extracted from the source and background neutrals. The neutralization efficiency of negative ions is nearly 60% even at MeV beam energy, which makes negative ions the inevitable choice as the primary ion species for future neutral beam systems.

More recently the concept of plasma propulsion using electronegative gases was proposed [Chabert 2007]. In this concept negative ion plasma is produced by using molecular gases containing fluorine, chlorine etc from which electrons are filtered by magnetic filtering and thus resulting in an ion-ion plasma. Both positive and negative ions from the ion-ion plasma are accelerated by an alternating accelerating field to provide thrust. Acceleration of both positive and negative ions also reduces the space charge formation on the thruster body as the mutual recombination is faster. This is one of the basic disadvantages of present thrusters.

Diagnostics of electronegative plasmas are thus required for fulfilling diverse applications. However this is often challenging. Generally the negative ion density (n_-) is inferred indirectly from the measurement of the absolute values of the electron density (n_e) and positive ion density (n_i), based on the assumption that the plasma is quasineutral i.e. $n_i \approx n_e + n_-$. The electron and positive ion densities are generally obtained using Langmuir probes. However, measuring the positive ion density is not straight forward in electronegative gases due to the presence of a wide range of ionic species. Hence the probe assisted pulsed Laser photodetachment and cavity ring down spectroscopy are the most commonly used techniques. Probe assisted photodetachment is based on measuring the electron current using a Langmuir probe placed inside the laser beam path. A transient increase in electron current is observed when the incoming laser annihilates all negative ions along its way by creating an electron-positive ion plasma $n_e \approx n_+$. This non-equilibrium electron-positive ion plasma lasts for a few microseconds before the perturbed plasma column equilibrates with the surrounding. The fractional negative ion density can be obtained from the ratio of the electron saturation current to the background prior to detachment.

The above method can provide only the relative fraction of negative ions. For the absolute measurement of negative ions, it is important that the accurate electron number density be obtained from a Langmuir probe. There are some major applications where the electron density is not straightforward to measure. One such example is high power radio frequency discharges involving multiple frequencies. The electron saturation current may be difficult to obtain in the case of depositing plasmas due to contamination on probes surfaces. Application of Langmuir probes in strongly magnetized plasmas is another such example where electron saturation current is difficult to obtain owing to complicated electron motion around the probe. Moreover positively biased Langmuir probe for collecting electron saturation current can disturb the local equilibrium of the plasma surrounding the probe. In order to address these

issues we researched into the practical application of the resonance hairpin probe for measuring electron density. The main advantage is that the (1) probe is electrically floating – this minimizes the perturbation to the plasma (2) Measurement of the time-varying electron density is possible. The subject of this investigation is the hairpin probe, which is employed as a diagnostic for electronegative plasma. Principally the hairpin measures electron density in collision-less plasmas. In this thesis we investigate the hairpin probe as a diagnostic for negative oxygen ion and other parameters in the discharge in conjunction with laser photodetachment. An independent technique is also investigated in which the hairpin probe is systematically biased to negative values either in dc or in pulsed dc mode for obtaining additional information including the negative ion density.

This chapter is organized as follows: Section 1.1 presents a general overview of the plasma, its fundamental properties through highlighting the role of the electron density in sustaining plasma discharges. Section 1.2 and 1.3 presents a summary of useful diagnostics for measuring electron and negative ion densities. A brief review of hairpin probes is presented in section 1.4. Section 1.5 gives the objective of the work followed by an outline of the thesis in section 1.6.

1.1 General overview of plasmas

The term plasma describes an ionized gas in which electrons are freed from neutral atoms resulting in the existence of positively charged ions and free electrons in a state of quasineutral equilibrium. In some plasmas, where abundance of negative ions are found, then the plasma can be classified into two categories namely: electropositive and electronegative plasma depending on their relative concentrations. Electropositive plasmas are the plasmas made up of electropositive gases like argon, nitrogen etc having electrons and positive ions only as charged particles. Electronegative plasmas are those which are made up of electronegative gases like chlorine, oxygen, hydrogen etc. In these plasmas the total positive ion density (n_+) is equals to sum of the electron (n_e) and total negative ion densities (n_-) i.e. $n_i \approx n_e + n_-$.

The species in the plasma can have the same or different temperature. Therefore plasmas can be categorized on the basis of particle temperatures. Plasmas having locally identical temperatures for all species are termed as equilibrium plasmas. An example of this type of plasma are fusion plasmas where the particles temperature are $>10^6$ Kelvin. On the other hand in the plasmas having large differences in the species temperature,

are defined as non-equilibrium plasmas also known as low temperature plasmas where electrons have high temperatures compared to the ions ($T_e >> T_i$, T_n with $T_i \approx T_n$ where T_i, T_e and T_n are the positive ion temperature, electron temperature and neutral gas temperature respectively). In low temperature plasmas, ions and neutrals are generally at room temperature (300-1500 Kelvin) whereas the electron temperature can be found in the range of 10,000-100,000 Kelvin (0.5-10 eV). The temperature is typically related to the operating pressure of the discharge. At high pressure collisions will be dominant and the particle will exchange energy which will lead to a local thermal equilibrium condition. The collision frequencies are small in low pressure discharges which results in a higher temperature difference between the electrons and ions. Such plasmas are regarded as non-equilibrium plasmas. However not only the pressure but the discharge length (basically product of discharge length and pressure) is responsible for characterizing equilibrium and non-equilibrium plasmas. This research work will focus on low pressure non-equilibrium plasmas.

Plasmas are characterized by mainly two parameters; namely particle densities (electron, neutrals, positive and negative ions) and its temperature. However the electron density (n_e; due to the lighter mass of the electrons), is one of the basic plasma parameters which can provide useful information about the state of the plasma. Electrons are mainly responsible for electron impact ionization that helps in sustaining the plasma. Positive ions are considered to be at near equilibrium with the background gas. In multi-component plasmas the electron density measurement can indirectly provide information about the negative ions and positive ion species. The state of a reactive discharge is affected sensitively by the parameters of the applied plasma processes, e.g. thin film growth or etching rates. Thus monitoring the electron density is an essential feature for ensuring defect free plasma processing. It is also required for understanding various plasma properties, power coupling into the plasmas, and the plasma chemistry. Furthermore there are many basic plasma parameters which depend on the electron density and characterize a gas to be plasma. In this section we present a brief overview of those basic properties of a plasma that depend on the electron density.

1.1.1 Fundamental properties of plasmas

Plasma frequency

The plasma frequency is the most fundamental collective effect exhibited by plasmas. It was first observed in 1929, in relation to the large fluctuations in the velocities of electrons in a low pressure mercury arc [Tonks 1929]. In equilibrium, the electric fields of the electrons and ions cancel each other out. However, due to the thermal motion of the particles, this field free equilibrium cannot be maintained. In order to explain the concept of the plasma frequency, it is useful to consider the motion of the center of masses of the electrons and of the ions (rather than the motion of all of the individual particles). If the center of mass of the electrons is now displaced from that of the ions, an electric field is set up (as the charges no longer cancel) which acts to attract the electrons and ions back together. This acts as a restoring force and sets up a simple harmonic motion of the electrons about the center of mass of the ions. This amounts to a continual conversion of electrostatic energy to kinetic energy and back again. This process takes place at the electron plasma frequency (ω_{pe}) given as follows (see section 2.2 for details)

$$\omega_{pe}^2 = \frac{n_e e^2}{\varepsilon_0 m} \tag{1.1}$$

Where m is the mass of the electrons, e is electron charge and ε_0 is vacuum permittivity. On substituting all the constant parameters it gives:

$$f_{pe}=9\sqrt{n_e}(\text{inHz}) \tag{1.2}$$

Here the electron density (n_e) is in m^{-3}. Thus the electron density is directly linked to the electron plasma frequency, which lies in the microwave (GHz) region for laboratory plasmas.

Debye sheath

The Debye sheath is a fundamental property of plasmas which depends on both the electron density and temperature. It is a layer in plasmas which has a greater density of positive ions, and hence an overall excess positive charge, that balances an opposite negative charge on the surface of a material with which it is in contact. A Debye sheath arises in a plasma because the electrons usually have a temperature an order of magnitude or greater than that of the ions and are much lighter. Consequently, they are

faster than the ions by at least a factor of $\sqrt{M/m}$ where M is the ion mass and m is the electron mass. At the interface to a material surface, therefore, the electrons will fly out of the plasma, charging the surface negatively relative to the bulk plasma. This negative potential is constantly maintained by the influx of energetic electrons that actively replenish the negative charge every time they are lost due to neutralization by positive ions at the surface. Hence the net current eventually reaches zero at a specific negative potential which is defined as the floating potential. The floating potential is typically of the order of few kT_e below the plasma potential and depends on the mass of positive ions and the electron temperature.

The potential distribution in the sheath can be obtained from the solution of Poisson's equation,

$$\nabla^2 \emptyset = -\frac{e}{\varepsilon_0}(n_i - n_e) \tag{1.3}$$

Assuming Boltzmann distribution for the electrons ($n_e = n_0 \exp(e\phi/kT_e)$) and for a small change in the sheath potential ($e\phi \ll kT_e$), such that the positive ion density is fixed ($n_i = n_0$) the equation (1.3) after Taylor's expansion of exponent term and neglecting all the higher order terms of ϕ gives,

$$\frac{d^2\emptyset}{dx^2} = \frac{e^2 n_0}{\varepsilon_0 k T_e}\emptyset \tag{1.4}$$

Where n_0 is the plasma density far away from the charged conductor at potential $\emptyset_0$ and $\emptyset$ is the potential at a distance x from the conductor. The solution to this equation can be written as,

$$\emptyset = \emptyset_0 exp\left(-\frac{|x|}{\lambda_D}\right) \tag{1.5}$$

Where the Debye length is defined as

$$\lambda_D = \sqrt{\frac{\varepsilon_0 k T_e}{e^2 n_0}} \tag{1.6}$$

Thus quasineutrality, which is the basic criterion for an ionized gas to be plasma, will exist if the dimensions of the system are large compare to the Debye length. Also for Debye shielding to be statistically valid there must be a large number of particles N_D in a Debye sphere.

Plasma permittivity

Another fundamental and important property depending on the electron density is the dielectric constant or permittivity of the plasma. Plasma permittivity defines the phase velocity of electromagnetic waves propagating through it and thus forms a basis of microwave diagnostics. If the plasma is located in a high frequency electromagnetic field of angular frequency ω, then the plasma permittivity (ε_p) as a function of ω, and plasma frequency ω_{pe}, is given by the relation (see section 2.2 for details)

$$\varepsilon_p = \varepsilon_0 \left(1 - \frac{\omega_{pe}^2}{\omega^2}\right) \tag{1.7}$$

Where ω_{pe} is defined by equation (1.1).

The effect of electron-neutral collisions on the plasma permittivity is neglected in the above expression (the effect of electron-neutral collisions on the plasma permittivity is discussed in the next chapter). Also for weakly or non magnetized plasmas the electron cyclotron frequency (ω_{ce}) can also be neglected compare to ω (i.e. $\omega_{ce} << \omega$).

As appear from the equation (1.7) for frequencies above the plasma frequency i.e. $\omega_{pe} << \omega$, the dielectric constant of plasma is positive. Hence, the refractive index ($\eta = \sqrt{\varepsilon_p}$) will be real. This would seem to imply that high frequency electromagnetic waves can propagate through plasma. On the other hand, for frequencies below the plasma frequency, the dielectric constant is *negative,* which would seem to imply that the refractive index $\eta = \sqrt{\varepsilon_p}$ is *imaginary.* Hence low frequency electromagnetic waves are reflected from the plasma boundary.

1.1.2 Plasma discharges

This section is mainly concerned a brief overview of plasma discharges namely: DC, radio frequency, wave heated discharges, helicon discharges etc. In most of the discharges it is commonly known that the electrons are responsible for creating and sustaining the plasma. The most commonly used method of generating and sustaining a low-temperature plasma for technological and technical application is by applying an electric field to a neutral gas. Any volume of a neutral gas always contains a few electrons and ions that are formed by the interaction of cosmic rays or radioactive radiation with the gas. These free charge carriers are accelerated by the electric field and new charged particles may be created when these charge carriers collide with atoms and molecules in the gas or with the surfaces of the electrodes. This leads to an avalanche of

charged particles that is eventually balanced by charge carrier losses, so that a steady-state plasma develops. The most important collision processes for the production and sustaining of a plasma are electronic excitation by means of collisions with energetic plasma electrons (i.e. electron impact excitation) and ionization by means of collisions with either energetic electrons (i.e. electron impact ionization) or metastable species of the support gas (i.e. penning ionization). Sometime the discharge is operated with pulsed voltages to enhance the higher instantaneous ionization and excitation and hence obtain better efficiencies at low power.

Along with the electron collisions in the plasma as a source of ionization, the electrons are also responsible for gaining energy from the oscillating radio frequency (rf) field applied onto the electrode as in case of capacitive coupled plasmas (CCP). Since the applied frequencies are in the MHz range (which is small compared to the electron plasma frequency), the electrons can easily follow rf field while heavy ions can only follow time-averaged electric fields. Another design of plasma source in which the rf powered electrode is isolated from the plasma is an inductively coupled plasma (ICP) discharge. In an ICP discharge the electrons are accelerated by an azimuthal electric field produced by a time varying magnetic field because of a time-varying electric current in the coil. The coil is isolated from the plasma and thus provides a low pressure high density plasma operation compared to a CCP. Another way of power coupling is based on the resonance between electrons in a magnetic field and microwave field and is called electron cyclotron resonance (ECR) discharge. In ECR discharges the gyrating electrons gain energy from the electric field of a right hand circularly polarized wave, which accelerate the electrons on a circular path, which increases the collisions and sustains the plasma. Electrons are also responsible for absorbing the energy from an rf wave that propagates along the plasma. In this type of source the microwave source is replaced by a radio frequency powered antenna responsible for creating resonating waves. This type of heating mechanism is mainly the principle of helicon discharges. Thus most of the heating mechanisms discussed above in different discharges are mostly governed by the electrons.

1.2 Conventional methods of measuring the electron density

The electron density can be measured by means of well known plasma diagnostic techniques such as electrostatic probes, emission and absorption spectroscopy, microwave techniques such as microwave transmission and cut-off,

hairpin probe and self-excited electron resonance spectroscopy (SEERS). The diagnostics are typically classified in terms of invasive or non-invasiveness to the plasma and the density range for the operation of the diagnostic. This section presents a brief overview on the principles behind electrical and microwave techniques.

Electrostatic probes

The electrostatic probe for plasma diagnostics was invented by Irving Langmuir in 1926 and it is commonly known as the Langmuir probe. It is an invasive technique in which a piece of conductor (planar, spherical or cylindrical) is inserted inside the plasma and a voltage-ampere characteristic is drawn by biasing the conductor with respect to other conductors in contact with the plasma such as the vacuum vessel or any reference electrode.

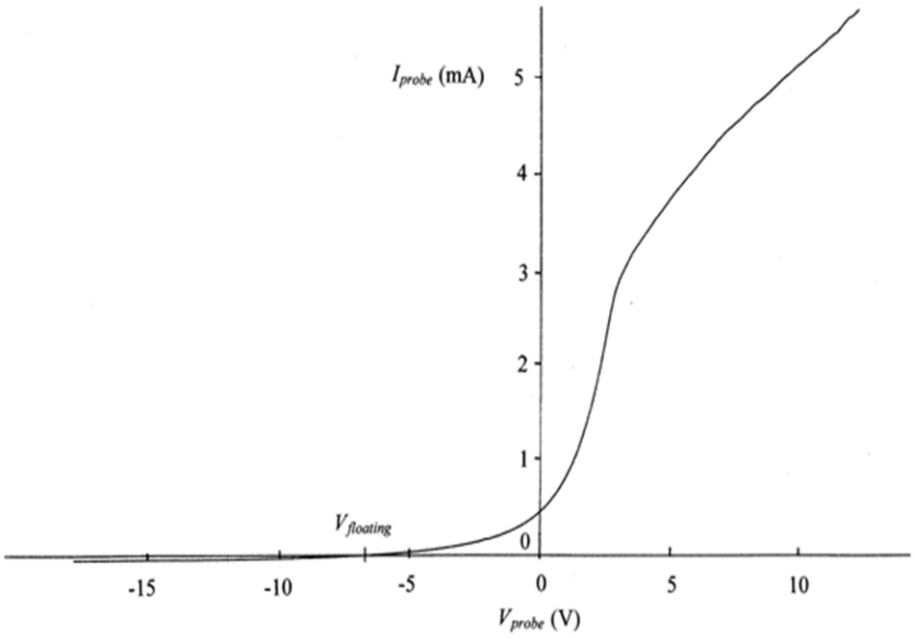

Figure 1.2: A typical Langmuir Probe Characteristic Curve.

When the bias voltage of the probe is set to a value much more negative than the floating potential one obtains a saturation current that corresponds to positive ions if the secondary electron emission is small. Similarly, when a positive potential is applied to the probe, typically a few volts above the plasma potential an electron saturation region

is obtained purely comprised of electrons. The typical characteristic so obtained is schematically shown in figure 1.2.

Following the simplest assumptions, [Langmuir 1924] the transition region from the electron saturation to the ion saturation is characterized by a slope which corresponds to the plasma electrons obeying the Maxwell-Boltzmann distribution $n_e = n_0 exp\left(\frac{V_B - V_p}{kT_e}\right)$. Thus the electron component of probe current is given by

$$I + I_i = I_e = \frac{1}{4} e n_0 \bar{v_e} A exp\left(\frac{V_B - V_p}{kT_e}\right) \tag{1.8}$$

Here n_0 is bulk plasma density, V_B is probe bias, V_p is plasma potential, T_e is electron temperature, A is the area of the probe and $\bar{v_e}$ is the mean electron speed given by $\bar{v_e} = (8kT_e/\pi m)^{1/2}$.

The electron saturation current is therefore given by

$$I_{es} = \frac{1}{4} e n_0 \bar{v_e} A \tag{1.9}$$

The positive ions exiting the plasma have a directed speed at the sheath edge which is given by the Bohm velocity $v_B = \left(\frac{kT_e}{M}\right)^{1/2}$. The typical ion saturation current is therefore given by,

$$I_{is} = -e n_s \left(\frac{kT_e}{M}\right)^{1/2} A \tag{1.10}$$

Where n_s is the density at the sheath edge related to bulk density by $n_s \approx 0.61 n_0$ at low pressure [Chabert and Braithwaite, 2011].

If the contribution of the ion current is eliminated from the net current drawn by the probe, then the electron temperature can be easily obtained from the slope of the characteristic curve plotted between as the log of electron current verses the probe bias. This is a straight line as shown below:

$$ln\left(\frac{I_e}{I_{es}}\right) = \frac{1}{kT_e}\left(V_B - V_p\right) \tag{1.11}$$

Hence the electron density can be obtained from the electron saturation current by substituting the mean electron speed (which is a function of T_e) and the probe area as given below:

$$n_0 = \frac{I_{es}}{e\bar{v_e}A} \tag{1.12}$$

One of the drawbacks of this technique are due to its invasive nature thus it can significantly perturb the plasma, particularly in a strong magnetic field. Inaccurate measurement of electron saturation current is possible if insulating films get deposited

on the probe surface. Furthermore in rf plasmas additional care must be taken in restoring the dc shape of the Langmuir probe characteristic. Active and passive compensation is used so that the probe can easily follow the rf plasma potential [Chabert and Braithwaite 2011]. However the Langmuir probe is the most popular diagnostic method as it uses simple equipment and a number of plasma parameters including, plasma potential, floating potential, electron and ion density, electron temperature can be readily obtained by analyzing the voltage-ampere characteristic.

Microwave diagnostics

The microwave diagnostic technique uses the frequency dependent permittivity of the plasma (equation 1.7) which changes the characteristic wavelength of the wave. The relative phase shift between the incident and the transmitted wave through the plasma medium is related to the electron density from the measurement of refractive index for that characteristic frequency [Heald 1978]. This is the principle of microwave interferometry.

The typical formula for obtaining the electron density using this technique for a wave of frequency ω which is chosen above the plasma frequency is given below,

$$\Delta\phi \approx \frac{e^2}{2c\varepsilon_0 m\omega}\int n_e dl$$

Here $\Delta\phi$ is the change in phase shift. Thus the line integral of the electron density can be obtained by measuring the change in phase shift. Microwave interferometry is a simple and non-invasive method to determine the line-integrated electron density; however a local measurement of density is not possible.

Another type of microwave diagnostic technique is known as microwave reflectometry. In this technique a wave with a frequency below the cutoff frequency is launched into the plasma. As a consequence the wave will be reflected from the so-called critical density layer. One can deduce the position of that layer by measuring the phase shift of the probing wave with respect to a reference wave or by measuring the time-of- flight of a short microwave pulse to the reflecting layer and back. Multiple-fixed or swept frequency systems are employed for measuring the electron density profile. It is generally not for diagnosing the central part of the density profile since the density gradient is too small here. The above techniques are commonly used in high density plasmas such as tokamaks and in laboratory plasmas as well.

The Hairpin probe is also a microwave technique. However its methodology for extracting the density is very different than the above discussed techniques. Using the hairpin probe, we launch a local electric field by means of a U-shaped quarter wave resonator wire which has a characteristic frequency that depends on the permittivity of the medium around the wire. On changing the permittivity, as happens in the plasma, the characteristic frequency gets shifted. The shifts in the characteristic resonance frequency in the two media are related to the electron density as (a detailed description can be found in chapter 2).

$$n_e = \frac{f_r^2 - f_0^2}{0.81}$$

Here the frequencies f_r and f_0 are in GHz and the electron density n_e is in 10^{16} m^{-3}. Figure 1.3 shows two resonance peaks: one corresponds to the vacuum resonance (f_0) and the second corresponds to the resonance in the presence of plasma (f_r).

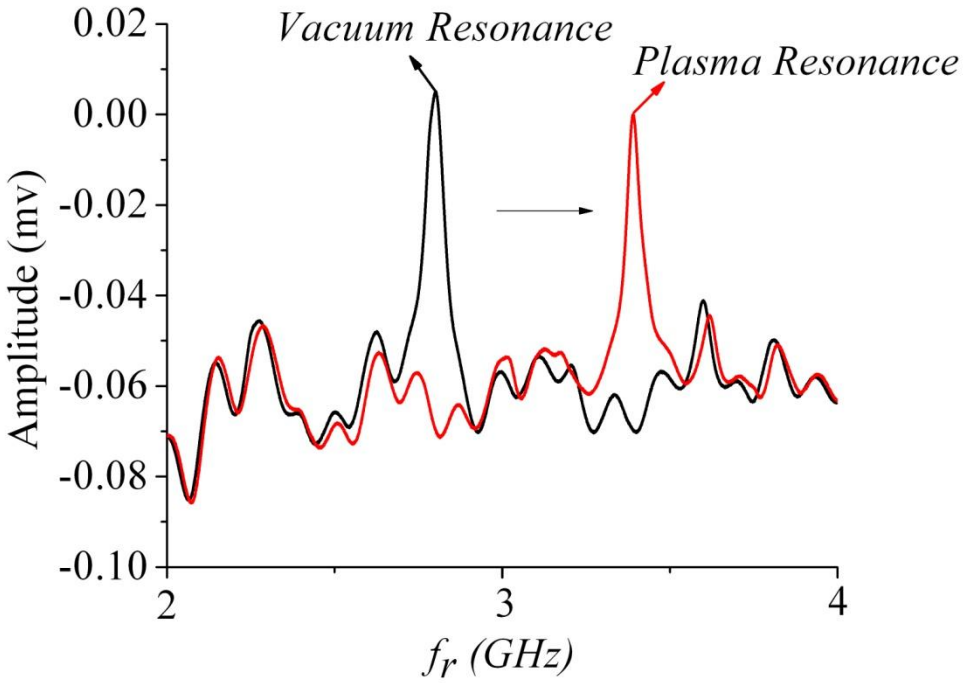

Figure 1.3: Resonance signal of a hairpin probe in vacuum and in plasma.

Thus the relative shift in the resonance frequency with and without the plasma allows one to obtain the electron density. This technique allows us to obtain a local measurement of the electron density in the plasma and therefore is highly promising.

1.3 Conventional methods of measuring negative ions

The measurement of negative ion density and temperature is commonly done by indirect techniques i.e. usually electrons and positive ions are monitored which gives information about negative ions. These indirect techniques mainly include electrical probes and laser based diagnostics. In this section we present a brief overview on these diagnostic techniques that are used for measuring negative ion density and temperature.

Langmuir probes are the one of the oldest ways for diagnosing of plasmas (a more detailed discussion can be found in section 1.2). Several theories have been developed based on Langmuir probe characteristics for estimating the negative ion parameters. Most of the theories were based on the ratio of the saturation current at the plasma potential to the positive ion saturation current. In 1988, Braithwaite and Allen [Braithwaite 1988] proposed an analytical expression which relates the negative ion density ratio to the ratio of negative saturation current to positive ion saturation current for a spherical Langmuir probe. It was the first time that the multi-valuation of the Bohm criterion in electronegative plasmas was discussed. This theory was well accepted and used by various authors [Amemiya 1990, Nikitin 1996]. More recently Shindo et al [Shindo 2001] used the same technique by comparing the ratio of the saturation current of positive ions and electrons in a noble gas plasma with that in an electronegative plasma to estimate the negative ion density. However the input parameter to these techniques like mass of positive ions, mass of negative ions and temperature ratio, make it difficult to use in complex industrial gas mixtures.

Another diagnostic technique based on electrostatic probes is the two-probe technique which was proposed by Chabert et al [Chabert 1999]. As the name suggests, this technique uses two electrostatic probes at the same time. One probe is used to measure the modified Bohm flux and another probe is used to measure the electron thermal current. The negative ion density is estimated by comparing the ratio of electron thermal current and modified Bohm flux to the ratio obtained by a fluid model developed by Sheridan et al [Sheridan 1999]. Initially the technique was employed for collision-less plasmas which were further developed by Curley et al [Curley 2008] to make use in modestly collisional plasmas. However the use of two probes is impractical in some plasma tools. Also the accuracy will again depend on the accuracy of the measured electron density.

Optical methods have also been developed for measuring absolute negative ion densities in which the cavity ring down spectroscopy (CRDS) [Booth 2006] is the most

promising one. In CRDS a pulsed laser is passed up and down through the plasma chamber via the use of highly reflecting mirrors located at each end of the chamber to create an optical cavity and so significantly increase the optical path length of the laser pulse through the plasma and the decay of the laser light escaping through one end of the cavity after each pass of the laser pulse through the plasma chamber is recorded. The time constant associated with the exponential decay in the laser energy escaping the cavity is determined. By comparing the CRDS signals with plasma on and plasma off, the absolute negative ion density can be measured. One of the main issues related to this technique is that this method only allows a line averaged density measurement whereas the negative ion density varies spatially within the plasma and local density variations are not considered in the results obtained with this method. Another issues related to this technique is the deposition or etching at the surface of glass windows, which affects the laser light.

Another well known diagnostic technique for electronegative plasmas is based on the detachment of electrons from the negative ions with a laser pulse followed by the detection of the electron density [Bacal 2000]. In this technique a pulsed laser beam of photon energy higher than the electron affinity of the negative ions is passed through the plasma. When operating in the saturation regime of laser flux it creates an electropositive channel. The negative ion density is determined by the difference in the background electron density and the peak electron density after photodetachment. Diagnostic of multiple negative ions is also possible using this technique. This is done by tuning the laser frequency (photon energy) just higher than the electron affinity of the specific negative ion to be diagnosed.

Measurement of the time varying electron density during the pulsed laser also gives the information of the negative ion temperature. To estimate the negative ion temperature it is assumed that the decay in the peak electron density in the laser channel is due to the diffusion of negative ions from the surrounding plasma [Bacal 2000]. The negative ion temperature is thus estimated from the recovery time and the radius of the laser beam. Furthermore two laser beam technique is also used to measure the negative ion temperature in which the first laser is used for photodetachment and the second laser is fired with some delay to measure the recovery of negative ions [Stern 1990]. In this thesis we have extensively studied this technique and proposed the use of hairpin probes with laser photodetachment to obtain negative ion parameters.

1.4 Hairpin probe

In this section we briefly present the background of the hairpin probe. The history of the hairpin probe is not too old, till 1970's the common plasma diagnostics for characterizing electron density were based on radio frequency techniques like microwave interferometers, faraday rotation and resonance cavity shift. These techniques were suitable for spatially averaged densities, and therefore they are ideal for homogeneous plasmas. Around 1971, Stenzel and Gould [Stenzel 1971] invented the microwave resonance probe for electron density measurements in collision-less weakly magnetized plasmas. The resonance probe had the advantage that the probe is electrically floating. This means the probe draws no net current from the plasma. Therefore a major advantage is that no reference electrode is necessary as required for Langmuir probes. This significantly reduces the perturbation introduced in the plasma. Stenzel and Gould used this technique extensively for studying the upper hybrid resonance in an afterglow decaying plasma [Stenzel 1971]. A detailed description of the probe was later published by Stenzel in 1976 [Stenzel 1976]. Figure 1.4 represents the design of the hairpin probe proposed by Stenzel. The probe had two loop antennas, 1.5 mm in diameter and separated by 4 mm. The hairpin was mounted in-between the two loops and was completely isolated from the two loops. The hairpin was made with a silver wire having diameter 0.1 mm and the length and width of the hairpin was 8 mm and 2 mm respectively.

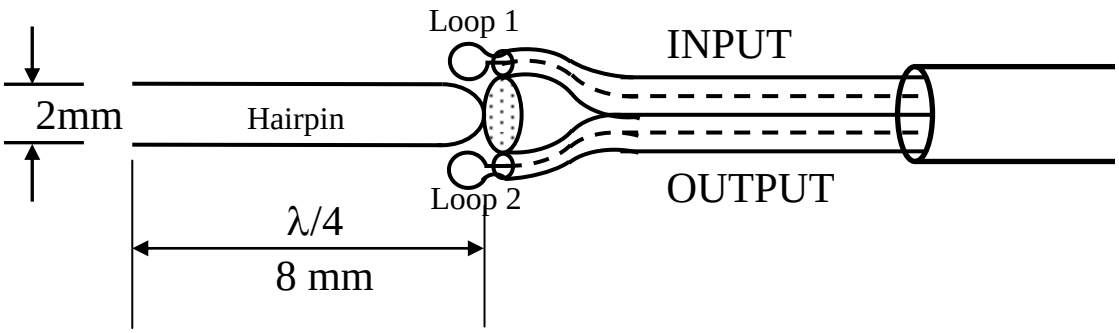

Figure 1.4: Schematic of the microwave resonator probe by Stenzel.

One of the disadvantages with Stenzel's probe was due to its bulky design. This was the reason for its rare application by few researchers ([Kim 1995], [Werner 1996], [Grabowski 1998]). In order to reduce the probe dimension Hebner et al [Hebner 2001]

demonstrated a hybrid system in which a coaxial cable loop antenna was used for exciting the hairpin and a remote horn antenna was used as a sensor.

In 2004 Peijak et al [Piejak 2004] introduced an innovative design of the microwave probe after which it became popular as a hairpin probe due to its characteristic shape. One basic advantage was that a single loop antenna is required for both excitation and detection of the resonance condition. Following this pioneering paper some renewed interest was created on the application of hairpin probes for direct application in commercial plasma tools [Karkari 2006, Curley 2010] and also in laboratory plasma studies [Karkari 2005, 2007]. Important papers include those by Braithwaite et al [Haas 2005] who addressed the effects of space charge sheath around the hairpin probe. Around the same time, Piejak and Braithwaite from Open University, UK [Piejak 2005] and Karkari et al [Karkari 2005] from Dublin City University, Ireland came up with novel designs of floating hairpin probes for rf plasmas. Curley et al [Curley 2008] measured the negative ions by comparing the electron density using a hairpin probe with the positive ion density using an additional ion flux probe. Ganguly et al [Sands 2007] demonstrated the use of a hairpin in sub-atmospheric pressure plasmas. Recently Sugai et al presented a detailed theoretical work on the application of hairpin probes in high pressure plasma [Xu 2009]. Sirse and Karkari et al [Sirse 2010, Conway 2010] have demonstrated the use of hairpin in conjunction with pulsed laser photodetachment for electronegative plasma diagnostics while Gogna and Karkari [Gogna 2010] addressed the issues related to the application of hairpin in magnetized plasmas.

1.5 Objective and motivation of the thesis

One basic limitation with hairpin probes is due to the sheaths around the resonator pins which affect the accuracy of the measured values at lower densities (below 10^{16} m^{-3}). The sheath is a boundary layer around the surface of the probe which is deficient of electrons. Therefore the effective permittivity seen by the hairpin is because of both the vacuum permittivity (ε_o) of the sheath and the true plasma permittivity (ε_p). The influence due to the sheath is significant at plasma densities below 10^{16} m^{-3}, as the effective sheath width becomes comparable to the separation between the pins. Hence the electron density measured by the hairpin is underestimated. This problem can be severe in the case of radio frequency discharges due to a high level of oscillation in the plasma potential resulting from sheath rectification. Even for a few

10's of volts rf plasma potential oscillations, the stray capacitances between the hairpin and the insulated probe stem can result in a substantial sheath thickness for low plasma densities of about 10^{16} m^{-3}. Also the presence of negative ions can modify the sheath thickness. Therefore the behavior of a sheath around the cylindrical pins is important for applying the hairpin probe technique in electronegative plasmas. A systematic study is therefore devoted to the numerical simulation of sheaths around cylindrical probes in electronegative plasmas.

One fundamental idea proposed by Peijak et al [Piejak 2004] for the compensation of the sheath width around the hairpin is based on step front sheath model. Such a method requires information of the electron temperature for obtaining an initial estimation of the sheath width. Therefore additional diagnostics are required for obtaining the temperature of the plasma. In line with the above model, Piejak [Piejak 2004a] also proposed a biased hairpin probe. In that technique the hairpin was biased up to the plasma potential in order to nullify the sheath. Braithwaite et al [Haas 2005] further refined the theory of negative and positive biased hairpin probes by including the role of electrons on the finite sheath width. However biasing of the probe to a positive potential is impractical for magnetized and deposition plasma conditions. Another fundamental limitation of the hairpin is that the measurable density range falls within 10^{15} to 10^{18} m^{-3}. One can calculate that there is very minimal benefit of pushing the upper range of microwave frequency required for the resonance. At electron densities ~ 10^{19} m^{-3}, the electron plasma frequency (f_{pe}) is above 28 GHz. Hence the dimension of the quarter wavelength $\lambda/4$ probe will be a length of typically 2.6 mm. This makes it rather impractical for designing a hairpin probe as the physical length of the resonator must be much larger than the separation between the resonator wires as compared with the wire radius. To address this issue we investigate the negatively biased hairpin probe. A negative bias creates an ion sheath around the hairpin which shifts the measurable frequency range to the lower frequency side when dealing with high density plasmas and yet the underestimated value may be calibrated to get the actual density.

Another important application addressed in this thesis is the measurement of density and temperature of negative oxygen ions using conventional photodetachment in association with a hairpin probe which replaces the Langmuir probe. In addition an independent technique is proposed for measuring the negative ion density and the associated plasma properties by using a pulse biased hairpin probe. A transient negative potential is used for driving the negative ions and electrons from the vicinity of the probe. On the sudden removal of the applied potential, the background electrons quickly

rush in to shield the ion space charge. This results in the observance of a transient electron density that corresponds to the background positive ions as similar to photodetached electron density in the case of pulsed laser photodetachment technique.

1.6 Outline of the thesis

The outline of this thesis is as follows: chapter 2 presents the detailed principle of the resonance hairpin probe. This chapter also describes different designs of the hairpin probe. A detailed description of the underlying techniques used for finding the steady state and time resolved electron density is presented together with experimental data.

In chapter 3 a detailed discussion is presented for different methods/models of sheath correction. A technique for measuring accurate electron densities in low density plasmas with the application of negative dc bias on the hairpin is presented. The results are compared with the correction based on step front sheath model. Finally, high density plasma diagnostics with negatively dc biased hairpin probe is proposed. Chapter 4 is devoted to the systematic theoretical investigation of sheaths particularly in the context of sheaths around cylindrical objects in electronegative plasmas.

The application of floating hairpin probes with laser photodetachment for electronegative plasma diagnostics is presented in chapter 5. The photodetachment signals are investigated both inside and outside the beam to avoid the laser ablation from the probe surface. The steady state negative ion density is experimentally measured using this technique in an oxygen based ICP discharge and also the time resolved negative ion density in argon/oxygen based pulsed dc magnetron discharge. The response of the plasma following photodetachment is discussed by comparing the plasma potential and electron density evolution. Finally an independent technique to measure the negative ion temperature is systematically investigated using the temporal evolution of the plasma potential during photodetachment and compared with those obtained by the evolution of the electron density.

In chapter 6 we presented a novel application of the hairpin probe to measure electronegative plasma parameters without using laser photodetachment. The temporal evolution of the electron density during the application of a sharp negative pulse to the hairpin is used for this purpose. This technique is experimentally investigated in both electropositive as well as in electronegative plasmas. The dependency of the diagnostic

on the applied pulsed parameters is also discussed. The limitation of this technique is presented at the end of the chapter.

Finally the summary, conclusions and future scope of the work are given in chapter 7.

Chapter 2

The resonance hairpin probe

In this chapter we discuss the fundamental principle behind the resonance hairpin probe for measuring the electron density in collision-less non-equilibrium plasmas with different designs of the hairpin probe. The experimental set-up for obtaining the probe resonance frequency is presented and its application for measuring the electron density in two important cases is demonstrated; (1) steady state plasmas, in which the electron density remains constant over the period of scanning of the frequency applied to the hairpin and, (2) the technique behind time-resolved measurement of the electron density with experimental results in a pulsed dc magnetron discharge.

2.1 Resonance frequency of the hairpin probe

The hairpin probe is based on measuring the frequency dependent permittivity of plasma by means of a U-shaped wire. Since the resonator design resembles the hairpin, it is therefore commonly called as a hairpin probe. The hairpin has its own characteristic resonance frequency which depends on its physical dimensions and the permittivity of the medium surrounding it. This section presents the resonance frequency formulation of the hairpin probe with the assumption of a transmission line and its equivalent LCR circuit. The effect of the hairpin resonator width on resonance frequency is also experimentally investigated in vacuum.

2.1.1 Transmission line model

In the simplest case, the hairpin probe can be modelled as a parallel wire transmission line having length L, wire radius a separated by distance $w \sim 2h$ ($L >> w$) which is shorted at one end and open at the other. Figure 2.1 shows the transmission line equivalent of the hairpin and the front view of the transmission line showing the electric and magnetic field lines at resonance.

When a current or voltage waveform is launched in a transmission line then it gets reflected from the open end because of the impedance mismatch. The transmitted and the reflected waves interfere either constructively or destructively depending on the

length of the transmission line. If the length of the transmission line is equal to the integral multiple of the quarter wavelength of the wave launched, the incident and reflected waves interfere constructively and thus support a standing wave. In the case of the hairpin probe a current waveform is fed via a loop sitting near to the short circuit end of the hairpin. At resonance, the hairpin supports a standing wave and the short circuit end of the hairpin will be a current anti-node (voltage node) and the open end will be a current node (voltage anti-node). Thus the probe will be sensitive at the open end where the electric field is a maximum.

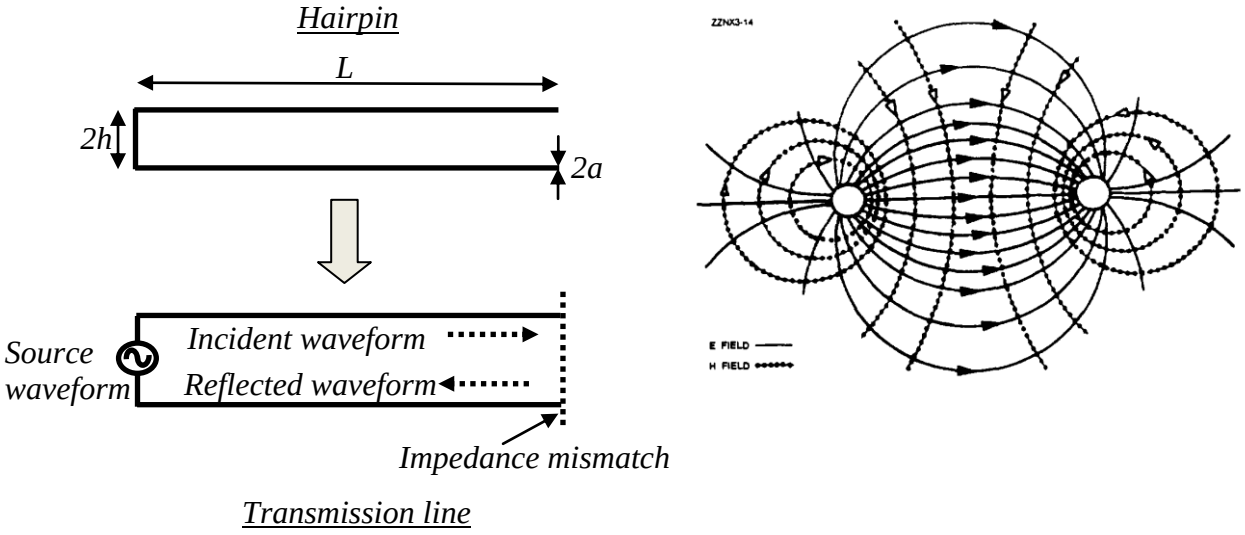

Figure 2.1: Transmission line equivalent of the hairpin and the front view of electric and magnetic field-lines in a transmission line.

In the resonance condition the length of the transmission line or hairpin is given by the odd multiple of the wavelength of the waveform launched, i.e.

$$L = (2k+1)\frac{\lambda}{4}, \text{ for } k = 0, L = \frac{\lambda}{4} \text{ (fundamental)} \tag{2.1}$$

Here k is an integer and λ is the wavelength. The frequency and wavelength are related by the equation

$$f = \frac{c}{\lambda} \tag{2.2}$$

Equations (2.1) and (2.2) above give the resonance frequency of the hairpin

$$f = \frac{c}{4L} \tag{2.3}$$

When the medium surrounding the hairpin is not vacuum but it is a dielectric medium having dielectric permittivity ε, then equation (2.3) can be written in the form

$$f = \frac{c}{4L\sqrt{\varepsilon}} \tag{2.4}$$

Thus the resonance frequency of the hairpin given by equation (2.4) is inversely proportional to its length and to the square root of the permittivity of the medium surrounding it.

2.1.2 LCR circuit equivalent of a transmission line

The electrical circuit of a transmission line is composed of distributed electrical elements, namely: the resistance of the line R_l given by the dc conductivity σ_l with the skin depth δ_l at frequency ω, conductance G_l given by the conductivity (σ_p) of the surrounding medium, distributed inductance L_l and the distributed capacitance C_l as shown in figure 2.2. The capacitance and inductance (which depends on the permittivity of medium and absolute permeability respectively), resistance and conductance is given by the relations [Xu 2009]

$$R_l = \frac{1}{2\pi a\sigma_l\delta_l}, \quad L_l = \frac{\mu_0}{\pi} ln\left(\frac{h}{a} + \sqrt{\left(\frac{h}{a}\right)^2 - 1}\right) \tag{2.5}$$

$$C_l = \frac{\pi\varepsilon_0\varepsilon}{ln\left(\frac{h}{a} + \sqrt{\left(\frac{h}{a}\right)^2 - 1}\right)}, G_l = \frac{\pi\sigma_p}{ln\left(\frac{h}{a} + \sqrt{\left(\frac{h}{a}\right)^2 - 1}\right)} \tag{2.6}$$

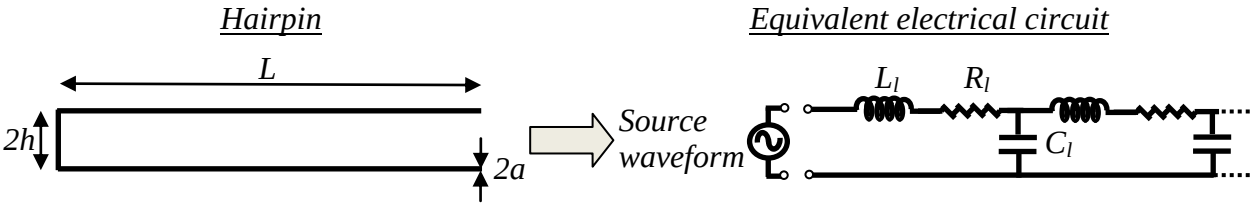

Figure 2.2: Equivalent electric circuit of the hairpin with distributed electrical elements.

The propagation constant of an electromagnetic wave exciting transmission line is given by $\gamma_l = \alpha_l + j\beta_l$. Where α_l is the attenuation constant and β_l is the phase constant. For a low-loss transmission line α_l and β_l is given by the distributed parameters as [Xu 2009]

$$\alpha_l \cong \frac{1}{2}\left[R_l\sqrt{\frac{C_l}{L_l}} + G_l\sqrt{\frac{L_l}{C_l}}\right], \beta_l \cong \omega\sqrt{L_l C_l} \tag{2.7}$$

Resonance occurs when the wavenumber satisfies $\beta_l L=(2k+1)\pi/2$ for the integer k. Thus on substituting β_l in equation (2.7), the fundamental resonance for k=0 gives $\omega =$

$\pi/2L\sqrt{L_l C_l}$. Substituting the values of the inductance and capacitance from equations (2.5) and (2.6) gives

$$f = \frac{1}{4L\sqrt{LC}} = \frac{c}{4L\sqrt{\varepsilon}} \tag{2.8}$$

Here $c = 1/(\varepsilon_0\mu_0)^{1/2}$.

Thus the expression for the hairpin resonance frequency obtained by the transmission line model and its LCR circuit equivalent suggest that the measurement of the resonance frequency of a U-shape wire gives a measurement of permittivity of the medium surrounding the probe.

2.1.3 Effect of hairpin dimension on vacuum frequency

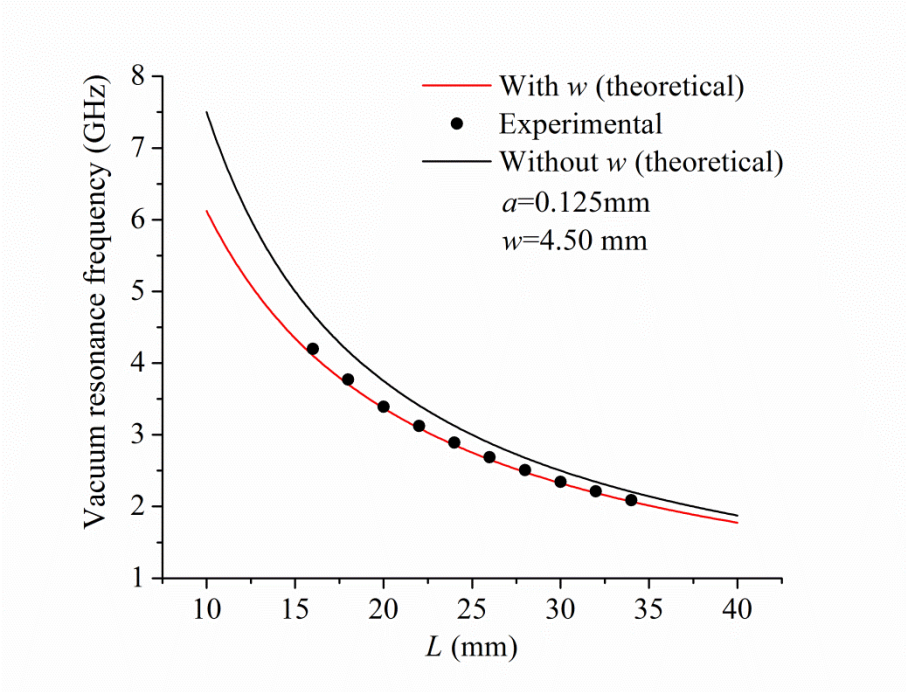

Figure 2.3: Experimental and theoretical plot of resonance frequency in vacuum, f_o, as a function of the length, L, of the resonator pins.

The dependence of resonance frequency on the physical dimension of the hairpin was outlined in the previous section. To validate the dependence a simple experiment was performed in vacuum. The experimental and theoretical vacuum resonance frequency (f_0) as a function of the length of the hairpin is shown in figure (2.3) with w ($f_0 = c/2(2L + w)$) [Sands, 2007] and without w ($f_0 = c/4L$). The width ($w=2h$) of the resonator is kept constant. The resonance formula, f_o, without w is based on the assumption of an infinite parallel wire transmission line which neglects the finite width,

w, of the resonator. However in the real experiments the effective length of the resonator includes the finite *w* i.e. the total length of the resonator is given by *(L+w/2)*. In figure 2.3 we observe that the experimentally measured vacuum resonance frequency (f_o^m) agrees well with equation (2.3) while for the shorter probe lengths f_o^m deviates from f_o. Thus the most general formula for the resonance frequency of the hairpin including the width of hairpin is given by the relation $f_0 = c/2(2L + w)$. Hence the width of the hairpin is taken into account when calculating the vacuum resonance frequency. However the electron density measurement by the hairpin probe is related with to the relative shift in the resonance frequency as discussed in the sections below.

2.2 Cold plasma permittivity

The response of a plasma particle to an externally applied electric field depends on its frequency. For steady state or low frequency fields this response is generally termed as the conductivity on the other hand the plasma response to a high frequency field is termed as permittivity [Chabert and Braithwaite 2011]. Thus before proceeding to the dependence of electron density on hairpin resonance frequency it is important to discuss the concept of plasma permittivity. In this section we discuss the plasma response to small amplitude oscillating electric fields and obtain the cold plasma permittivity in two cases, namely: collision-less and collisional.

2.2.1 Plasma response to high frequency electric field

Consider a plasma excited by an externally imposed high frequency electric field. The electric field will be induced by imposing an oscillating potential $V(t) = V_0 \sin \omega t$ at time $t = 0$ across boundaries on opposite sides of a plasma having length l (implicitly >> λ_D) in the x direction. For simplicity the plasma will be assumed to be infinite in extent (or at least >> l) in the other two directions so that their effects can be neglected. Since the plasma is assumed to be electrically neutral, each species must have the same equilibrium number density, n_e. Now, given that the electrons are much less massive than the ions (i.e., $m \ll M$) thus the lighter electrons will give the primary inertial response to an applied electric field in plasma. Also they have the same charge (modulo a sign), hence it follows that the electric field induced oscillations of the electrons are of much higher amplitude than those of the ions. In fact, to a first approximation, the electrons oscillate whilst the ions remain stationary. Also for

simplicity the thermal motions of the particles can be neglected and a zero initial drift is assumed.

In the simplest case a slab consisting entirely of one charge species is displaced from its quasineutral position by an infinitesimal distance x. The resulting charge density which develops on the leading face of the slab is $\sigma = en_e x$. An equal and opposite charge density develops on the opposite face. The x-directed electric field generated inside the slab is of magnitude $E_x = -\sigma/\varepsilon_0 = -en_e x/\varepsilon_0$. The electric field together with the equation of motion gives an oscillatory solution with a frequency given by electron plasma frequency (a detailed discussion can be found in the next section). Thus there will be a cut-off in frequency defined by the electron plasma frequency. Plasma electrons will be unresponsive for any applied frequency above this frequency whereas the electrons will oscillate with the applied frequency lower than this.

2.2.2 Dielectric property of the plasma

(1) Collision-less

In the collision-less plasma the mean free path of electrons is large compared to the length of the plasma (l as considered in section 2.2.1). In this situation apart from electric force there will not be any additional force will exerted onto the electrons (again the magnetic force is not considered). Also a cold plasma is assumed, where one or more species is assumed to have no thermal energy. The motion of electrons in the applied electric field will be governed by Newton's second law of motion

$$m\ddot{x} = -eE \tag{2.9}$$

Where E is the applied electric field given by $E = E_0 \sin\omega t$.

The solution of the differential equation (2.9) is given by

$$x = \frac{eE_0}{m_e\omega^2}\sin\omega t$$

Assuming that the electrons and ions are evenly distributed throughout the plasma, the electric field induced displacement of an individual electron generates an effective electric dipole moment in the x direction. The electric dipole moment in the x direction will be given by the equation

$$p = -p_0 \sin\omega t \tag{2.10}$$

Where p_0 is given by the relation

$$p_0 = \frac{e^2E_0}{m_e\omega^2} \tag{2.11}$$

Above equation gives the magnitude of the dipole moment of an individual electron induced by the applied electric field. If n_e is the electron density per unit volume of the plasma then the dipole moment per unit volume will be given by multiplying equation (2.11) by n_e. The effect of magnetic field and collisions are not included in the above formulation, further ions and neutrals are assumed to be stationary.

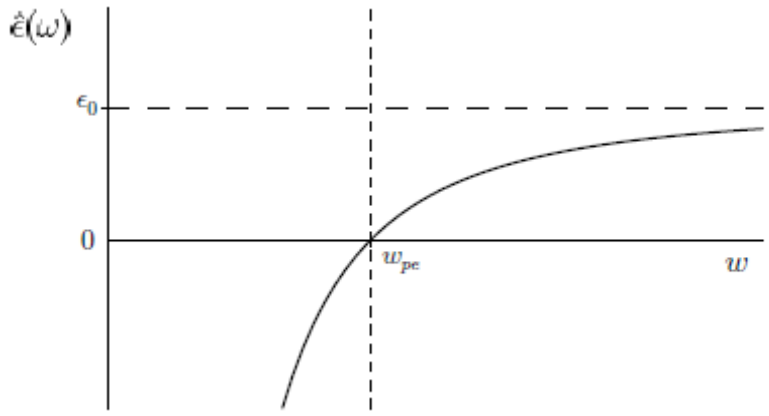

Figure 2.4: Frequency dependence of plasma permittivity.

The dipole moment per unit volume induced in the medium by the electric field is given by the relation

$$p = (\varepsilon - 1)E \tag{2.12}$$

Simplifying equation (2.12) with (2.11) (multiplied by n_e for the dipole moment per unit volume) gives the plasma permittivity

$$\varepsilon = 1 - \frac{\omega_{pe}^2}{\omega^2} \tag{2.13}$$

Thus the plasma permittivity is a function of applied frequency. This frequency dependent permittivity is plotted in the figure 2.4.

The value of $\varepsilon(\omega) \rightarrow 1$ for $\omega >> \omega_{pe}$. In this case the driven component of the electric field approaches the externally applied electric field in this “vacuum" limit. Since the plasma permittivity is negative for $\omega < \omega_{pe}$, the externally applied electric field is shielded out of the plasma or cut-off in this frequency range. The vanishing of $\varepsilon(\omega)$ for $\omega = \omega_{pe}$ indicates that this is a “normal mode" of oscillation of the plasma.

(2) Collisional

In the collisional plasma, typically at high discharge pressure, the mean free path is short compared to the discharge length. In this case the electrons will collide with the background ions and neutrals. The collision will create another force to the electrons moving in the applied electric field. The interaction of the electrons with the ions and neutral particles in a plasma can be represented by a friction term in the electron equation of motion.

$$m\vec{\ddot{x}} = -e\vec{E} - \nu_e m\vec{\dot{x}} \tag{2.14}$$

Where ν_e is the effective collision frequency. The collision term represents the rate of change of momentum and therefore the force exerted on the electrons by the ions and neutrals of the plasma. Doing the same exercise as in the previous section the equation of motion yield a complex dielectric function of

$$\varepsilon = 1 - \frac{\omega_{pe}^2}{\omega(\omega - j\nu_e)} = 1 - \frac{\omega_{pe}^2}{\omega^2 + \nu_e^2} - j\frac{\nu_e}{\omega}\frac{\omega_{pe}^2}{(\omega^2 + \nu_e^2)} \tag{2.15}$$

Under the condition of $\omega > \omega_{pe}$ (typically in the GHz range) and pressure up to 500 mTorr (which is typically the case fulfilled in all the discharges used in this thesis), the collision frequency is very small compared to the wave frequency i.e. $\nu_e \ll \omega$. Thus the permittivity given by the equation (2.15) takes the form of equation (2.13).

2.3 Electron density measurement from plasma permittivity

This section presents a simple analytical expression which relates the vacuum resonance frequency and plasma resonance frequency of the resonance hairpin probe to the electron density. Since the plasma studied in this thesis is collision-less, the formula for electron density is derived from the collision-less dielectric permittivity described in section 2.3.2.

The resonance frequency of a hairpin depends on the permittivity of the medium surrounding it and its physical dimension as shown in equation (2.4). Also in collision-less, non-magnetized and non-equilibrium plasmas the permittivity is a function of the electron density and the frequency of the penetrating electric field. Thus using a hairpin probe in the plasma can quantify the electron density. Again if the plasma is located in a high frequency electromagnetic field of angular frequency ω, then the cold plasma permittivity as a function of ω, and plasma frequency ω_{pe}, is given by the relation

(2.13). If the probe is in vacuum, where $\varepsilon = 1$, then the resonant frequency is determined by the physical dimension of the probe. From equation (2.14):

$$f_0 = \frac{c}{4L} \tag{2.18}$$

If the probe is immersed inside plasma, the resonance frequency will change accordingly with respect to its resonance frequency in vacuum due to the change in the permittivity around the resonator pins. Thus from equation (2.4), (2.13) and (2.18) we can derive the relation for the shifted resonance frequency in the plasma,

$$f_r^2 = f_0^2 + f_p^2 \tag{2.19}$$

Where $f_r = f_0/\sqrt{\varepsilon_p}$ (ε_p is plasma permittivity defined by equation (1.7)) is the resonance frequency of the hairpin in the presence of the plasma. Using the plasma frequency (f_p from equation (1.1)) we can write an expression for the electron density as a function of the resonance frequency in the plasma:

$$n_e = \frac{f_r^2 - f_0^2}{0.81} \tag{2.20}$$

Where the frequencies f_r and f_0 are in GHz and the electron density n_e is in 10^{16} m^{-3}. Thus with the relative shift in the resonance frequency with and without plasma the electron density can be obtained using equation (2.20).

2.4 Designs of hairpin probes

The typical design of the hairpin depends on the particular method used for determining the resonance frequency. When the hairpin is in resonance, a significant amount of power is coupled to the hairpin from the external driving loop. Intense electric fields generated around the hairpin can provide a signature of the resonance condition. In another type of design, the reflected power is measured in the 50 Ω transmission line supplying the microwave signal to the loop antenna. At the resonance frequency the reflected power detected using a directional coupler is found to reduce drastically owing to efficient power transfer to the hairpin followed with ohmic losses by the finite resistance of the wire. Based on these principles mainly two types of hairpin resonators are found in the literature, namely: transmission and reflection types as discussed below. The design of the probe differs slightly when the coupling loop is electrically isolated from the hairpin.

2.4.1 Transmission and Reflection type

The transmission type probe is comprised of two loop antennas constructed at the end of two 50 Ω lines. One of the loops functions as the transmitter of the microwave signal to the hairpin while the other, called the pick-up loop, acts as the receiver when the probe is driven at resonance for a characteristic frequency as shown in figure 2.5.

Figure 2.5: Schematic diagram of a transmission type hairpin probe.

For improving the signal to noise ratio the coupling between the driving loop and the pick-up loop is minimized by bending the plane of the pick-up loop in the perpendicular direction of the plane of the driving loop and the hairpin [Piejak, 2004].

Because of bulky construction of the probe comprised of two individual coaxial lines, this original design, as proposed by Stenzel [Stenzel, 1976], is less popular. In 2004, Peijak et al [Piejak, 2004] proposed measuring the resonance signal from the reflected power from the same coaxial line used for driving the hairpin. This eliminated the requirement for the second 50 Ω line which greatly simplified the construction of the probe. This is shown in figure 2.6 below.

Figure 2.6: Schematic diagram of a reflection type hairpin probe.

2.4.2 Floating hairpin probe

One of the limitations of the design proposed by Peijak et al [Piejak, 2004] for the reflection type probe is that the hairpin is directly attached to the loop antenna which is close to ground potential. Therefore its application to discharges having significantly large potential fluctuations, such as in the case of single and dual frequency confined narrow gap capacitive discharges, can result in severe arcing of the probe. The sinusoidal variation of the plasma potential can also result in sheath rectification and

drastic reduction of electron density around the hairpin pins. Therefore it is essential to design the hairpin to be electrically isolated from the coupling loop. In order to achieve this objective, a number of designs of floating hairpin probes were published around the same time by different groups. Important ones are by Piejak and Braithwaite et al [Piejak, 2005], Curley and Booth [Curley, 2008] and Ganguly [Sands, 2007]. The floating hairpin probe designed at Dublin City University, Ireland by Karkari and Ellingboe [Karkari, 2005] has a mechanism by means of which the short circuited end of the hairpin is mechanically attached by sandwiching between two cylindrical tubes. In this way the pins can be replaceable. One of the important aspects of designing a floating hairpin is that extensive care needs to be taken for minimizing stray capacitance between the loop antenna and the hairpin. This is generally achieved by providing a sufficient air-gap between the two components.

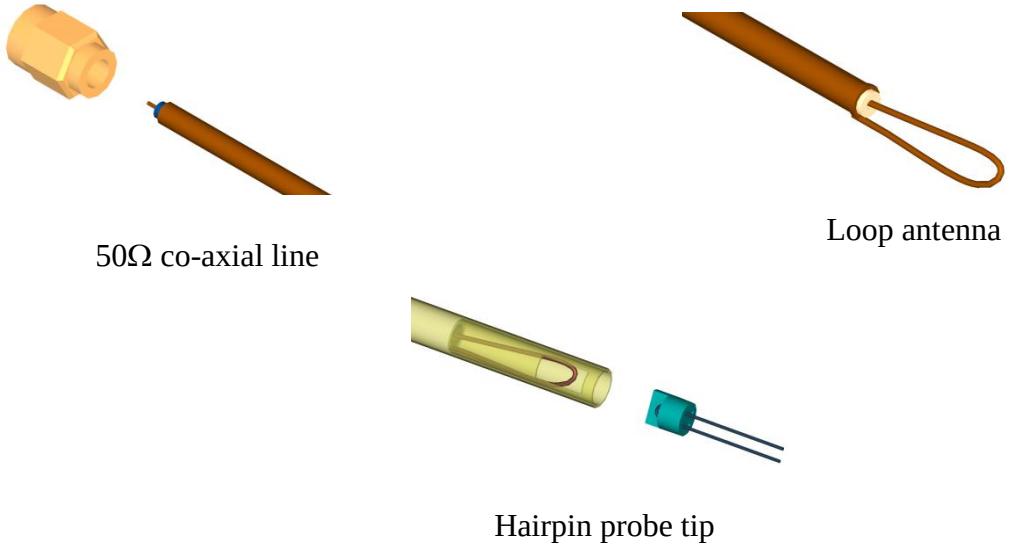

Figure 2.7: Schematic diagram of a floating hairpin probe.

A schematic of a floating hairpin probe is shown in figure 2.7. The probe design contains a 50 Ω coaxial line, a single turn driving loop of diameter nearly 3 mm and a hairpin resonator of length nearly 30 mm and width 2-4 mm which is completely isolated from the driving loop. Since the hairpin is inductively coupled to the driving loop, the position of the hairpin with respect to the driving loop will affect the quality of the signal. However one can identify a better quality resonance peak in the reflected signal by varying the position of the hairpin with respect to the driving loop. But there is a trade-off between the quality of the resonance peak and floating the hairpin (capacitance between the driving loop and the hairpin should be much smaller compared to the capacitance between the hairpin and the plasma).

The signal quality of the resonance signal also depends on the material of wire chosen for the hairpin [Sands, 2007]. To improve the quality of the resonance signal the losses in the hairpin should be a minimum which can be reduced by choosing a wire material of higher conductivity (effect of other factors like length to width ratio, wire diameter, surface nicks etc on the quality of resonance signal are not discussed here). Wire materials used for hairpins in this thesis are molybdenum and gold coated tungsten.

2.4.3 Electrically biased hairpin probe

For our study, we need to externally bias the hairpin with respect to the plasma potential for varying the dimension of the sheath around the hairpin. When negatively biased, expulsion of electrons from the vicinity of the probe results in a shift of the resonance peak in the plasma towards the vacuum frequency. On the other hand, a positive bias up to the plasma potential will negate the sheath; hence the resonance frequency shifts to the true resonance value that corresponds to the actual plasma permittivity.

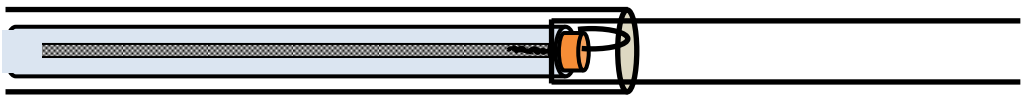

Figure 2.8: Schematic diagram of an electrically biased hairpin probe.

A schematic diagram of an electrically biased hairpin probe is shown in figure 2.8 and 2.9. The design and the method of obtaining the resonance frequency is the same as discussed in section 2.4.2. The hairpin remains electrically isolated from the driving loop while a hypodermic tube carries the electrical connection to the short circuited end of the hairpin. The use of a hypodermic tube also provides flexibility to change hairpin tip without interrupting the line of electrical connection. The hypodermic tube is electrically isolated from the plasma using an additional ceramic sleeve. A special vacuum compatible electric feed through is designed which have separate electrical connection for biasing the probe and SMA connection hermetically sealed for the microwave signal to the loop antenna.

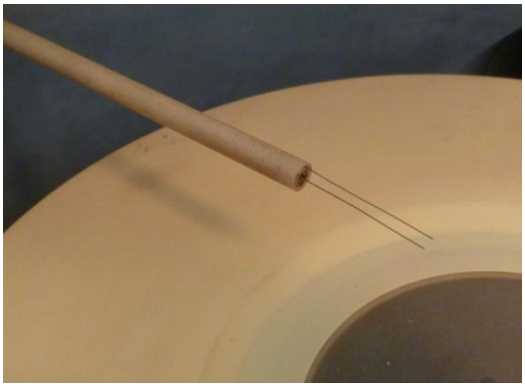

Figure 2.9: Electrically biased hairpin probe in Sentech SI 500 triple planar spiral antenna ICP etch system.

2.5 Detection of resonance frequency in steady state plasma

The technique used for the measurement of the resonance signal involves varying the input microwave signal and measuring the reflected microwave power at each frequency. The typical process takes 10 – 20 ms depending on the tuning frequency of the source. Additional delay can occur due to automation used for the detection of the resonance signal. In order to be able to determine the resonance frequency accurately, one should consider the plasma to remain in steady state during the diagnostics. The method for detecting the resonance peak in a steady state plasma is presented in the following section.

2.5.1 Schematic of the setup

The experimental set-up shown in figure 2.10 comprises a tunable microwave source (frequency range 1 – 8 GHz, power level 10 dbm). The microwave signal is fed into the loop antenna via a directional coupler placed between the microwave source and the 50 Ω coaxial line whose far end is attached to the loop-antenna as shown in the figure 2.10. The r.m.s amplitude of the reflected signal is obtained using a negative output schottky diode and displayed on an oscilloscope against the time axis, the time axis is linearly related to the frequency. As the applied frequency is tuned to the resonant frequency, significant microwave power is inductively coupled in to the resonator. Correspondingly, the reflected power output across the diode is reduced. In this way one can identify the resonance frequency corresponding to the drop in the reflected signal.

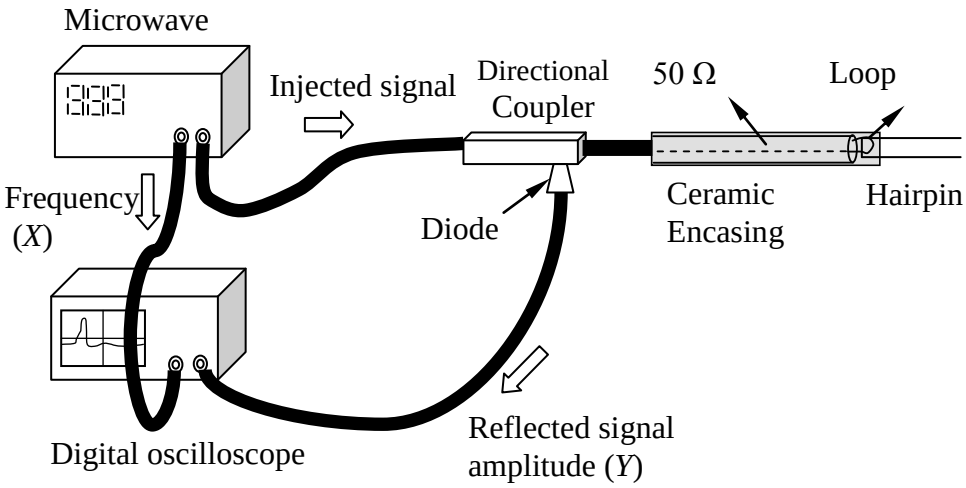

Figure 2.10: Schematic of floating hairpin resonance probe and the circuit for detecting the resonance peak.

2.5.2 Resonance frequency and its characteristics in vacuum

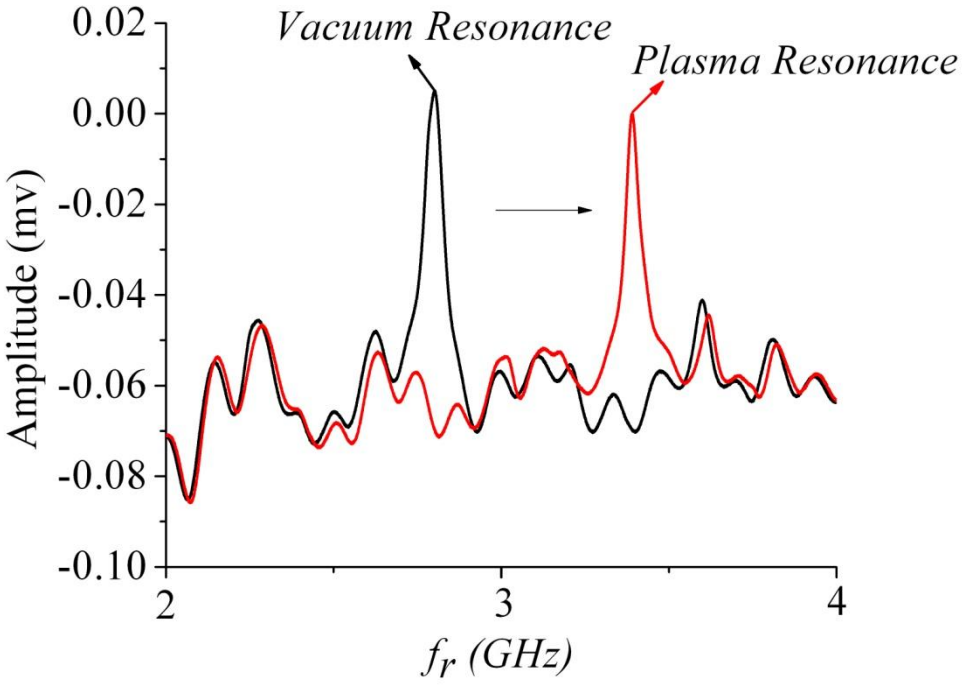

Figure 2.11: Amplitude of reflected signal in vacuum and in plasma for a sweep of frequency.

In figure 2.11, reflected signals are plotted, one under vacuum (black) and the other in plasma (red). The reflected signal is characterized by a negative amplitude signal which sharply drops to zero at the resonance frequency. The resonance frequency of the same probe shifts to higher value in plasma since the plasma permittivity $\varepsilon_p < 1$ while the resonance frequency of hairpin is inversely proportional to the square root of ε_p. The formula that relates the measured resonances in vacuum and in plasma to the electron density is given by equation (2.20). Hence we can estimate the steady state electron density in the plasma using equation (2.20).

2.6 Dynamical plasma systems and measurement of time-resolved electron density

2.6.1 Dynamical plasma systems

Plasma systems in which the variation in electron density is faster than the period of the sweeping frequency (10-20 ms) are considered as dynamical plasma systems. An example of a dynamical plasma system investigated in this thesis is a pulsed dc magnetron discharge operated at 10 KHz with a 50% duty cycle. The temporal evolution of the electron density in this case occurs at microsecond scales, which is faster than the sweeping period. Another example of a dynamical system discussed in this research is the temporal evolution of the electron density during pulse laser photodetachment of negative ions. During pulsed laser photodetachment, the electron density overshoots instantaneously (typically of the order of nanoseconds) and then drops back to equilibrium on a time given by the response time of the negative ions (typically few microseconds). The method of obtaining the time resolved electron density is discussed in the following section.

2.6.2 Detection of resonance peak in time-resolved mode

There are two methods of obtaining time-resolved electron density namely: step increment of frequency technique and the box-car technique. In the first technique the reflected signal from the hairpin is observed as a function of trigger pulse at a single frequency, however the box-car technique averages many signals at a discrete moment of the discharge. The details of the above techniques are as follows:

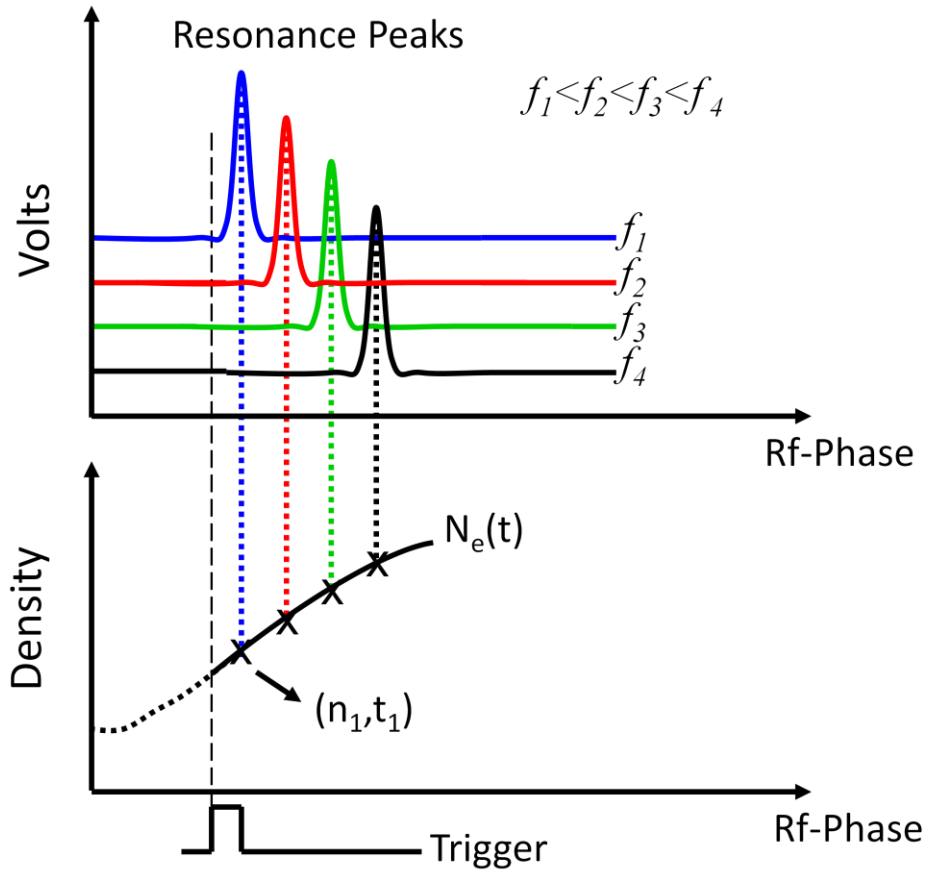

Fig 2.12: Amplitude of reflected signals at different frequencies and time varying electron density vs time.

The experimental setup to obtain the electron density in time-resolved mode by step increment of frequency is the same as in the case of a steady state plasma. The only difference is the oscilloscope is now synchronized with the trigger pulse. Figure 2.12 shows a schematic of the principle idea. The electron density is shown to be increasing as a function of time following the trigger pulse. If the microwave source is operated in the continuous wave (CW) mode it gives a single frequency output. If the probe is in resonance at any point of time during the trigger the reflected power shows a minimum at that point of time. If the electron density dynamic is repeating at each trigger pulse, it is possible to tune the CW to a next higher frequency, which will allow the probe to resonate at a later time for increasing density. The process can be repeated to obtain a spectrum of probe resonance frequencies as a function of time, and then it is straightforward to obtain the electron density using equation (2.20). In this way, by changing the frequency of the microwave we can get the time varying electron density.

The time resolution of the acquisition depends on both the acquisition limit of the oscilloscope and the quality factor of the resonance signal. The former condition can be improved by choosing a fast oscilloscope while the latter one is improved by improving the quality factor. A choice of a longer hairpin will improve the quality factor and hence the time resolution, but again there will be a compromise with the spatial resolution.

In the box-car technique, instead of sending a constant frequency to the resonator the signal is acquired at a discrete point of time. The delay is used to give the desired time width with a suitable delay from the reference time. The box-car integrator averages the data points over many cycles before moving to the next time step. In this way it produces the whole time resolved electron density profile. In this thesis we have used the step increment of frequency technique to measure the time resolved electron density.

2.6.3 Time-resolved electron density spectrum in a pulsed dc magnetron discharge

The step increment of frequency technique explained above is applied to measure the time evolution of the electron density in a pulsed dc magnetron discharge described in section 5.6.1. Figure 2.13 shows the spatio-temporal of electron density along the centre line (measured at a distance of 65, 75, 85, 95 mm respectively from the target). Corresponding time-resolved electron density for a one particular position (Z = 95 mm) is shown in the figure 2.14. The magnetron is operated with a 10 KHz pulsed dc at a moderate 100 W power with 30% O_2 and 70% argon and 10 mTorr discharge pressure. The applied pulse voltage waveform from a 100x voltage probe is displayed with a white line on the figure 2.13 with its magnitude on the right y axis. The distance of the probe from the target is shown on the left y axis in figure 2.13 whereas the electron density is represented by the colors.

The measurement of the time resolved electron density involves the increment of frequencies from the lowest to the highest electron density. At each frequencies the reflected signal from the probe are recorded. To improve the signal to noise ratio the background signal in vacuum is subtracted from each of the reflected signals at all frequencies.

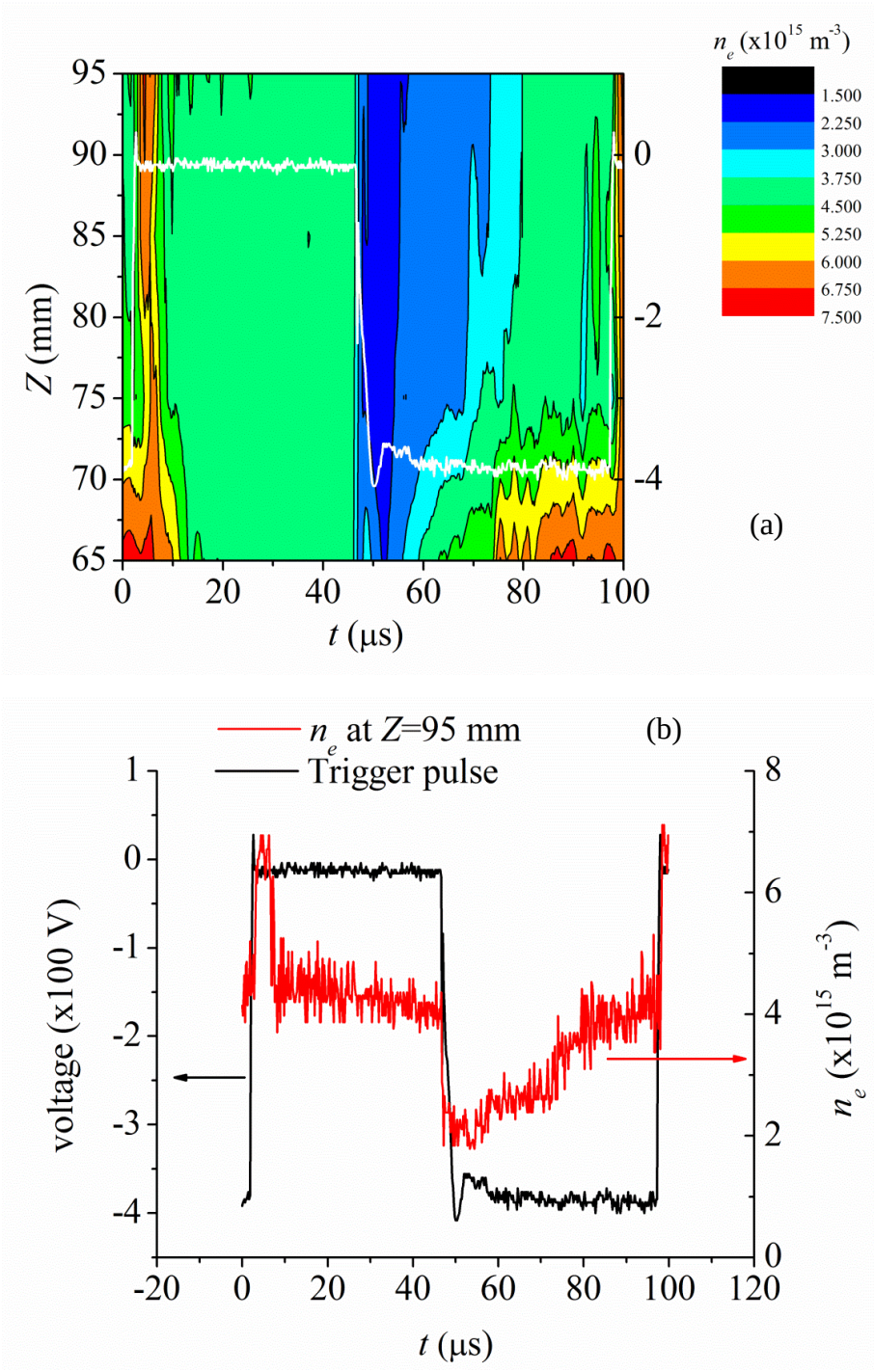

Figure 2.13: a) Spatio-temporal evolution b) temporal evolution of electron density in a pulsed dc magnetron discharge.

Chapter3

Sheath effects on electron density measurement by hairpin probe

3.1 Motivation

The hairpin probe theory assumes that the inter-spacing between the pins of the hairpin are uniformly filled with a homogeneous plasma. However such an assumption is rarely achieved due to the presence of sheaths around the resonator pins in plasma. The sheath is devoid of bulk electrons and is treated as a vacuum dielectric layer. This vacuum dielectric layer modifies the effective permittivity surrounding the hairpin. Hence an incorrect density is measured as obtained from the shift in the resonance frequency. In general, one avoids the problem by choosing the spacing between the pins to be much larger than typical sheath sizes. However, in low plasma densities that are below 10^{16} m^{-3} and in radio frequency discharges (due to fluctuation in rf potential) the sheath width is relatively large.

The effect of sheath width on the probe's resonance frequency is a fundamental problem. Although Stenzel [Stenzel 1976] considered this effect to be negligible provided the separation between the pins is far greater than the typical sheath dimensions. Until 2003 Hebner [Hebner 2001], Kim [Kim 1995] all used the hairpin probes without considering the influence of the finite sheath width. Peijak in 2004 [Piejak 2004] first recognized the problem. He systematically compared the measured electron densities with a Langmuir probe and an interferometry technique and found that the electron densities, particularly of the lower order of 10^{16} m^{-3} range, were found to be underestimated by over 40 % than those measured using interferometry. Finally he proposed a model for the correction of the density measured in the case of floating sheath.

The model for the floating sheath considers capacitance associated with infinitely long coaxial cylinders wires. From that Piejak et al [Piejak 2004] obtained the effective permittivity by providing the geometric sheath width based on a step front sheath model. Following this principle, several authors [Curley 2008, Piejak 2005] adopted this method for the correction of the electron density. Ganguly et al [Sands

2007] further modified the formula by taking into account the finite width of the resonator. A brief review of this model is presented in section 3.2.

However one major limitation associated with the above method were the dependencies on electron temperature and the initial guess of the electron density. This is required for estimation of the sheath thickness. Peijak [Piejak 2004] used a Langmuir probe for obtaining the electron temperature (T_e). Thus in terms of practical benefit, the use of hairpin posed no significant benefit as compared with a Langmuir probe.

Since then some useful suggestions were made such as the one unpublished paper by Peijak [Piejak 2004a] in which he suggested biasing the hairpin up to the plasma potential, thus helping to nullifying the sheath. Later Braithwaite et al [Haas 2005] applied this principle and proposed a model that includes the electrons in the sheath by biasing the hairpin probe. However again the major problem remains due to practical application of the hairpin when applied to magnetized plasmas and in plasmas where the plasma potential is fluctuating at large rf potentials, therefore biasing of the probe can introduce local perturbation, arcing etc. Furthermore it may be impractical to bias the hairpin in depositing plasmas as the surface conductivity is compromised due to any insulating depositions on the surface of the pins.

Therefore the question addressed in this chapter concerns whether one can obtain accurate electron densities independently without relying on another diagnostic for the additional information of electron temperature. Based on the above foreseen limitations we present an alternative approach that considers applying a negative dc bias to the probe for estimating the sheath width. This method is based on the well known Child-Langmuir sheath model. In this technique the sheath width is estimated by measuring the ion current corresponding to a finite negative potential applied to the hairpin.

3.2 Effective permittivity of the plasma and sheath

Figure 3.1 shows a side view and a front view of the sheaths surrounding the hairpin limbs. These sheaths are treated as a coaxial cylinder of radius *b* separated from each other by distance *2(h-b)* where *2h* is the width of the hairpin probe. Assume the capacitance of the sheath is C_s whereas the capacitance of the plasma between the midplane up to the surface of sheath is given by C_p. Following Piejak [Piejak 2004] we apply the method of images for obtaining the effective capacitance between the pins.

This reduces the problem to solving for the capacitance between the cylindrical wire and mid-plane (as shown in figure 3.1).

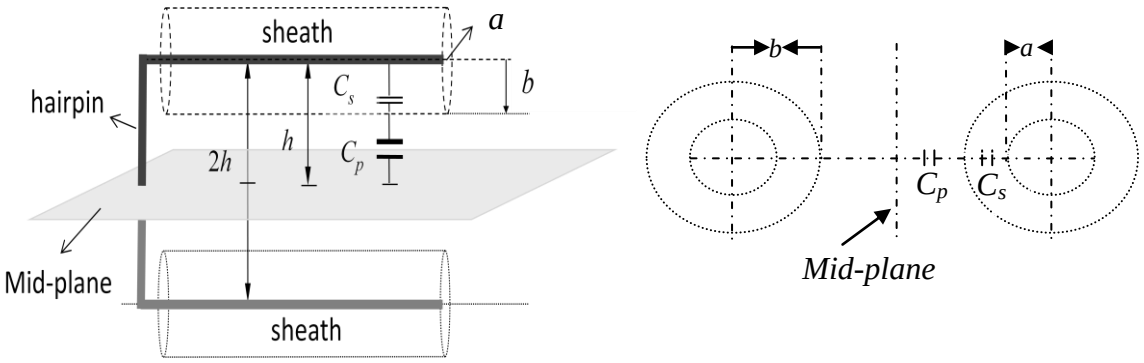

Figure 3.1: Schematic of the side view and the front view of the hairpin limbs with wire radius *a*, width *2h* and sheath radius *b*.

The capacitance per unit length between any cylindrical wires situated at a height *h* above a plane as given by Piejak [Piejak 2004] is

$$C = \frac{\pi \varepsilon_{eff}}{\ln\left(\frac{2h}{a}\right)} \tag{3.1}$$

Here ε_{eff} is the relative effective permittivity due to the plasma and the sheath. However one can also treat the effective capacitance by expressing effective capacitance in terms of series combination of capacitance of a cylinder of radius equivalent to the sheath around the hairpin having permittivity ε_o and a capacitance from the outer surface of the cylinder to the mid-plane filled with plasma having permittivity κ_p where $\varepsilon_p = \varepsilon_o \kappa_p$ This is expressed as follows:

$$C = \frac{\pi \kappa_p}{ln\left(\frac{2h}{b}\right) + \kappa_p ln\left(\frac{b}{a}\right)} \tag{3.2}$$

Equating these two expressions (3.1) and (3.2), we can obtain ε_{eff} in terms of the sheath dimension as follows:

$$\varepsilon_{eff} = \frac{\kappa_p \ln\left(\frac{2h}{a}\right)}{\ln\left(\frac{2h}{b}\right) + \kappa_p \ln\left(\frac{b}{a}\right)} \tag{3.3}$$

In the above formulation Piejak [Piejak 2004] neglected the wire and the sheath radius compared with the width of the hairpin probe. However at lower plasma densities, typically of the order of 10^{15} m^{-3}, and an electron temperature of 3eV, the Debye sheath is nearly 0.4 mm which is significant and thus cannot be neglected with respect to width

of the hairpin probe. The refined sheath capacitance formula by eliminating the assumption of small sheath width is shown below.

Again the capacitance between a mid plane and a wire of radius *a* considering the wire radius in the formula is given by

$$C_{eff} = \frac{\pi\varepsilon_{eff}}{\ln\left[\frac{h}{a}+\sqrt{\left(\frac{h}{a}\right)^2-1}\right]} \approx \frac{\pi\varepsilon_{eff}}{\ln\left[\frac{2h-a}{a}\right]} \tag{3.4}$$

Using the same equation the capacitance between the mid plane and the sheath of radius *b* is given by

$$C_p = \frac{\pi\kappa_p}{\ln\left[\frac{h}{b}+\sqrt{\left(\frac{h}{b}\right)^2-1}\right]} \approx \frac{\pi\kappa_p}{\ln\left[\frac{2h-b}{b}\right]} \tag{3.5}$$

Here *b* is the radius of the sheath boundary.

The effective capacitance is equated to the series equivalent of the plasma capacitance given by (3.5) and the sheath capacitance. In order to obtain C_s a hypothetical vacuum cylinder of radius *b* is assumed and vacuum in the remaining space *(h-b)*. Thus first by equating C_{eff} with series equivalent of C_{wp} and C_s we can find the sheath capacitance C_s. Here C_{wp} is the capacitance between the mid plane and the hypothetical cylinder of radius *b* without plasma in equation (3.5) by replacing κ_p with ε_0 and C_{eff} is given by (3.4). Thus we can write

$$C_{eff} = \frac{C_s C_{wp}}{C_s + C_{wp}} \tag{3.6}$$

On substituting the value of C_{eff} and C_{wp} we can get the value of the sheath capacitance which is given by

$$C_s = \frac{\pi\varepsilon_0}{\ln\left[\frac{2h-a}{a}\right]-\ln\left[\frac{2h-b}{b}\right]} \tag{3.7}$$

The series combination of (3.5) and (3.7) results in C_{eff}, which is equivalent to (3.4), by doing this we can obtain a relationship between the effective permittivity ε_{eff} as a function of κ_p, *a* and *b*,

$$\varepsilon_{eff} = \frac{\kappa_p \ln\left[\frac{2h-a}{a}\right]}{\kappa_p\left[\ln\left[\frac{2h-a}{a}\right]-\ln\left[\frac{2h-b}{b}\right]\right]+\ln\left[\frac{2h-b}{b}\right]} \tag{3.8}$$

From equation (3.8), when $b = a$ as in the case of negligible sheath width, we observe that the effective permittivity is equal to the plasma permittivity i.e. $\varepsilon_{eff} = \kappa_p$. Again when the sheath radius is comparable with the half width (mid-plane of the pins) we can substitute $b=h$ which gives the effective permittivity reducing to the vacuum permittivity i.e. $\varepsilon_{eff} = \varepsilon_o$. The equation is similar to one obtained by Ganguly et al [Sands 2007]. Therefore equation (3.8) is better suited for a negative biased hairpin as discussed further in section 3.4.

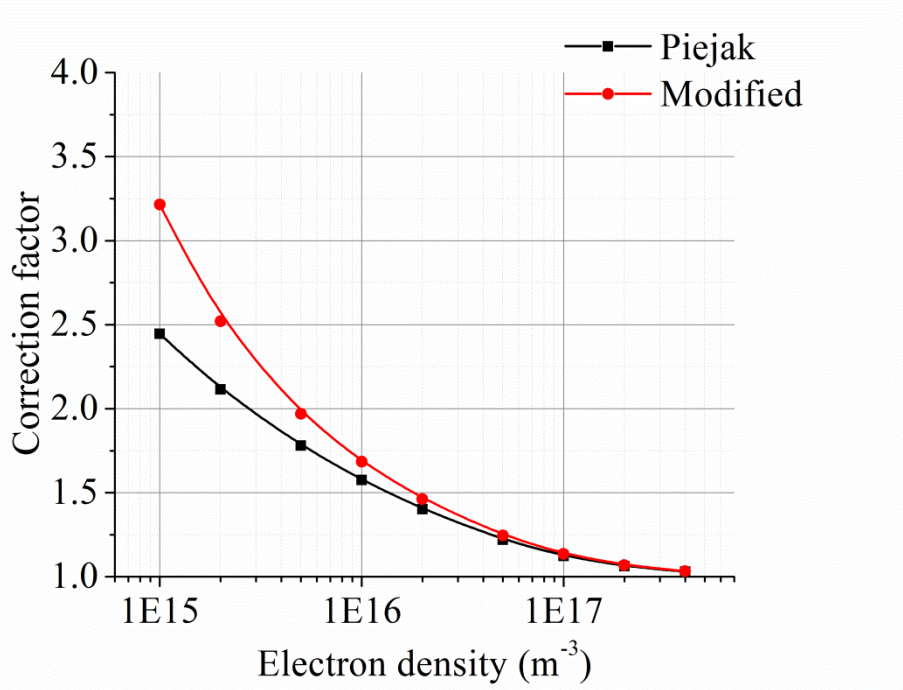

Figure 3.2: Correction factor due to the sheath as a function of the electron density estimated by the Piejak formulation [Piejak 2004] and the modified formulation. The electron temperature is 3eV, wire radius is 0.125mm and the hairpin probe length and width are 30mm and 3mm respectively.

When the sheath width and wire radius is neglected with respect to the width of hairpin probe, it gives a similar expression to that derived by Piejak [Piejak 2004]. Therefore by assuming b, $a << h$ equation (3.8) can be rewritten as follows,

$$\kappa_p = \frac{\left(f_o^2\right)\ln[2h/b]}{(f_r)^2 \ln[2h/a] - \left(f_o^2\right)\ln(b/a)} \tag{3.9}$$

Here we have substituted $\varepsilon_{eff} = f_0^2/f_r^2$ which can be experimentally measured. On substituting κ_p from (2.13) in (3.9) we get

$$f_{pe}^2 = \frac{f_r^2 - f_o^2}{1 - \frac{f_o^2}{f_r^2}\Lambda}, \text{ with } \qquad \Lambda = \frac{\ln(b/a)}{\ln(2h/a)} \tag{3.10}$$

Thus n_e(corrected) = n_e(uncorrected)*correction factor where the correction factor is given by $f_r^2/(f_r^2 - f_0^2\Lambda)$. For the Piejak formulation, Λ is defined in equation (3.10), whereas for the modified formulation (when the sheath width and wire radius are not neglected in comparison with the width of the hairpin probe) it is given by $\Lambda = (ln((2h-a)/a) - ln((2h-b)/b))/ln((2h-a)/a)$.

Figure 3.2 shows the comparison of correction factor obtained by the Piejak formulation and the modified formulation. For estimating the sheath width, the step front sheath model is used as described in Section 3.3. The Electron temperature is taken to be 3 eV. As observed in the figure, the correction factor obtained by both formulations agrees fairly well when the plasma density is higher than $2*10^{16}$ m^{-3}. However the correction factor by Piejak's model is found to be insufficient for lower densities because the sheath sizes are larger compared with the pin separation.

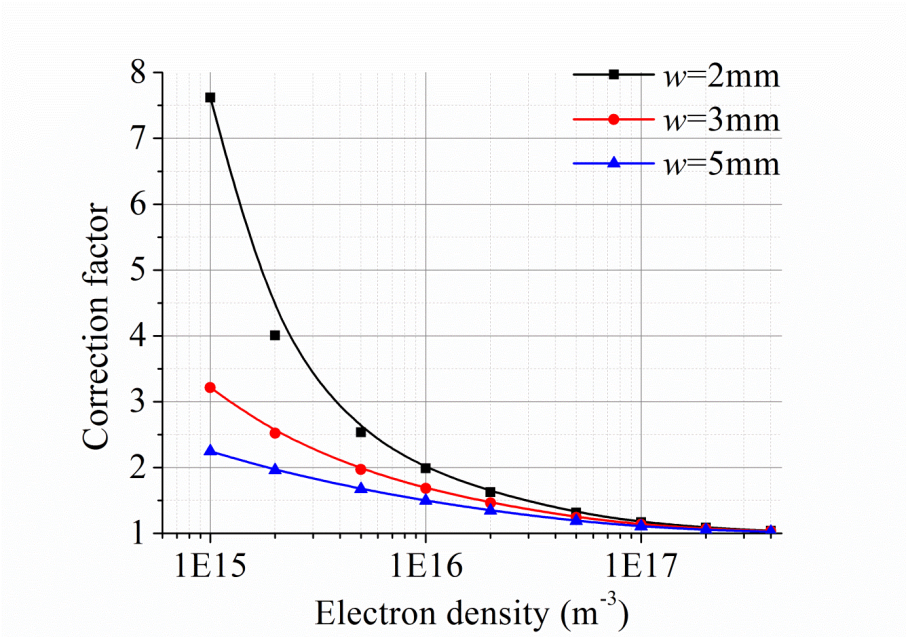

Figure 3.3: Correction factor due to sheath as a function of electron density estimated by modified formulation for different widths of the hairpin probe. The electron temperature is 3eV, wire radius is 0.125mm and the hairpin probe length is 30mm.

Shown in figure 3.3 the correction factor is significantly reduced by increasing the width of the hairpin probe from 2mm to 5mm for a constant plasma density and electron temperature. However the compromise for going to larger width hairpins would

be on spatial resolution. As expected the correction factor also decreases with a decrease in electron temperature, as observed in figure 3.4. In all cases (figure 3.3-3.4) it is observed that the sheath correction is less significant when the plasma density is of the order of 10^{16} m^{-3} or higher. However the sheath correction is recommended for plasma densities of the order of 10^{15} m^{-3} and electron temperatures in the range of 1-5 eV or higher.

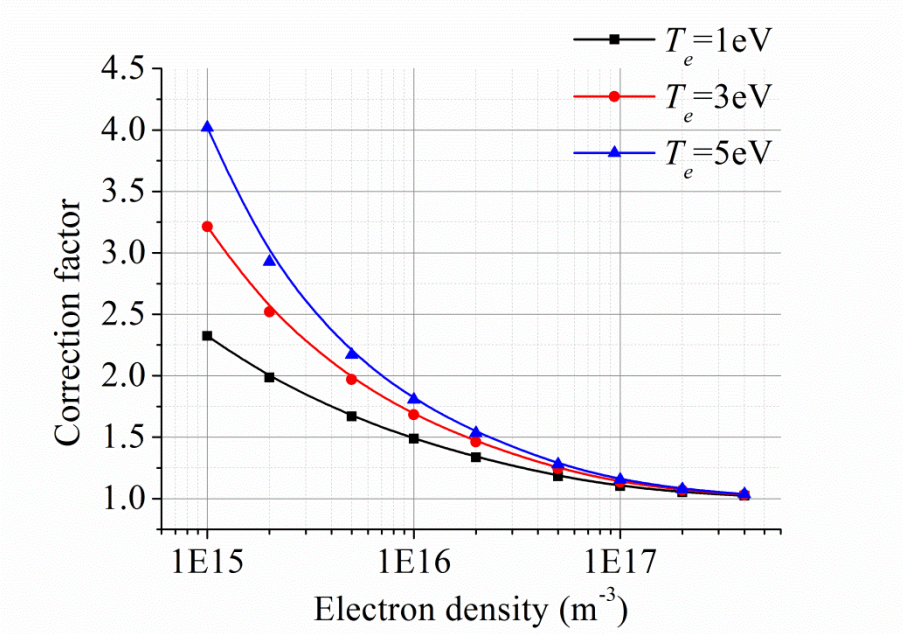

Figure 3.4: Correction factor due to the sheath as a function of electron density estimated by the modified formulation for different values of electron temperature. Wire radius is 0.125mm and hairpin probe length and width are 30mm and 3mm respectively.

3.3 Sheath corrections and limitations of present model

The simplistic approach to correct for the presence of sheath is to provide the sheath width in equation (3.10) [Piejak 2004]. The sheath width can be calculated by using the well known Child-Langmuir sheath model or by using the step front sheath model. The Child-Langmuir sheath model is based on the assumption that the sheath potential should be much larger compared to the electron temperature (when measured in electron Volts) [Chabert and Braithwaite 2011]. However this may not be truly applicable for the hairpin probe because it is a floating probe, and is found to overestimate the sheath width if applied [Piejak 2004]. Thus the step front sheath model is the possible solution for evaluating the sheath width as suggested by Piejak et al [Piejak 2004]. In the step front sheath model an electron free collision-less sheath is

assumed with cold positive ions. The equations governing the sheath are the ion flux continuity equation; ion momentum equation and the Poisson's equation

$$\frac{d}{dr}(rnv) = 0 \tag{3.11}$$

$$\frac{d}{dr}(rnv^2) + rn\frac{d\varphi}{dr} = 0 \tag{3.12}$$

$$\frac{1}{4\pi}\frac{d}{dr}\left(r\frac{d\varphi}{dr}\right) + rn = 0 \tag{3.13}$$

Here *r*, *v*, *n*, and φ are the radius, ion velocity, ion density and electrical potential, respectively.

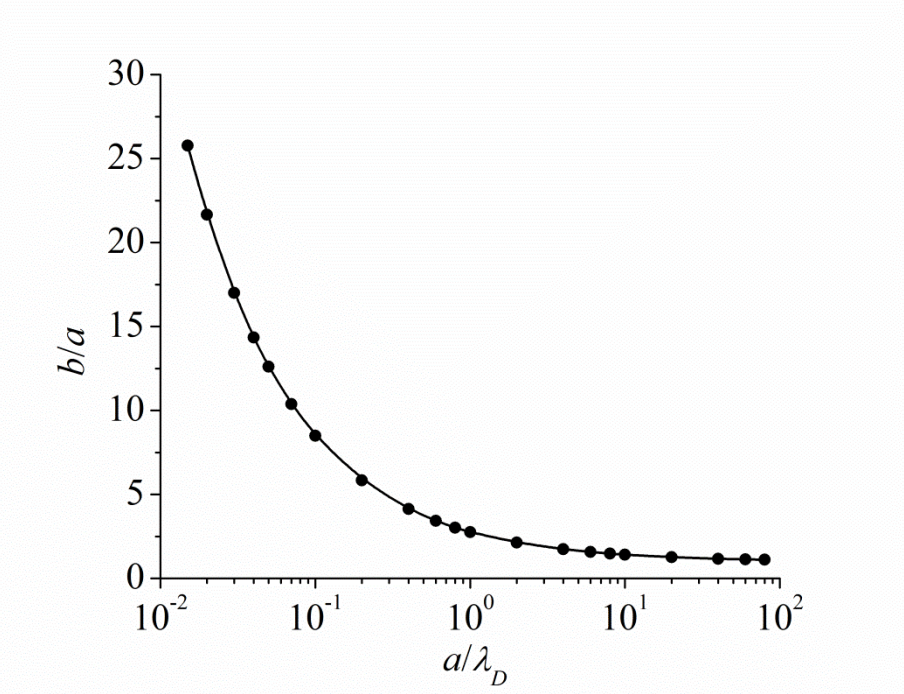

Figure 3.5: Plot of ratio of sheath radii to probe radii as a function of probe radii to Debye length from the step front sheath model.

The solution of the above equations with the boundary conditions $\eta_b = 0$, $\eta_b' = -1$ and $\eta_a = -ln(b/a\varrho) = -ln(\xi_b/\varrho.\xi_a)$ provides the ratio of sheath radius to wire radius (b/a) as a function of (a/λ_D). Here η_b and η_a are the electric potential normalized by the electron temperature. ϱ is the mass ratio defined by $\varrho = (M/2\pi m)^{1/2}$. ξ_a and ξ_b are the radius normalized by the Debye length. Subscripts *a* and *b* represent the probe surface and the position of the sheath edge respectively.

Figure 3.5 shows the plot of b/a as a function of a/λ_D obtained by numerically solving equations (3.11) to (3.13) for argon. From figure 3.5 it is possible to deduce the sheath width for a specific value of a/λ_D to estimate the corrected electron density using

equation (3.10). Piejak et al [Piejak 2004] compared the value of *b/a* by the step front sheath model with that obtained by the Child-Langmuir sheath model and found that the ratio *b/a* is overestimated at lower values of a/λ_D when using the Child-Langmuir sheath model. However for $a/\lambda_D>0.3$ both models gives nearly the same values of *b/a* (see figure 4 in reference Piejak 2004). In practical situations, for example plasma having a density $1x10^{15}$ m^{-3} to $1x10^{16}$ m^{-3}, 3 eV electron temperature and a wire radius 0.125mm for the hairpin probe, typical values of a/λ_D are between 0.3 to 1. Thus it appears that any one of the models can be used to estimate the sheath width for the electron density correction.

The major drawback of this approach is that it invokes the use of a theoretical sheath model which requires additional plasma parameters. For example in the step front sheath model (SFSM) information of both the electron temperature and electron density are required initially for obtaining λ_D. Thus a separate diagnostic such as a Langmuir probe is needed for measuring the electron temperature, otherwise one needs to provide a guess value as applied by [Piejak 2004]. However n_e still remains an unknown parameter. Therefore an approximate λ_D is first obtained using the uncorrected n_e which gives an initial value of *b/a*. This allows one to obtain Λ by substituting *b/a* in equation (3.10). On obtaining the first round correction, the new n_e is again used for refining λ_D and the process is iterated until the n_e value saturates to the actual density.

As evident, the above procedure has two major limitations. (1) The requirement of an independent diagnostic for determining T_e and initial guess for n_e that is necessary for calculating the sheath width. (2) The SFSM is only true for the floating sheath and may not be valid for rf sheaths. This problem is common in industrial plasma tools that apply capacitive radio frequency discharge. The amplitude of rf oscillation in plasma potential can vary from a few 10's to 100's of Volts such as in the case of narrow gap capacitive coupled plasmas used for nano-device fabrication plants. In such a scenario the floating potential is driven more negative as compared to a floating sheath where the rf oscillation is almost zero.

3.4 Sheath correction by a negative dc biased hairpin probe

The above limitations motivate for formulating an alternative method for the sheath correction. In this section a negative dc biased hairpin is proposed. The principle of sheath correction using this technique is discussed. The experimental set-up is presented in section 3.4.3 followed by the experimental results and discussion in

sections 3.4 and 3.5 respectively. Finally, a high density plasma diagnostic is proposed using this technique.

3.4.1 Basic principle

If the hairpin is biased to a negative dc potential without affecting the plasma parameters, it will lead to the drawing of a net positive ion current. The negative potential also leads to an increase in the sheath width and hence a decrease in the resonance frequency. On estimating the sheath width from the measured voltage and current along with the corresponding measured resonance frequency, it is possible to deduce the corrected electron density using equation (3.10). Alternatively the resonance frequency can be plotted using equation (3.10) as a function of sheath width (*b*) for a fixed plasma density and compared with the measured value of the resonance frequency as a function of sheath width for different bias voltages.

However the estimation of the sheath width from the measured current and voltage for a cylindrical sheath relies on solving Poisson's equation (as in the case of step front sheath model) with defined boundary conditions and depends on the electron temperature and electron density. Thus in the simplest case the sheath width can be estimated by a Child-Langmuir sheath model given by

$$b^2 = \frac{4}{9}\varepsilon_0 \left(\frac{2e}{M}\right)^{1/2} \frac{V^{3/2}}{j_i} \tag{3.14}$$

Here j_i is the positive ion current density, b is sheath width, M is the mass of the positive ion and V is the voltage on the probe with respect to the plasma potential. Using the above equation one can obtain the sheath width by providing the ion current density at the respective applied voltage to the probe. However, the Child-Langmuir sheath model neglects electron space charge in the sheath and thus it can be applicable only for a large negative bias that exceeds the electron temperature i.e. $eV << -kT_e$.

One advantage of applying this planar Child-Langmuir sheath model is to eliminate the complexity arising in the case of the cylindrical sheath solution which requires prior knowledge of the electron temperature and electron density. However, use of the planar Child-Langmuir sheath assumption for cylindrical sheaths can only be applicable for a thin sheath i.e. for low bias voltage (lower sheath width), it leads to an overestimate of the value of sheath width for low density plasmas where the sheath sizes are bigger. In the following section we found that the assumption of a planar Child-Langmuir sheath model is valid and in agreement with the SFSM correction for

higher plasma densities, and overestimates the correction at low plasma density. However the overestimation at low plasma density is still in the acceptable range for all practical purposes.

3.4.2 Resonance frequency dependence on the sheath width

The theoretical curve of probe resonance frequency (f_r) as a function of sheath width (b) is plotted in figure 3.6. The relationship between the resonance frequency and the sheath width is obtained from equations (3.8) and (1.7). In these equations we substituted the values ε_{eff} and κ_p which resulted in a bi-quadratic equation in f_r given by:

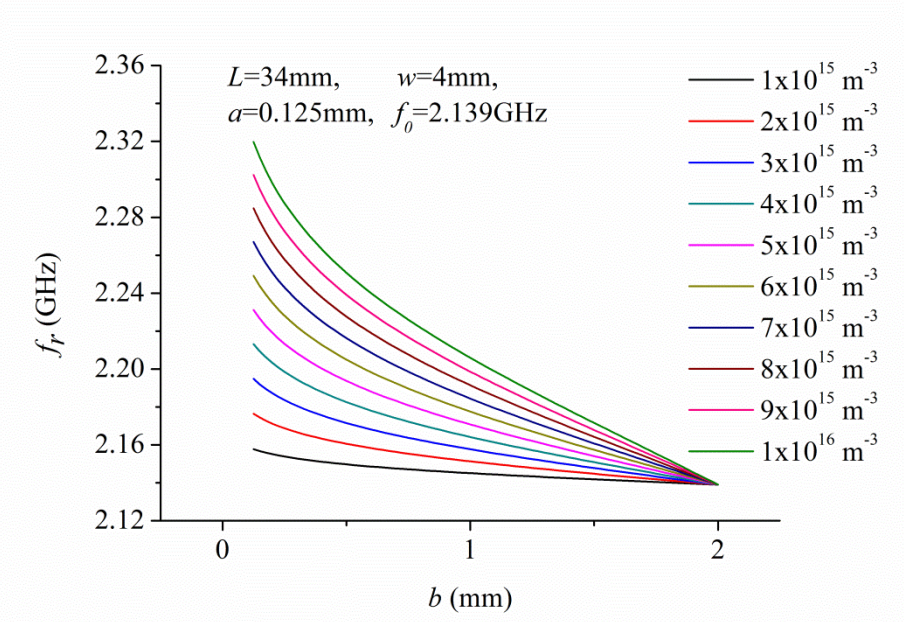

Figure 3.6: Plot of the resonance frequency of a hairpin as a function of the sheath width for various electron densities.

$$f_r^4 A - f_r^2 A\left(f_{pe}^2 + f_0^2\right) + f_{pe}^2 f_0^2 (A - B) = 0$$

Where $A = \ln\left(\frac{2h-a}{a}\right)$ and $B = \ln\left(\frac{2h-b}{b}\right)$.

One of the possible solutions of the above equation is plotted in figure 3.6 for a range of plasma densities, particularly in the range where the sheath correction is expected to be significant. In the above solutions the value of the sheath width b is arbitrarily varied from the probe surface up to the mid-plane of the hairpin. As shown in figure 3.6 the corresponding resonance frequency at which the sheath vanishes (i.e. $b=0.125\ mm$) is

the ideal resonance frequency for that electron density. The larger the sheath width the lower is the resonance frequency, approaching to the vacuum frequency as the sheath width engulfs the space between the pins completely.

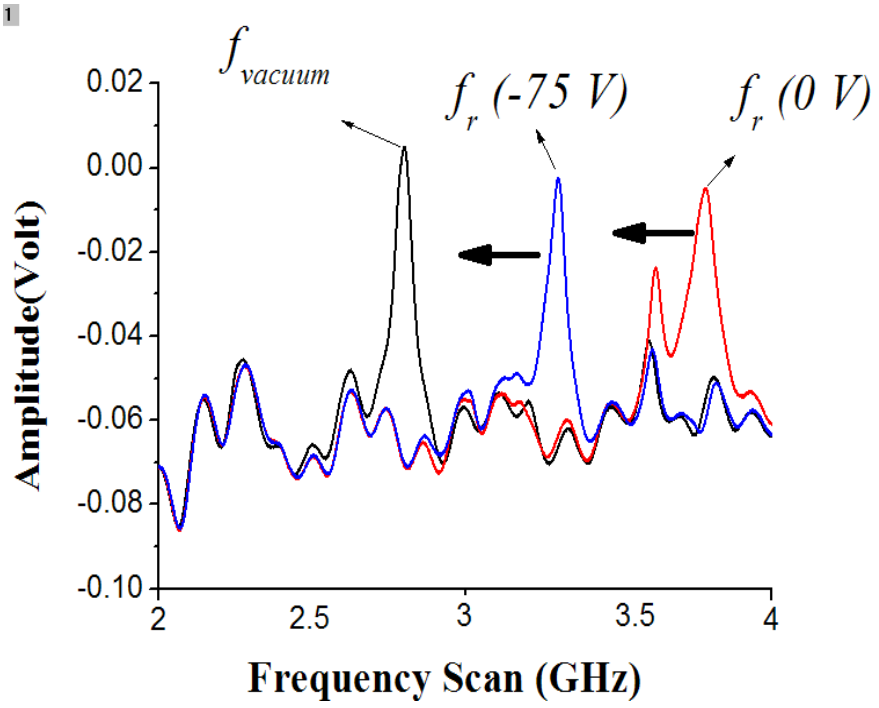

Figure 3.7: Amplitude of reflected signal vs frequency with and without bias.

The experimental realization of the probe resonance frequency shifting towards the vacuum frequency with the application of a negative bias is shown in figure 3.7 in an argon plasma. The resonance spectrum is measured in an ICP discharge (a detailed description of the setup can be found in section 3.4.3) with an L-shaped hairpin probe (L~25 mm, W~3mm and f_0 =2.809 GHz) purposely built that allowed aligning the pins in the uniform plasma region. As shown in figure 3.7 applying a negative bias increases the space charge sheath around the resonator prongs and hence decreases the resonance frequency. For a sufficiently large negative bias, the probe measures the resonance frequency that approaches that obtained in vacuum.

3.4.3 Experimental setup

The experiment is performed in an Inductive Coupled Plasma (ICP) system. The schematic of the setup is shown in figure 3.8 with a detailed description in section 5.4.1. An argon discharge is generated between the helicon antenna of diameter 30 mm and the cylindrical chamber of internal diameter of 200 mm. The helicon antenna is

mounted at the centre of the cylindrical chamber and powered by a 13.56 MHz ENI ACG10B signal generator.

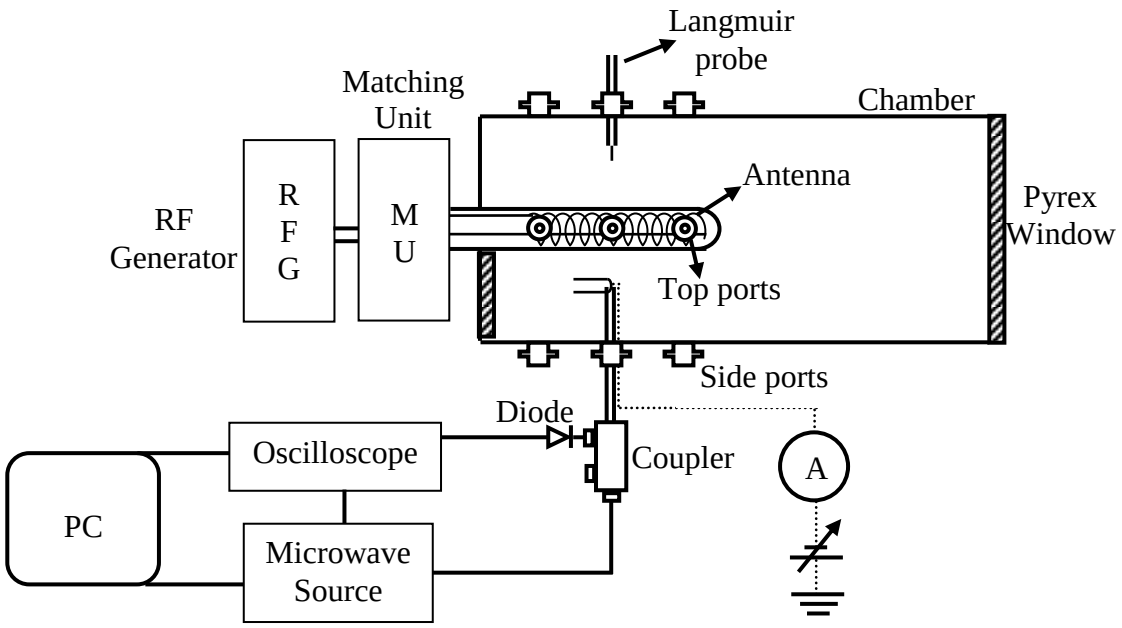

Figure 3.8: Top view of the ICP reactor with the hairpin probe and its measurement circuit and Langmuir probe connected.

The hairpin tip (dimensions of the hairpin probe tip are mentioned in figure 3.6) is set at right angles to the axis of the probe feed-through and hence resembles the L-shape of the english alphabet. This design of the hairpin allows the probe to be in a uniform plasma having a negligible density gradient along the length of the hairpin. The hairpin probe is installed through one of the side ports such that it is approximately 40 mm distant from the helicon antenna. The hairpin probe tip is connected to a dc power supply for biasing it with a negative potential. The current during the applied bias is measured across a 50 Ω resistor with respect to ground. The microwave generator, dc power supply and oscilloscope are controlled by LabVIEW. Briefly, a voltage ramp is generated and the corresponding resonance frequency and current at each bias voltage is collected. A Langmuir probe is also installed from the opposite port to measure the electron temperature that is required to compare the results obtained for sheath correction using the step front sheath model.

3.5 Results

The experimental data showing current drawn by the hairpin as a function of the applied negative bias is plotted in figure 3.9. The floating potential is at ~ 12 Volts. The different sets of data points correspond to different background densities achieved by varying the external ICP power from 30 W to 50 W. In the above experiment the background neutral pressure in the chamber was kept at 10mTorr with argon as the working gas.

As the probe bias is increased the resonance frequency shifts towards lower frequencies. This is plotted in figure 3.10. The resonance frequency shift with the applied negative bias and correspondingly the sheath widths are plotted in figure 3.11.

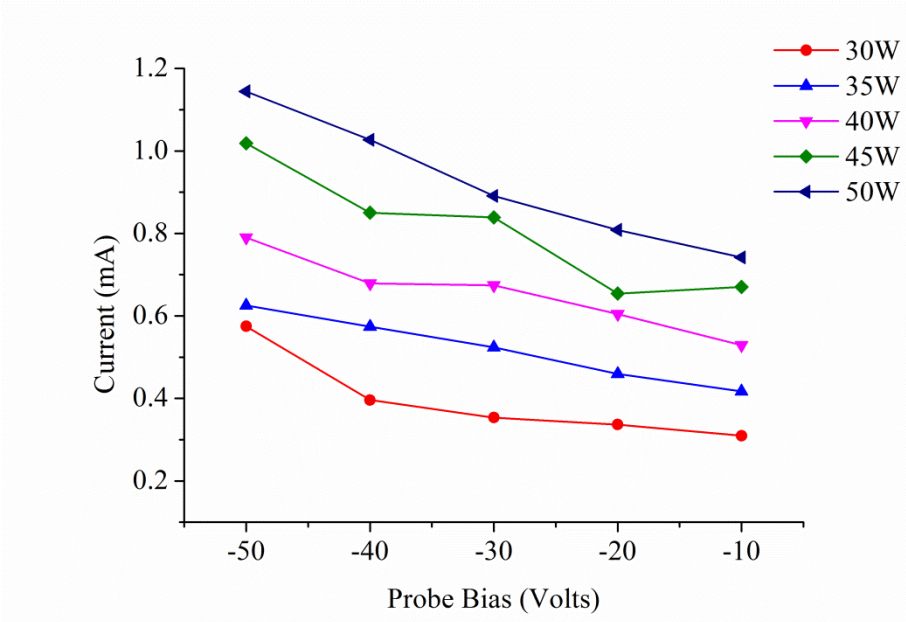

Figure 3.9: Measured Current as a function of the probe bias for various rf powers. The pressure is kept constant at10 mTorr.

The theoretical values of resonance frequency as function of a range of sheath widths are plotted in figure 3.12 for various electron densities. On the same plot, measured values of the resonance frequency corresponding to 40 W and 50W ICP power from figures 3.10 and 3.11 are also shown. The agreement between measured and theoretical value of resonance frequency with sheath width (b) suggests that a negative dc bias hairpin probe is a possible option for estimating the sheath corrected electron density.

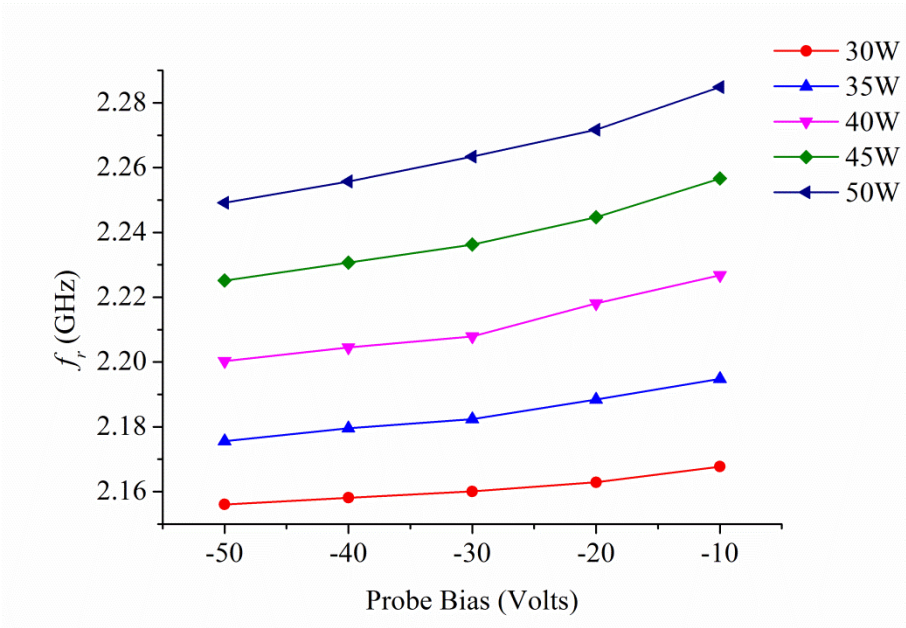

Figure 3.10: Measured resonance frequency as a function of probe bias for various rf powers at 10 mTorr operating pressure.

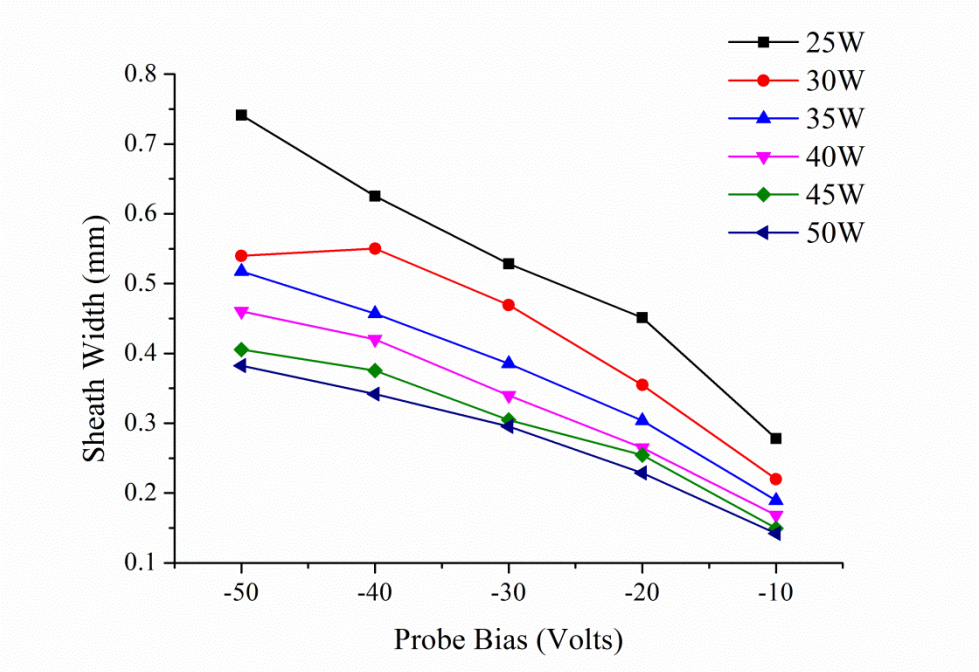

Figure 3.11: Sheath width estimated by the Child-Langmuir sheath model as a function of probe bias for various rf powers at 10 mTorr operating pressure.

Corresponding sheath corrected and sheath uncorrected electron densities at 40W ICP power and 10mT gas pressure are plotted in figure 3.13 as a function of probe bias. The sheath corrected electron density is obtained by using equation (3.10) with the modified expression for Λ and providing the sheath width from figure 3.11. It is clear from figure 3.13 that the probe bias up to -50V has no change in the corrected electron density

which is consistent with the fact that biasing the probe should not modify the plasma parameters surrounding it.

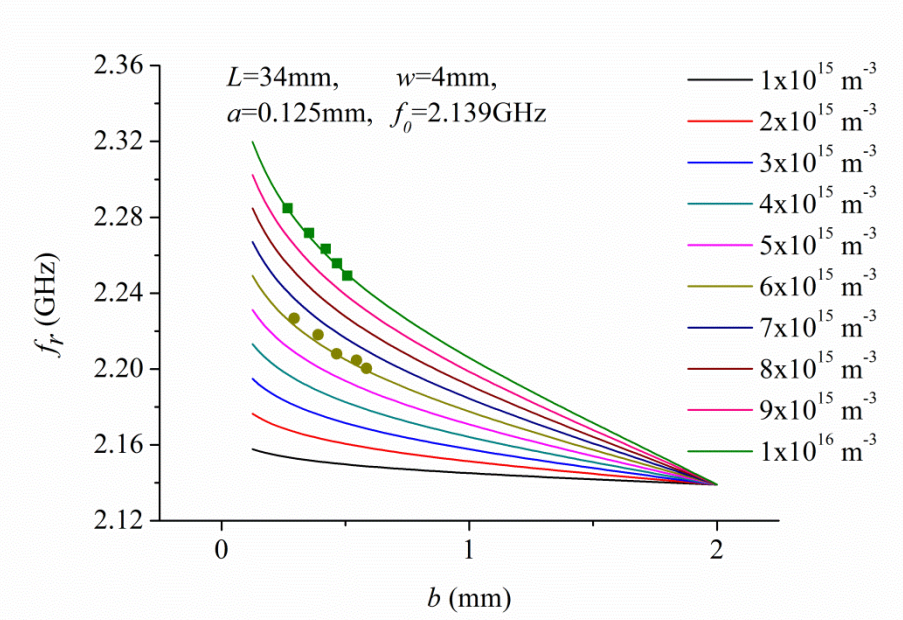

Figure 3.12: Plot of resonance frequency as a function of sheath width from theory (line) and experiments (Dots: square-50W, circle-40W).

In figure 3.14 we considered the plasma density in the range less than $5x10^{16}$ m^{-3} as the sheath corrections are significant. By applying the same principle we compared the corrected electron density obtained by a negative dc biased hairpin probe at different ICP powers with the SFSM as shown in figure 3.14. As shown in figure 3.14, the difference between the corrected and the raw density (uncorrected) is found to be 41% when the ICP power was operated at 25W as compared to 10% when the ICP power was raised to 100W. Also observed is a small discrepancy between the planar Child-Langmuir sheath model and the step front sheath model by approximately 12 %. However as the density increases by increasing the rf power, the difference is reduced to within 5 %. For obtaining the corrected electron density using the SFSM, the electron temperature was measured using a Langmuir probe and it was found to be ~3eV independent of the rf power. Finally the sheath width is calculated using the SFSM and equation (3.10) for estimating the corrected electron density. The overestimation in the sheath width at lower densities is attributed to simplifying the problem to a planar Child-Langmuir sheath model.

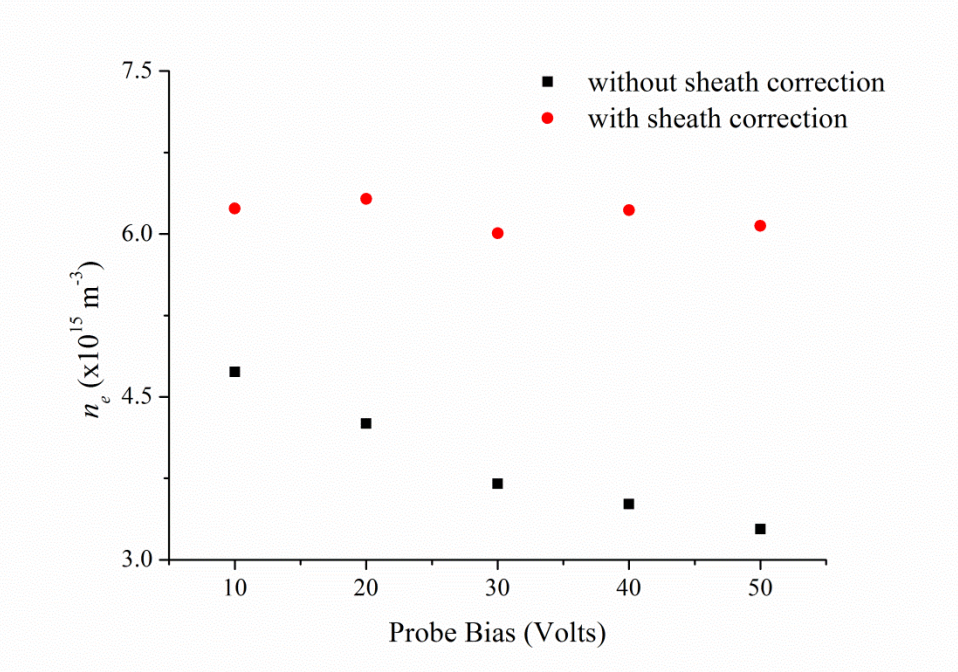

Figure 3.13: Plot of sheath corrected and sheath uncorrected electron density as a function of probe bias corresponding to 40W ICP power and 10 mTorr gas pressure.

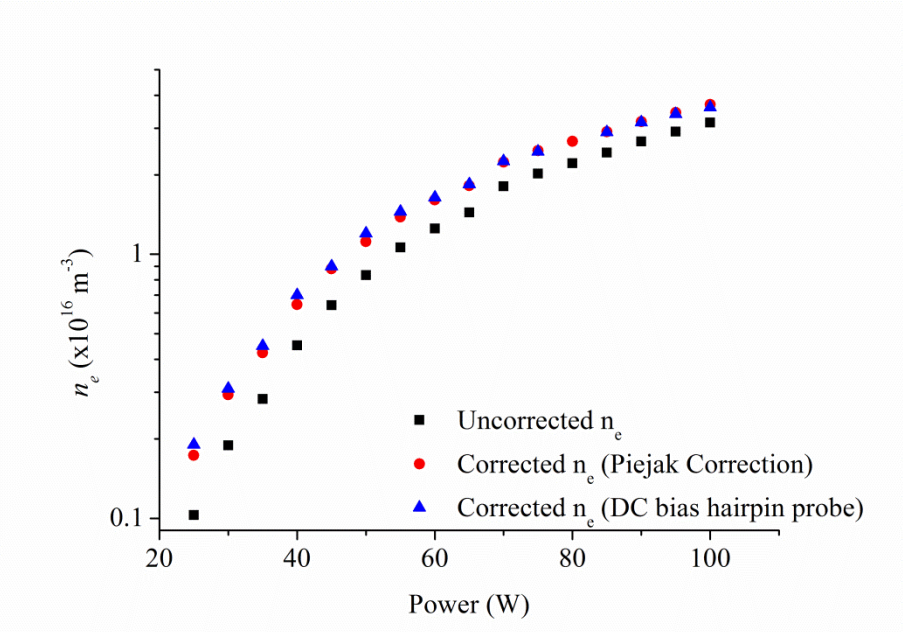

Figure 3.14: Uncorrected and corrected electron density by the step front sheath correction and dc bias hairpin probe (*w*~4mm) in an argon plasma as a function of rf power at 10 mTorr operating pressure.

3.6 Discussion

The modified formula obtained for the sheath correction shows significantly higher correction compared to Piejaks correction. At low plasma density (1x10^{15} m^{-3})

the correction is about 25% higher than the Piejak correction for an electron temperature of about 3 eV. Thus at low plasma densities, neglecting sheath width with respect to the width of the hairpin to obtain the sheath correction is not a good approximation. Using the modified sheath correction formula the effect of the hairpin probe width on sheath correction is investigated. At $1x10^{15}$ m^{-3} electron density and 3eV electron temperature the sheath correction is reduced from 85% to 50 % by changing the hairpin width from 2mm to 5mm which is still significant. Also, the hairpin of width above 5mm is impractical to use because it affects the quality of the signal. Thus changing the hairpin width is not a feasible solution to reduce the sheath effects at the expense of spatial resolution.

The results presented in section 3.4 highlight the effective use of a negatively biased hairpin for compensating underestimated densities due to the finite sheath around the hairpin. An advantage clearly seen is that the sheath width can be found independently without relying on the electron temperature as required in the case of the SFSM. The negatively biased hairpin is based on the space charge limited current collection by the probe. In the simplest case the sheath width can be estimated by the planar Child-Langmuir sheath model i.e. using equation 3.14. Using this planar Child-Langmuir sheath model eliminates the complexity of the sheath estimation as in the case of the cylindrical probe which requires prior knowledge of the electron temperature, electron density and numerical solution of Poisson's equation for cylindrical geometry. However the assumption of a planar sheath can overestimate the sheath width compared to the cylindrical sheath because for a fixed probe area and given bias the current collected by planar probes is small compared to cylindrical probes. The overestimation can be higher in low density plasmas where the sheath sizes are bigger, however in high density plasmas the assumption of a planar sheath can be applicable for cylindrical sheaths [Chabert 2011]. This fact is apparent from figure 3.13. The discrepancy is found to be higher at low density but as the density increases the planar Child-Langmuir sheath model and the step front sheath model both give a reasonably good match to the corrected density. Another uncertainty posed with the dc biased hairpin is that the applied negative bias should be measured with respect to the plasma potential. In order to overcome this limitation, we assumed the floating potential that can be conveniently measured. The plasma potential can be approximated with the basic assumption of a finite electron temperature and the gas used. Since the applied negative bias is significantly larger compared to the plasma potential, therefore the error associated with

this assumption (neglecting plasma potential with respect to the applied bias potential) is minimal.

One should also be careful about the magnitude of the bias voltage because the planar Child-Langmuir sheath model used in the calculation cannot be applicable when the sheath sizes are much greater than the probe dimension. In this study we found that the theoretical and measured value of resonance frequency as a function of sheath width matches very well for a probe bias of less than -50 volt but the results can deviate for higher bias voltages. The corresponding electron density also remains constant with probe bias after sheath correction as shown in figure 3.13 (red dots). Finally the electron density is corrected using the negative dc hairpin probe and compared with the step front sheath correction (the only available and widely accepted technique to correct for the sheath). Good agreement between these two techniques validate the assumption of the planar Child-Langmuir sheath model for estimating the sheath width from the measured current and voltage and hence the corrected electron density.

The above method can also be useful for measuring higher plasma densities which is currently limited (below 10^{18} m^{-3}) due to the practical range of the microwave source, choice of vacuum resonance of the resonator and the dispersion of the resonance signal due to electron thermal motion. To address this issue a finite sheath around the hairpin is created by applying a negative dc bias thus bringing the resonance signal in the measurable range and finally the underestimation in the electron density due to the sheath is corrected by the technique described above. Unfortunately no results are presented in this thesis for high density plasma diagnostics using this technique. Hopefully the work will continue in the future.

3.7 Summary and conclusions

In this chapter we studied the effect of the sheath on the electron density measurement by the hairpin probe. A modified formula for sheath correction is derived which excludes the assumptions of previous formulations and is thus applicable for a wider range of electron densities. Based on the modified formula the effect of the probe width and electron temperature on the sheath correction is presented. It is concluded that even by increasing the hairpin probe width the correction cannot be reduced significantly. The negative dc biased hairpin probe is also studied to estimate the corrected electron density due to the sheath. The agreement between the corrected electron density obtained by the negative dc biased hairpin probe and modified sheath

correction formula (providing sheath width by SFSM) confirm the validity of negative dc biased hairpin probe to use for the sheath correction. Finally a high density plasma diagnostic is proposed using a negatively dc biased hairpin probe.

In particular this method is better with respect to a positive biased hairpin because a negative potential can be applied even to an insulating surface while the perturbation to the plasma is significantly reduced. In addition one major advantage is that additional information regarding the electron temperature is not required for the estimation of the sheath width. Another advantage addressed is the usefulness of the biasing technique for shifting the resonance frequency to a lower frequency range. This is necessary if the measurable densities are greater than 10^{18} m^{-3} which demands an impractical size of the hairpin. For example a 1 – 8 GHz source can measure electron densities up to 8×10^{17} m^{-3}, provided the vacuum resonance is 1 GHz. This would imply that the required length of the hairpin is 75 mm. Also at very high plasma densities, electron thermal motion results in the dispersion of the resonance signal.

Chapter 4

Theoretical investigation of the sheath around a cylindrical probe in electronegative plasmas

4.1 Motivation and background

The hairpin probe measurement is greatly affected by the presence of a sheath as discussed in the previous chapter. These effects are dominant in low density plasmas where the sheath sizes are bigger. Since electrons are lighter in mass, the sheath properties are mostly described by electronic parameters such as the electron density and electron temperature. However along with the electrons, the sheaths are also influenced by the presence of other charged species in the plasma. Electronegative plasmas are one of the examples in which the majority of the electron population is replaced by negative ions, and hence the sheath and discharge properties are mainly governed by these particles. Negative ions are heavier in mass compared to electrons, and thus having lower temperature they affect the positive ion fluxes collected by the surface and can change the sheath dimensions. Thus before applying hairpin probes to electronegative plasmas it is important to understand the sheath properties in the presence of negative ions. Since hairpin probes consist of two cylindrical pins, in the simplest case it is adequate to investigate a single cylindrical pin interaction with an electronegative plasma, thereafter assuming the effect will be the same on the other pin. Thus the problem is reduced to investigating a cylindrical probe (similar to a cylindrical Langmuir probe) interaction with an electronegative plasma.

The presence of negative ions and their influence on Langmuir probe was first addressed in 1935 [Spencer-Smith, 1935]. Since then significant research on the theory of plasma probe interaction in electro-negative plasma have been published [Braithwaite 1988, Amemiya 1999, Franklin 2000, Kono 2001, Sheridan 1999]. Most theories addressed the modification in the positive ion flux collected by the probe caused by the presence of negative ions.

An important observation found from numerical studies of the sheath at a spherical probe by Braithwaite and Allen [Braithwaite, 1988] found a parameter range where the positive ion flux becomes multi-valued. They proposed that the sheath forms at the first location where charge neutrality is violated. However this leads to a discontinuity in the ion flux at some values of the negative ion concentration [Sheridan

1999]. Leading to the discontinuity in the ion flux this theory predicts very well the beginning of sheath i.e. the point at which charge neutrality is violated first. However as proposed by J E Allen [Allen 2004] this theory can't be used to estimate the positive ion flux leaving the discharge.

Relaxing the plasma approximations, Sheridan et al in 1999 [Sheridan 1999] put forward a fluid model to compute the flux of positive ions from a low-pressure planar electronegative discharge. The flux continuity equation, momentum conservation equation and Poisson's equation governing the transition from quasineutral plasmas to the sheath were solved as an initial value problem using the boundary conditions u_0, η_0, $\varepsilon_0=0$, $\tilde{n}_0 = (1+\alpha)$ for $q=0$ and $\tilde{n}_0{}^2(\tilde{n}_0 - 1 - \alpha) = 2q^2$ for $q>0$ at the centre of the discharge. Here u_0, η_0, ε_0, $\tilde{n}_0$ and q are normalized parameters described in reference [Sheridan 1999]. For addressing the multi-valued ion flux, Sheridan et al proposed the correct solution is the one which gives the larger value of flux. The physical interpretation of this multi-valuation in the positive ion flux was briefly discussed by Kono et al [Kono 2003]. According to Kono, when the positive ion attains the modified Bohm speed in the presence of negative ions, quasineutrality breaks down and the space charge begins to develop until all the negative ions are repelled by the potential. Once all the negative ions are repelled, the space charge starts decreasing because the modified Bohm speed is smaller than the Bohm speed without negative ions i.e. $(kT_e/M)^{1/2}$. Positive ions start decelerating which again creates a positive space charge and the process continues to form oscillatory solutions until the actual Bohm speed is gained by the positive ions. Finally, using a fluid model Franklin [Franklin 2000] analyzed the influence of the positive ion thermal motion on the oscillatory solutions. He found that the oscillatory solution is mainly due to the unphysical assumption of a significant difference between the temperatures of the ions. By considering the finite temperature of positive ions Franklin found that the oscillations in the electric field are suppressed.

In this study we followed a similar approach to that proposed by Sheridan et al [Sheridan 1999]. Thus, without assuming quasineutrality the equations governing the sheath around cylindrical probes are solved from the bulk plasma to the edge of the probe. The profile of the electric potential is obtained with respect to different plasma parameters. Finally, the sheath width is obtained by using curvature criterion [Crespo 2006] for different sets of parameters range. Before dealing with the electronegative plasma sheath, we first discuss the Bohm criterion in electropositive plasmas.

4.2 Bohm speed in electropositive plasma

The transition from a quasineutral plasma to the plasma sheath is not abrupt. There is a transitional layer that exists between the plasma and the sheath (as shown in figure 4.1) to maintain the continuity of ion flux. This layer is known as the presheath region which has a length several times that of the Debye length. In this region ions get accelerated and acquire a finite velocity known as the Bohm velocity. Thus there must be a finite electric field in this region.

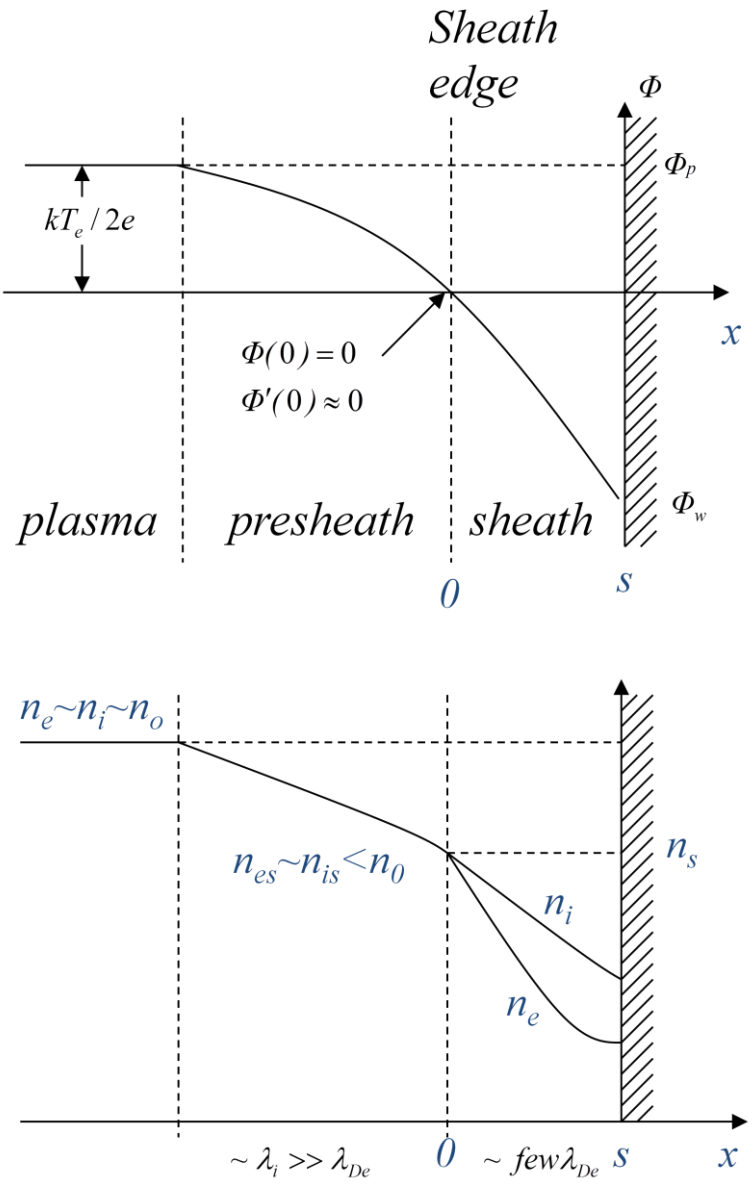

Figure 4.1: Spatial profile of the electric potential and charged particles densities in the plasma, presheath and sheath region.

We assume a simple system in which we consider:

i) Maxwellian distribution of electrons with temperature T_e

ii) Cold positive ions i.e. $T_i=0$

iii) $n_{es}=n_{is}$ at the edge of the sheath and presheath

The positive ion flux and acceleration of positive ion is given by the continuity equation and the momentum equation, which are given by equation 4.1 (neglecting ionization and momentum transfer collisions).

$$n_i(x)u_i(x) = n_s u_s$$

$$\frac{1}{2}Mu_i^2 + e\emptyset = \frac{1}{2}Mu_s^2 \tag{4.1}$$

Where n_s and u_s are the positive ion density and positive ion fluid speed at the sheath edge, $n_i(x)$ and $u_i(x)$ are the ion density and velocity respectively at any position from the surface inside the sheath, $\emptyset$ is electric potential and M is the mass of positive ions. On substituting the ion fluid speed from the momentum equation into the continuity equation, we obtain the ion density in the sheath as a function of the electric potential as

$$n_i = n_s\left(1 - \frac{2e\emptyset}{Mu_s^2}\right)^{-1/2} \tag{4.2}$$

The electron density distribution is given by the Boltzmann relation as

$$n_e = n_s exp\left(\frac{e\emptyset}{kT_e}\right) \tag{4.3}$$

The electric potential ($\emptyset$) in the sheath can be obtained by using the Poisson equation,

$$-\frac{d^2\emptyset}{dx^2} = \frac{e}{\varepsilon_0}(n_i - n_e) \tag{4.4}$$

Here ε_0 is the permittivity of free space. By substituting n_e and n_i from (4.2) and (4.3) in to (4.4), we obtain a non-linear equation governing the sheath potential, electron density and ion density as

$$\frac{d^2\emptyset}{dx^2} = \frac{en_s}{\varepsilon_0}\left(exp\left(\frac{e\emptyset}{kT_e}\right) - \left(1 - \frac{2e\emptyset}{Mu_s^2}\right)^{-1/2}\right) \tag{4.5}$$

The above equation is a second order non-linear differential equation whose first integral can be obtained analytically by multiplying $d\emptyset/dx$ and integrating with respect to x, along with the boundary conditions ($\emptyset = 0$, $d\emptyset/dx = 0$ at x=0).

$$\frac{1}{2}\left(\frac{d\emptyset}{dx}\right)^2 = \frac{en_s}{\varepsilon_0}\left(\frac{kT_e}{e}exp\left(\frac{e\emptyset}{kT_e}\right) - \frac{kT_e}{e} + Mu_s^2\left(1 - \frac{2e\emptyset}{Mu_s^2}\right)^{-1/2}\right) \quad (4.6)$$

Above equation can be integrated numerically to obtain the value of $\emptyset$. However it is straightforward to see that the term on the right hand side of equation (4.6) should be positive for a solution to exist. Using the Taylor's expansion for small $\emptyset$ and imposing this positive condition, the right hand side gives

$$u_s \geq u_B = \sqrt{\frac{kT_e}{M}} \quad (4.7)$$

Where u_B is called the Bohm velocity. The equation (4.7) is known as the Bohm sheath criterion, which implies that the ion flow speed at the sheath boundary must be at least as great as the ion acoustic speed. To acquire this velocity there must be a finite electric field in the bulk plasma over some distance. This region is known as the presheath region, and is typically much wider than the sheath. The potential drop in the presheath region to accelerate ions to the Bohm speed can be estimated by

$$Mu_B^2/2 = e\emptyset_s \quad (4.8)$$

Where $\emptyset_s$ is the potential at the sheath edge with respect to the plasma potential. On substituting the value of the Bohm speed u_B in equation (4.8) we get $\emptyset_s = kT_e/2e$. Thus to accelerate ions to Bohm velocity, the potential drop in the presheath region is of the order of the electron temperature.

4.3 Equilibrium properties of sheaths in the presence of negative ions

4.3.1 Bohm criterion in the presence of negative ions

As discussed in the case of electropositive plasmas, the Bohm criterion signifies the breakdown of quasineutrality resulting in the beginning of a space charge region. It is an inequality that states that the ion flow speed at the plasma sheath boundary must be at least as great as the ion acoustic speed. The Bohm criterion gets modified due to the presence of negative ions in the plasma, because of their higher mass compared to electrons. Using sonic flow at the sheath edge, Wickens and Allen in 1978 [Wickens 1978] obtained the modified Bohm speed in plasmas having two electron temperatures. The expression is then generalized to negative ion containing plasmas given as (a detailed derivation can be found in the next section)

$$u_s = u_B \left(\frac{1+\alpha_s}{1+\alpha_s\gamma}\right)^{1/2} \tag{4.9}$$

Where $u_B = \sqrt{kT_e/M}$ is the Bohm speed in electropositive plasmas, γ is the ratio of the electron temperature to the negative ion temperature, and α_s is the ratio of the negative ion density to the electron density at the sheath edge. Because of the low temperature of the negative ions compared to electrons, they can be repelled by the sheath edge potential, thus α_s must be different from α_0 (ratio of the negative ion to the electron density in the bulk plasma). If $\emptyset_s$ is the potential at the sheath-presheath edge with respect to the plasma, then by assuming a Maxwellian distribution for electrons and negative ions, α_s can be related to α_0 as

$$\alpha_s = \alpha_0 exp\left(\frac{e\emptyset_s(1-\gamma)}{kT_e}\right) \tag{4.10}$$

From the equation (4.9) we found that the speed of positive ions, at the sheath edge is dependent on α_s and γ. For large values of γ and modest values of α_s the positive ion speed at the sheath edge is reduced significantly. Ignoring collisions $\emptyset_s$ can be expressed as

$$\frac{e\emptyset_s}{kT_e} = \frac{1}{2}\left(\frac{1+\alpha_s}{1+\alpha_s\gamma}\right) \tag{4.11}$$

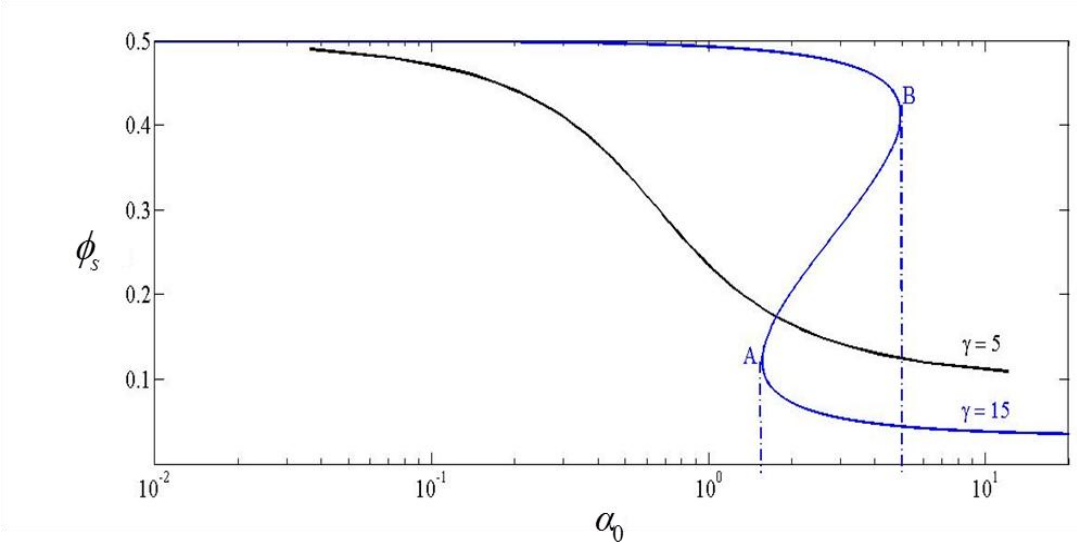

Figure 4.2: Plot of the sheath edge potential as a function of the electronegativity (α_0) [Braithwaite 1988].

Equations (4.10) and (4.11) can be solved to obtain $\emptyset_s$ as a function of α_0 (ratio of negative ion density to electron density in the bulk plasma). The curve of $\emptyset_s$ as a function of α_0 for different values of γ is shown in figure 4.2. It is clear from the figure

that as the electronegativity increases the potential at the sheath-presheath edge decreases For a specific range of α_0 the Bohm criterion in electronegative plasmas can also be satisfied at more than two positions (blue curve in figure 4.2 from A to B) i.e. three values of $\emptyset_s$ for given value of α_0 and γ. This multi-valuation of the Bohm criterion in electronegative plasmas was first discussed by Braithwaite and Allen [Braithwaite 1988]. According to Braithwaite and Allen the multiple solution exists for $\gamma \geq 5 + \sqrt{24} \approx 9.9$.

4.3.2 Basic formulation of the model

In this section we present the basic formulation of the sheath surrounding cylindrical probes. The steady state fluid equations of continuity and momentum for the positive ions are written in a cylindrical coordinate system [Chung 2006]. For simplicity we restrict our analysis to weakly collisional plasmas with negative ions, positive ions and electrons. This is an appropriate assumption since the study in this thesis is limited only to collision-less plasmas. Thus the parameter range is chosen such that the mean free path λ_{mfp} for electron-neutral and ion-neutral collisions can be neglected inside the sheath. However we consider weak collisionality within the pre-sheath region defined by a collision frequency υ_{iz}. The collisions in the pre-sheath govern the positive ion flux to the probe. The probe is a cylindrical wire with its lengths $l_{probe} >> r_p$; where r_p is the wire radius and $r_p \leq \lambda_D$ the Debye length of the plasma.

When the wall losses of negative ions dominate over volume recombination (for low pressure plasmas) then the negative ions will exist in thermal equilibrium with each other, obeying the Boltzmann distribution function. In other words the negative ion density should be determined mainly by transport. To satisfy this, the following relation must hold in a region with length L_{Boltz} [Kono 2001]: $\frac{L_{Boltz}^2}{D} \ll \frac{n_-}{k_a n_g n_e}$ Here D, n_e, n_g, k_a and n_- are the diffusion coefficient, electron density, neutral gas density, electron attachment rate co-efficient and negative ion density respectively. Thus the characteristic time of loss of negative ions via diffusion should be much smaller than the recovery time of negative ions via electron attachment. Thus we can write

$$n_- = n_{-0} exp\left(\frac{e\varphi}{kT_-}\right) \tag{4.12}$$

Also for the electrons we can write,

$$n_e = n_{e0} exp\left(\frac{e\varphi}{kT_e}\right) \tag{4.13}$$

Assuming, $\varphi < 0$ is the probe potential with respect to the plasma, n_{e0} and n_{-0} represent respective densities in the bulk plasma, e = electronic charge, k = Boltzmann constant.

Because $\varphi < 0$, a non-neutral layer of positive ions is formed around the probe and extends up to a certain radius from the probes surface. Beyond this region is a diffused quasineutral boundary layer called the "pre-sheath" region having a very weak electric field, while the plasma quasineutrality condition $n_{+s} \approx n_{es} + n_{-s}$ is considered to be valid in the pre-sheath region. Assuming the positive ions fall radially towards the probe surface, thus neglecting the orbital motion of ions, the positive ion flux $J_+ = n_+ v_+$ is given by the continuity equation as,

$$\frac{d}{dr}[n_+ v_+] + \frac{n_+ v_+}{r} = \vartheta_{iz} n_e \tag{4.14}$$

Here n_+ and v_+ are the ion density and velocity respectively at any radial position from the probe and ϑ_{iz} is ionization frequency. Acceleration of ions towards the probe is governed by the momentum conservation equation:

$$\frac{d}{dr}[n_+ v_+^2] + \frac{n_+ v_+^2}{r} + \frac{kT_+}{M}\frac{dn_+}{dr} = \frac{en_+}{M}\left(-\frac{d\varphi}{dr}\right) \tag{4.15}$$

Here M is the mass of positive ions.

For obtaining φ we use the Poisson equation;

$$-\frac{d^2\varphi}{dr^2} - \frac{1}{r}\frac{d\varphi}{dr} = \frac{e}{\varepsilon_0}(n_+ - n_- - n_e) \tag{4.16}$$

Here ε_0 is the free space permittivity. By substituting n_e and n_- from (4.12) and (4.13) in (4.16) and using the following normalizing parameters;

$$\xi = \frac{r}{\lambda_D}, \quad \tilde{n} = \frac{n_+}{n_{+0}}, \quad u = \frac{v_+}{C_s}, \quad \psi = -\frac{e\varphi}{kT_e},$$

$$\beta = \frac{T_+}{T_e}, C_s = \sqrt{\frac{kT_e}{M}}, \quad q = \frac{\lambda_D}{\Lambda}, \quad \Lambda = \frac{C_s}{v_{iz}}, \qquad \gamma = \frac{T_e}{T_-} \tag{4.17}$$

We obtain the following dimensionless equation;

$$\frac{d}{d\xi}(\tilde{n}u) + \frac{\tilde{n}u}{\xi} = \frac{q}{1+\alpha} e^{-\psi} \tag{4.18}$$

$$\frac{d}{d\xi}(\tilde{n}u^2) + \frac{\tilde{n}u^2}{\xi} + \beta\frac{d\tilde{n}}{d\xi} = \tilde{n}\frac{d\psi}{d\xi} \tag{4.19}$$

$$\frac{d^2\psi}{d\xi^2} + \frac{1}{\xi}\frac{d\psi}{d\xi} = \tilde{n}(1+\alpha) - e^{-\psi} - \alpha e^{-\gamma\psi} \tag{4.20}$$

Following the analysis of the quasi-neutral condition in the pre-sheath, we can consider that for weak electric fields, $d^2\psi/d\xi^2 \approx 0$ and $d\psi/d\xi \approx 0$. Therefore equation (4.20) is reduced to;

$$\tilde{n} = \frac{e^{-\psi} + \alpha e^{-\gamma\psi}}{(1+\alpha)} \tag{4.21}$$

By solving the set of equations (4.18), (4.19) and (4.20) we obtain,

$$\frac{d\psi}{d\xi} = \frac{\frac{-\Gamma_+^2}{(e^{-\psi} + \alpha e^{-\gamma\psi})\xi} + \frac{2\Gamma_+ q e^{-\psi}}{(1+\alpha)(e^{-\psi} + \alpha e^{-\gamma\psi})}}{\left[\frac{(e^{-\psi} + \alpha e^{-\gamma\psi})}{(1+\alpha)^2} + \frac{\beta(e^{-\psi} + \alpha\gamma e^{-\gamma\psi})}{(1+\alpha)^2} - \frac{\Gamma_+^2(e^{-\psi} + \alpha\gamma e^{-\gamma\psi})}{(e^{-\psi} + \alpha e^{-\gamma\psi})^2}\right]} \tag{4.22}$$

A condition for the normalized ion flux, $\Gamma_+ = \tilde{n}u$ at the sheath boundary ξ_s is obtained by imposing the condition at the sheath boundary where the space charge begins to develop resulting in sharp rise in electric field i.e. $\frac{d\psi}{d\xi} = \infty$. This condition is satisfied by equating the denominator of (4.22) to zero. This gives the normalized positive ion flux at the sheath boundary.

$$\Gamma_+ = \frac{(e^{-\psi_s} + \alpha e^{-\gamma\psi_s})}{(1+\alpha)} \sqrt{\beta + \frac{(e^{-\psi_s} + \alpha e^{-\gamma\psi_s})}{(e^{-\psi_s} + \alpha\gamma e^{-\gamma\psi_s})}} \tag{4.23}$$

By general inspection of (4.21) and (4.23), the square-root term in (4.23) corresponds to the normalized Bohm speed u_s for the positive ions, modified in the presence of negative ions:

$$u_s = \sqrt{\beta + \frac{(e^{-\psi_s} + \alpha_s e^{-\gamma\psi_s})}{(e^{-\psi_s} + \alpha_s\gamma e^{-\gamma\psi_s})}} \tag{4.24}$$

It can be verified that for electropositive plasmas ($\alpha_0 = 0$ i.e. $\alpha_s = 0$ from equation (4.10)), equation (4.24) reduces to the absolute Bohm speed $u_B = \sqrt{k(T_e + T_+)/M}$ which is similar to the one for electro-positive plasma for cold positive ion (i.e. $T_+ \approx 0$). Equation (4.24) is similar to the one obtained by Sheridan et al [Sheridan 1999] for planar discharge with $\beta = 0$. Equation (4.24) gives multiple solutions for specific values of α_s and γ as discussed in section 4.2.1.

To obtain the complete potential profile and the position of the sheath edge the quasineutral assumption is relaxed as proposed by Sheridan et al and the set of equations (4.18) to (4.20) is solved numerically from the plasma to the probe using an adaptive step size Runge-Kutta scheme. The four unknowns in these equations are $\tilde{n}$, u, ψ and $d\psi/d\xi$, hence four initial values are necessary to be defined for these parameters in order to solve the coupled equations, which is described in the following section.

4.3.3 Boundary Conditions

The equations are solved from $\xi \rightarrow \infty$ to any arbitrarily small value of ξ. Far away from the probe i.e. in the plasma ($\xi >> r$), we assume the quasineutral condition such that the normalized density $\tilde{n} = 1$, where ψ and $d\psi/d\xi \approx 0$. To obtain the initial value of u at the defined position in the plasma $\xi >> r$ from where the equations (4.18) to (4.20) are integrated; we consider the following: First we drop the ionization collision term on the right hand side of (4.18) and integrate with respect to ξ to obtain,

$$\xi \tilde{n} u = a \tag{4.25}$$

From (4.25), (4.19) and (4.20) one can obtain u for specific values of $\xi >> r$. Here a is the normalized current density defined as: $a = \frac{J_D}{e n_{+o} C_s}$ here, $J_D = \frac{I_+}{2\pi\lambda_D}$ is the Debye current density and $I_+ = 2\pi e r n_+ v_+$ is the positive ion current per unit length of the probe. Therefore one can solve (4.18) to (4.20) for obtaining the normalized electric potential, electric field, density and the velocity profile from the plasma to the probe surface.

4.3.4 Methods of finding the sheath boundary

The sheath thickness is mainly defined by the position of the sheath edge from the probe surface which is rather difficult to determine due to the smooth behavior of parameters describing the sheath. However this point can be located by high positive ion current density. Based on this there are different ways of interpreting the sheath boundary. One of the techniques, commonly known as the curvature criteria [Crespo 2006], interprets the sheath pre-sheath boundary as the point where the curvature of the electric potential becomes maximum i.e. $\frac{d\psi_c}{d\xi} = 0$. Where ψ_c represent the curvature of the normalized electric potential. Since there is no arbitrary parameter involved, the curvature criterion is a suitable solution to find the position of the sheath edge. Figure 4.3 shows the spatial profile of the electric potential and its curvature. The electric potential profile is obtained by numerically solving the sheath equations (4.18) to (4.20) from the plasma to the probe. Figure 4.3 clearly shows a maximum in the curvature of the electric potential profile. The value of ξ corresponding to this maximum is defined as the position of the sheath edge.

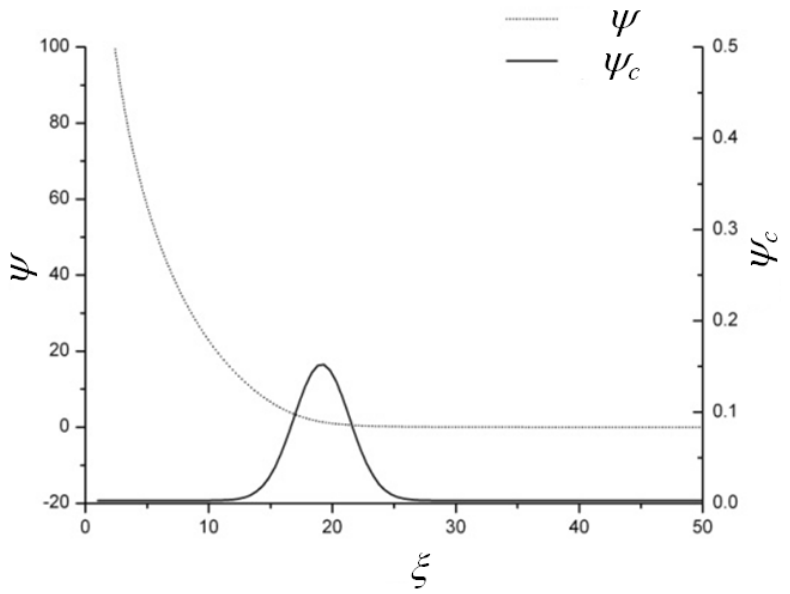

Figure 4.3: Normalized potential and its curvature as a function of the normalized distance from the probe surface (for a=10, α=0.5, γ=10, q=0 and β=0).

4.4 Numerical simulation results

The main focus of this study is to obtain the thickness of the sheath around cylindrical probes and the effect of the electronegative plasma parameters (α and γ) on it. For this purpose the model equations (4.18) to (4.20) are solved numerically using an adaptive size Runge-Kutta method from the plasma to the edge of the probe with the boundary conditions discussed in the previous section. However a choice of finite ξ is required to solve the model equation because the probe sees an infinite plasma. Therefore it is important to inspect the probe potential when this parameter is varied.

Figure 4.4(a) and 4.4(b) shows the variation of normalized probe potential as a function of ξ. Figure 4.4(a) is plotted for different values of α keeping q, a and γ constant, however figure 4.4(b) is plotted for different values of the normalized current density, keeping other parameters constant as described in the figure. As shown in figures 4.4(a) and 4.4(b), the potential at the probe first increases monotonically and then saturates as ξ is varied over a distance 10 λ_D to 100 λ_D. Thus a choice of ξ between 50 λ_D to 100 λ_D is reasonable for the parameter range used in this study. Therefore for our analysis we have chosen ξ = 100 λ_D as an upper limit of the integration to obtain the numerical solutions to the model equations. However in some of the figures the spatial variation is shown from the value below 100 λ_D. This is because the spatial behavior is almost the same from the upper limit shown to the point ξ = 100 λ_D.

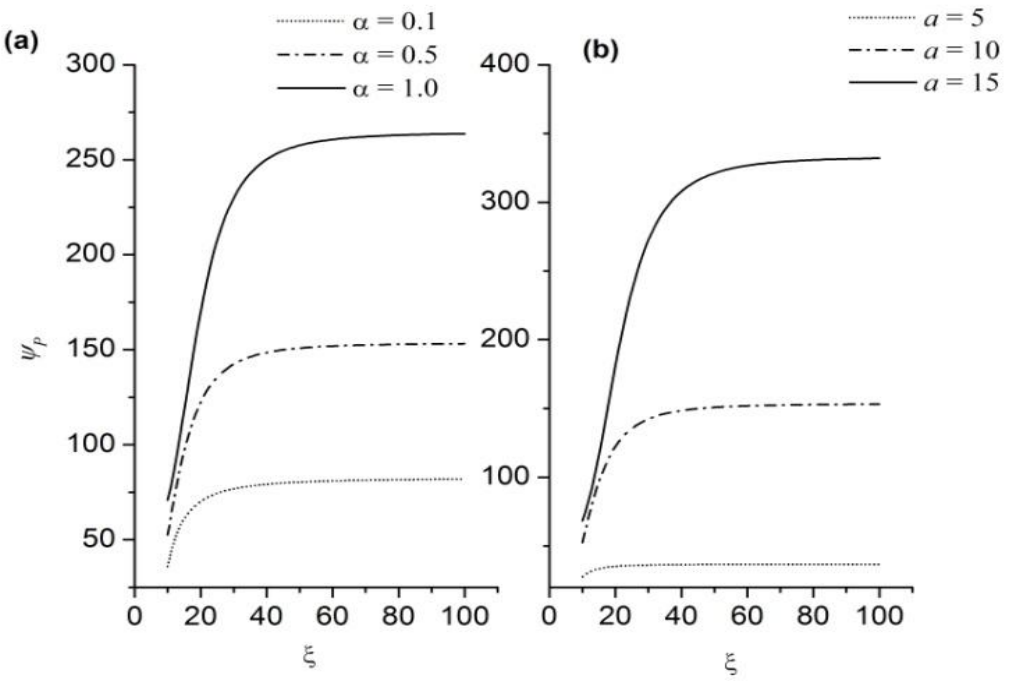

Figure 4.4: Effect of the integration length ξ on the probe potential (a) Parameters: γ=10, q=0, β=0 and a=10 (b) α=0.5, γ=10, β=0 and q=0.

4.4.1 Sheath potential

The normalized sheath potential profile is first obtained for different values of α by solving the complete set of non-linear equations numerically. In this calculation, the ionizing collisions in the pre-sheath are completely ignored by assuming $q = 0$. Ion thermal motion is considered to be infinitely small, i.e. $\beta \approx 0$. From figure 4.5 we observe that at a fixed value of the normalized positive ion current, the normalized sheath potential increases monotonically with α. Hence the sheath width also increases with the electronegativity for a constant value of normalized positive ion current. This result is a consequence of keeping the ion flux constant at the probe surface. As observed in equation (4.11); an increase in the electronegativity results in a drop in the pre-sheath potential as well as the positive ion speed at the sheath–presheath boundary. Consequently the positive ion flux at the sheath boundary should reduce. However we have chosen our boundary condition by defining a constant positive current density a using equation (4.25). To conserve this current, the sheath boundary expands radially such that the integrated surface charge density of positive ions is constant in the sheath region. This observation is found to be consistent with that obtained by Amemiya [Amemiya 1999].

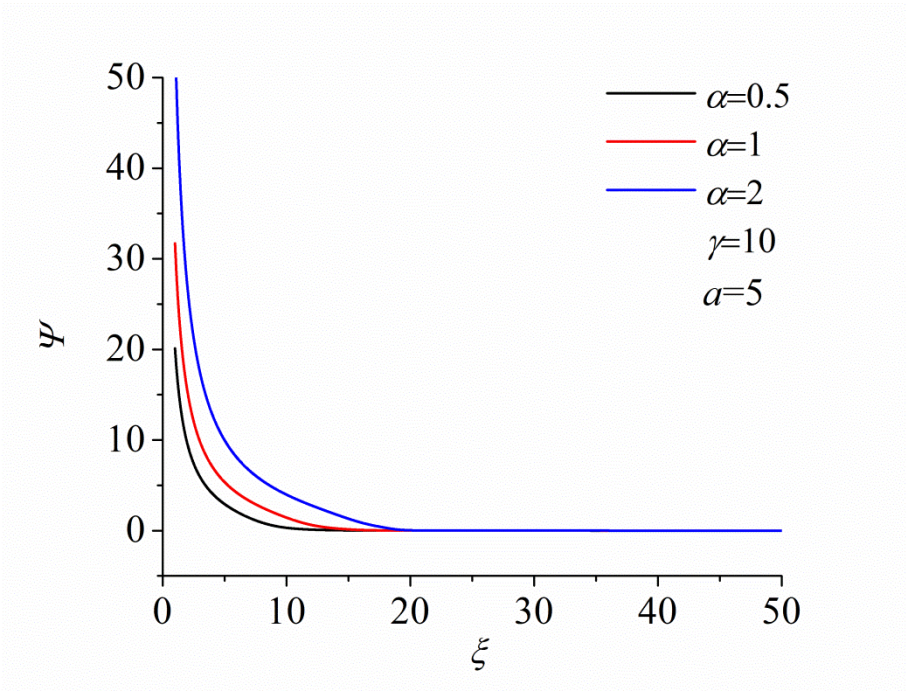

Figure 4.5: Plot of the spatial profile of the normalized sheath potential for different α. For these calculations we have chosen q=0, a=5 and β=0.

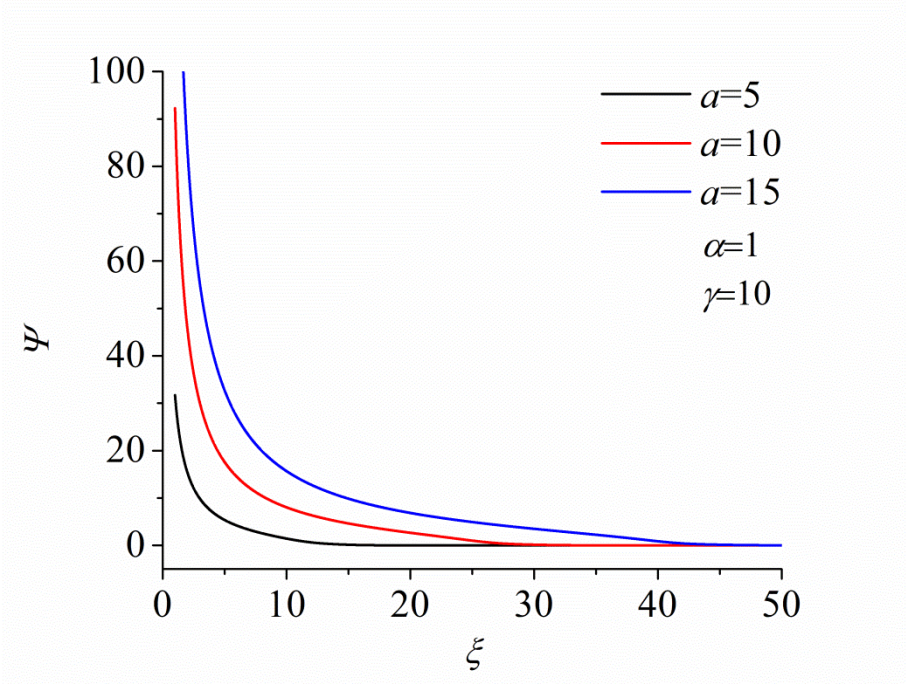

Figure 4.6: Plot of the spatial profile of the normalized sheath potential for different values of the normalized positive ion current a.

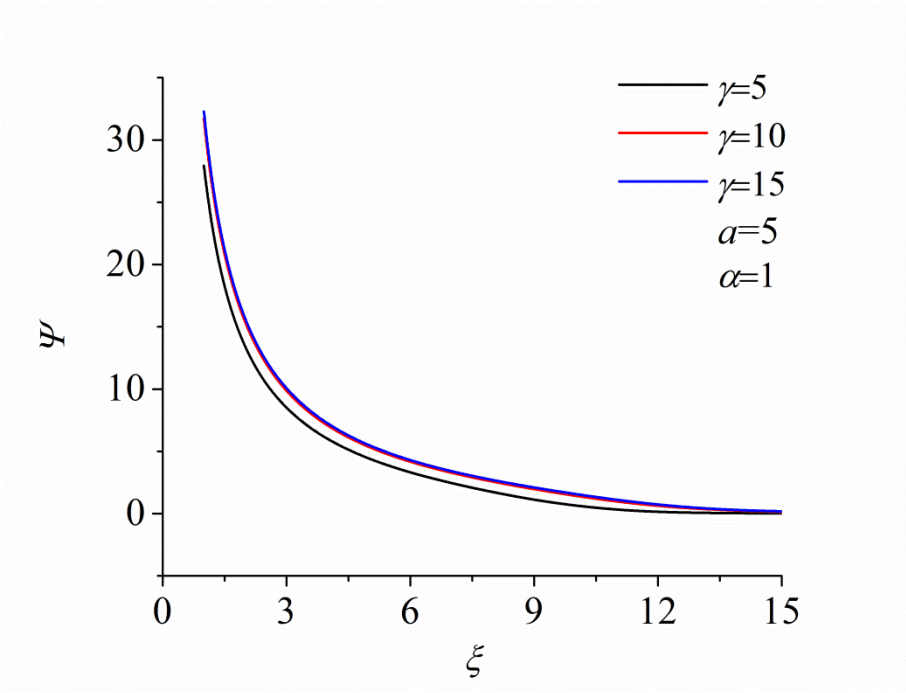

Figure 4.7: Plot of the spatial profile of the normalized sheath potential for different values of γ.

The effect of the normalized current density a and the temperature ratio γ is shown in figure 4.6 and figure 4.7. As shown in figure 4.6: with the increase in the normalized current density, the electric potential also increases and moves to the higher values of ξ. Thus for increase in the current density for a constant value of α and γ the sheath width also increases. As shown in figure 4.7 the effect of γ on the electric potential profile is not so significant. Hence changes in the temperature ratio γ won't change the sheath width significantly for constant values of a and α.

4.4.2 Sheath width as a function of probe potential

The motivation behind the sheath modeling surrounding cylindrical probes in electronegative plasmas is to obtain the sheath width. In this section we obtain the normalized sheath width as a function of the normalized probe potential using the curvature criterion described in previous section. The parameters chosen in this study are outside the parameter range where multiple solutions exists [Braithwaite 1988]. Again, in the calculations the ionizing collisions in the pre-sheath are completely ignored and ion thermal motion is neglected. This is an appropriate condition to approximately estimate the sheath dimensions. The normalized sheath width is obtained for two different values of α by choosing a constant value of γ (i.e. γ=10).

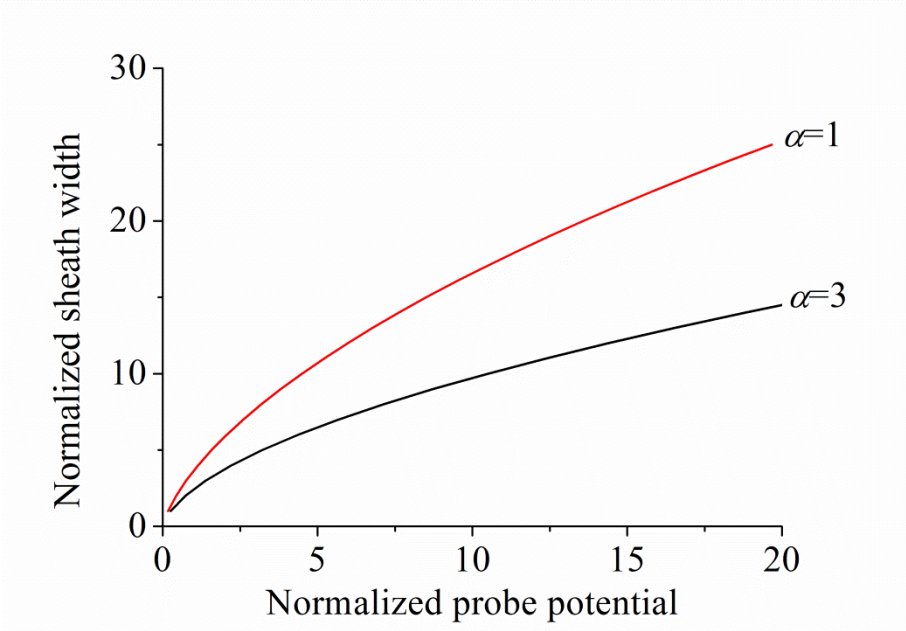

Figure 4.8: Plots showing the comparison of the normalized sheath width obtained for two different values of α using the curvature criterion.

The sheath thickness in figure 4.8 is found to be an increasing function of the probe potential. If a constant positive ion current is considered, then the potential of the object increases while ξ extends to larger values, implying a greater sheath width. This is shown in figure 4.5. However in figure 4.8 we observe a decrease in the sheath width for a given potential with increases in the electronegativity α. This is in favour of accurate hairpin probe measurement i.e. the smaller in the sheath width the smaller will be the underestimation in the measured electron density by the hairpin probe.

The above observation is consistent as increasing the electronegativity decreases the positive ion flux. Figure 4.9 shows how the positive ion current collected by the probe affected with an increase in the electronegativity. The positive ion current collected by the probe decreases with increase in α.

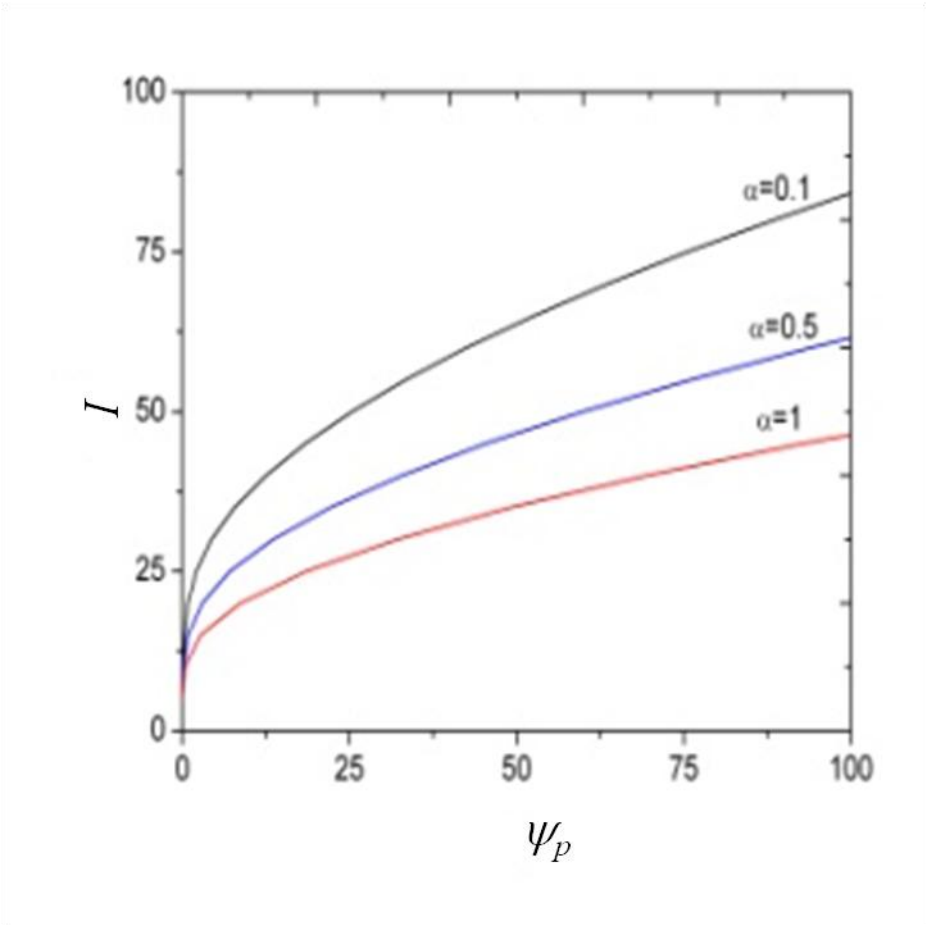

Figure 4.9: Theoretical IV characteristic curves for different values of ξ_p ,α and γ parameters for β=0, γ=10, ξ_p =5.

4.5 Summary and Conclusions

As discussed: the sheath around the cylindrical pins is an important parameter for the hairpin probe. Their effect can be substantial when *b/h* ~1 (where *b* and *h* are sheath width and probe half width respectively) because of its contribution to the effective permittivity. In this chapter we further studied the effect of negative ions on the sheath width. The model equations are solved in a cylindrical coordinate system without assuming quasineutrality in the presheath region. The sheath and presheath boundary is thus estimated on the basis of a curvature criterion i.e. the point at which the curvature of the electric potential is maximum.

Important results thus obtained show the enhancement of the sheath potential and the sheath width with electronegativity for similar positive ion fluxes to the cylindrical probe. The sheath sizes are typically of the order of 1-25 times the Debye length at a normalized probe potential of 2-20. This information is necessary for designing hairpin probes in the subsequent chapter for electronegative plasma

diagnostics. Furthermore the model equation also includes the positive ion temperature and collision frequency. Since the negative ions have nearly the same mass as that of the positive ions thus the cold positive ion assumption cannot be valid. Therefore the positive ion temperature should be included to better estimate the sheath width. The effect of collision frequency is also studied, however it is not presented in this chapter since it is not relevant to the scope of this thesis. Briefly, with increases in the collision frequency, the sheath width is found to be decreased for a fixed ion current density.

Chapter 5

Hairpin probe in conjunction with laser photodetachment for electronegative plasma diagnostic

5.1 Introduction

Most of the gases used in technological plasma applications used for the etching of semiconductors in the microelectronic and photonic industries are electronegative in nature. As a consequence it results in the formation of a significant fraction of negative ions in the plasma. The presence of negative ions has a dramatic effect on plasma processing. Powder formation in chemically active plasmas has been attributed to negative ions which accentuate the mechanism [Howling 1994]. The negative ions also affect the discharge structure and the sheaths as reviewed and discussed in Chapter 4. This has inspired a number of theoretical works since the 1990's and recent debates on the theories of electronegative discharges by Franklin, Lampe [Lampe 2003, Franklin 2005, Lampe 2006].

Some of the most important and interesting problems related to the existence of various kinds of instabilities and double layers are associated with electronegative plasmas [Chabert 2006]. Therefore diagnosis of negative ion discharges is important for the experimental verification of the above theories as well as for the quantification of basic discharge parameters for a wide range of applications. Probe assisted laser photodetachment is a commonly used technique for electronegative plasma diagnostics in which the temporal evolution of current to a positively biased Langmuir probe is measured. In this chapter we present the application of hairpin probes for measuring negative ion parameters; namely the negative ion density and temperature during laser photodetachment. Hairpins have several advantages compared with the conventional Langmuir probe, particularly in magnetized plasmas where Langmuir probes tend to deplete electrons. Additional limitations apply in the case of probe surfaces being exposed to oxide deposition, as in the case of pulsed magnetron sputtering [Dodd 2010]. The insulating films developed can severely hamper the accuracy of the measured electron saturation current. In some plasma reactors, typically those used in plasma manufacturing industries, there are large amplitude rf oscillations in the plasma potential. The presence of a Langmuir probe in such cases can severely disturb the plasma. Due to the above limitations, the hairpin is considered as a possible candidate

for the diagnosis of electronegative plasmas. This study is also important to benchmark the technique of pulse biased hairpin probes, which is presented in chapter 6.

The chapter is presented as follow: in section 5.2 principle behind pulsed laser photodetachment is discussed. Experimental results are presented in section 5.3 and 5.4 on oxygen negative ion density characterization in an inductive ion source at Dublin City University. In section 5.5 we present time-resolved negative ion density measurements for the first time using a hairpin probe in pulsed dc magnetron discharges and a comparison with Langmuir probe assisted photodetachment. This experiment was carried out at the Electrical Engineering Department of University of Liverpool following an invitation from Prof. James Bradley. In section 5.6 we discuss the measurement of the negative ion temperature. The discrepancy in measuring negative ion temperature on ignoring the ambipolar electric field created along the axis of the beam with the adjacent plasma is also discussed. This caused an overestimation in the measured negative ion temperature. In order to address this issue, we further used an emissive probe for measuring the plasma potential behaviour. As shown in this section, the negative ion temperature obtained from the plasma potential evolution is found to be lower compared with the negative ion temperature obtained from the electron density refilling time. Finally the summary and conclusion of the chapter is given in section 5.7.

5.2 Principle of probe assisted laser photodetachment

If the laser photon energy is tuned to a threshold value just enough for the photodetachment of weakly bound electrons to the negative ions, one can detach electrons from negative ions. This gives rise to a quasineutral equilibrium between electrons and the background positive ions. As time evolves, an equilibrium is reached between the electropositive plasma with the negative ion rich background plasma. This is caused by negative ions diffusing from the surrounding plasma into the electropositive region determined by their characteristic thermal speed. Thus by measuring the temporal evolution of the electron density before and after detachment, one can estimate the negative ion density. This is often done by using a Langmuir probe operating in the electron saturation regime, which is proportional to the electron density.

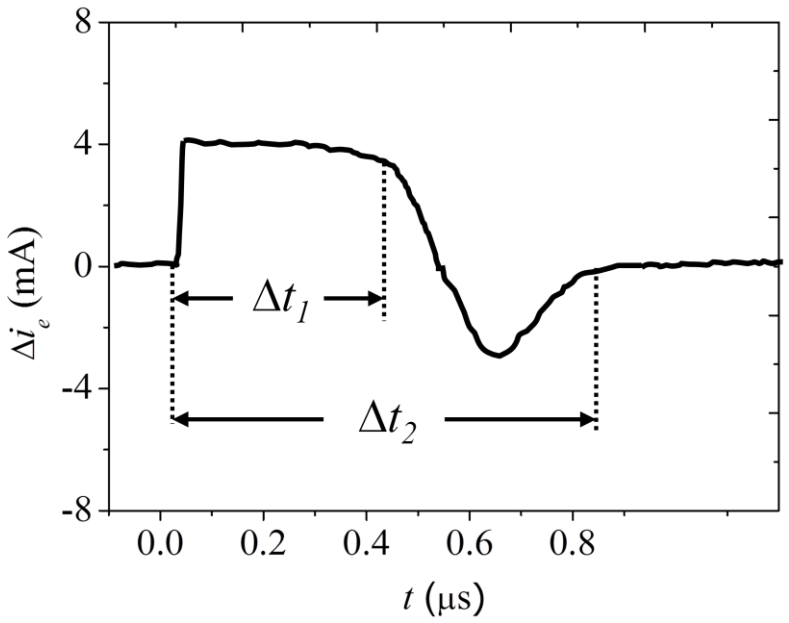

Figure 5.1: Typical photodetachment signal recorded by a cylindrical Langmuir probe at the axis of the laser beam [Devynck, 1989].

Let us consider n_{-0} and n_{e0} as the bulk negative ion density and electron density respectively. The fraction of the negative ion density is defined by a parameter $\alpha = n_{-0}/n_{e0}$. This can be conventionally determined by a Langmuir probe by taking the ratio of the peak in the electron saturation current following photodetachment with the background.

$$\alpha = \frac{\delta n_e}{n_{e0}} = \frac{\delta I_e}{I_e} \tag{5.1}$$

Here δn_e is the change in electron density and corresponding change in current δI_e. One can obtain the absolute negative ion density (n_{-0}) provided that the electron density is known prior to detachment with a good degree of certainty.

A schematic of the temporal evolution of the electron saturation current at the axis of the laser beam measured with a Langmuir probe is shown in figure 5.1 [Devynck, 1989]. Roughly, the signal is characterized by a peak in the electron saturation current relative to the background ($t<0$). This is followed by a plateau (for a period Δt_1 as shown in figure 5.1) in which the electron density and positive ion density are in equilibrium. The next phase is a decay in the electron saturation current. This phase is the signature of negative ions refilling the negative ion deficient region of the cylindrical volume, hence the electron density decays. One also observes that the electron saturation current, which is a representation of electron density, dropping

below the equilibrium level. This overshoot in the electron saturation current before reaching the equilibrium value (after a period Δt_2), reflects that some positive ions are expelled from the laser illuminated region because of the creation of an ambipolar electric field. We have addressed this problem in section 5.6 by applying an emissive probe which finds that the plasma potential sharply rises following photodetachment.

5.3 Hairpin probe with laser photodetachment

5.3.1 Probe alignment and laser

The alignment of the hairpin probe for the laser photodetachment experiment is quite tricky since the hairpin probe has two parallel cylindrical limbs. One also needs to be careful about avoiding the interaction of the high power laser with the end of the ceramic tube which encloses the coaxial cable and the loop. Keeping this in mind we designed a hairpin probe in such a way that its pin's are directed at an angle with respect to the probe feedthrough. In this way the laser is coincident with more than 90% of the hairpin probe while reflection from the ceramic holder encasing the loop was avoided because the ceramic was situated outside the laser beam volume. Figure 5.2 shows a schematic of the hairpin probe and laser beam.

To measure the absolute value of the negative ion density, the diameter of the laser beam should be sufficient enough to detach electrons from negative ions which influence the hairpin. In this experiment we have chosen a laser beam of diameter 6mm, thereby assuming that it is adequate for this purpose (the hairpin probe width is ~3mm).

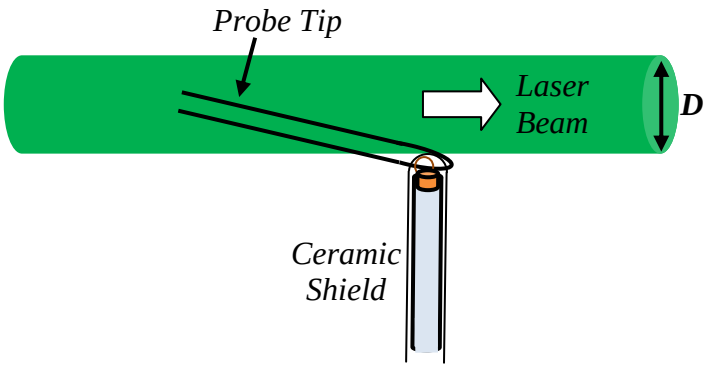

Figure 5.2: A schematic diagram of the hairpin probe and laser.

The experiment is carried out in the inductive oxygen discharge. Oxygen is well known for its electronegativity and because of its low value of detachment energy. The second harmonic corresponding to the 532 nm (2.33 eV) wavelength (green light) of the

laser is therefore suitable for photodetachment. This photon energy is however insufficient for causing photodissociation (5.12 eV) or ionization of the O_2 (E_{iz} = 12.07 eV) and O (E_{iz} = 13.6 eV) species [Shibata, 1997]. Whereas it is above the photodetachment energy for the two main oxygen negative ions O_2^- (Ed = 0.44 eV) and O^- (Ed = 1.46 eV). Therefore the laser beam is only responsible for removing the extra electron from negative ions. The photodetached electrons increase the net electron density, which is measured by the time-resolved technique discussed in section 2.6.2.

The laser setup used in the experiment comprises the following parts:

(1) Innolas Spitlight 600 Nd : YAG laser which has a bandwidth of <0.003 mm^{-1} operated at a frequency of 10 Hz. The second harmonic of the laser is generated using a temperature controlled type II KTP crystal. The resulting mixture of infrared and green light is then fed into a harmonic separation assembly composed of two dichroic mirrors that transmit infrared but reflect green light.

(2) A series of mirrors for reflecting the green light at 532 nm and steer the beam to the laser exit aperture.

(3) A small sheet of glass for reflecting part of the laser beam onto a Thorlabs Det210 fast photodiode that is used to trigger the oscilloscope.

The exit beam has a 6.0 mm diameter, which is steered using mirrors into the plasma chamber (describe in section 5.4.1) through a quartz window, and passes at a specific radial distance from the helical RF antenna enclosed inside the quartz exit port located at the far end of the chamber.

5.3.2 Photodetachment signal along the illuminated region

If the laser flux is sufficient, then it is possible to detach electrons from all negative ions in the path of laser beam (effect of laser flux on photodetachment fraction is further studied in section 5.3.4). In this experiment we fixed the laser flux at ~2000 J/m^2. Following the laser pulse, the electron density is expected to rise instantly and then fall to the equilibrium value after some time. When the hairpin probe is employed for detecting the rise and fall in the electron density, we adopt the step increment of frequency technique for obtaining temporal values of the probe resonance in the case of a time varying plasma density, as discussed in section 2.6.2. The procedure begins by tuning the input frequency to the hairpin slightly above that at the resonance frequency observed for the background plasma (before injecting the laser). The signal corresponding to 2.12 GHz as shown in figure 5.3 is the resonance frequency of the background plasma (t < 0 s) having a plasma density of about $3x10^{15}$ m^{-3} (data is taken

in an oxygen ICP discharge discussed in the section 5.4). In figure 5.3 the signals shown are normalized by subtracting the individual background dc level corresponding to the amplitude of the reflected signal when the probe is not in resonance. At t = 0 shown by the trigger pulse applied for firing the laser, all signals have been scaled to reduce the dc amplitude to zero prior to the laser pulse.

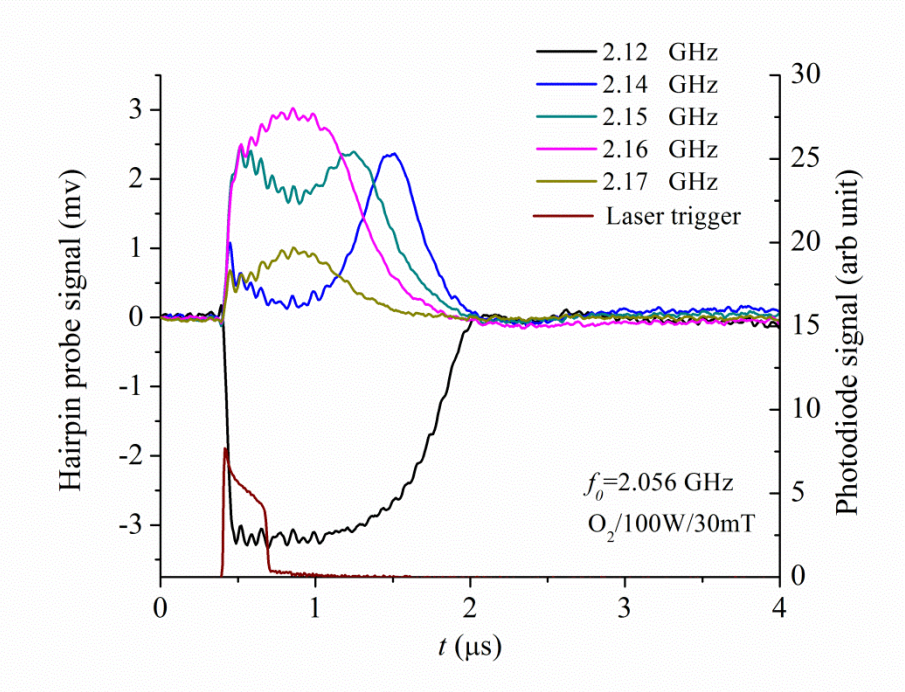

Figure 5.3: The hairpin probe signals on the axis of the laser beam following photodetachment of oxygen negative ions at t = 0 shown by the trigger pulse applied for firing the laser. The laser flux is kept constant a value of 2000 J/m^2.

The dip in the hairpin probe signal at 2.12 GHz shows that the probe is off resonance due to the generation of extra electrons from photodetachment of negative ions. The probe remains off resonance over a substantial period of time (approximately 1-2 μs) as the photoelectrons diffuse through the probe region. As the hairpin frequency is gradually increased to bring the probe back to a resonance with the increased electron density we observe that two distinct peaks begin to emerge. The first peak corresponds to the increasing electron density, and second corresponds to a decreasing plasma density following photodetachment. As the microwave frequency further increases the two peaks move closer together as the probe is gradually brought to resonance with the surrounding plasma, and when the hairpin driving frequency reaches resonance with the photodetached plasma electron density, the two peaks merge into a single peak. This is observed at 2.16 GHz as shown in figure 5.3, which corresponds to an electron density of about 5.4x10^{15} m^{-3}. The absolute negative ion density is obtained by the subtraction

of the background electron density from the electron density corresponding to the frequency of a single peak which is 2.4×10^{15} m^{-3} in the present case.

In the figure 5.3, although the electron density is the same during the rising and falling phase, however we observe some asymmetry in the resonance peaks in time. This is attributed to a sharp rise in density in the photodetachment phase followed by the slow decay in density in the diffusion phase as the surrounding negative ions refill the electropositive region.

5.3.3 Off-line of sight response

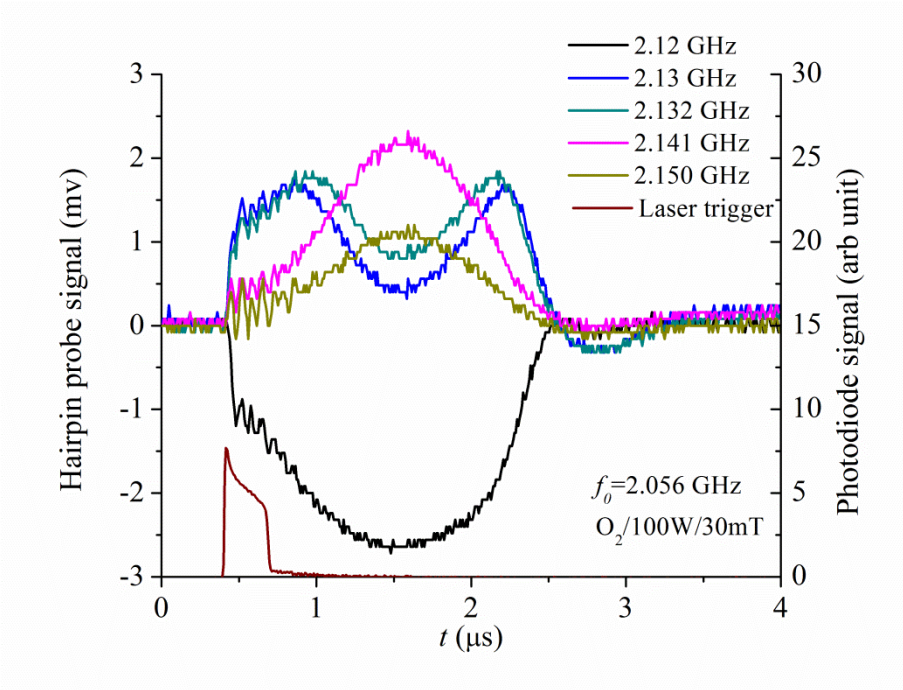

Figure 5.4: Hairpin signals recorded outside the laser beam (~4mm from the axis of the laser beam) as the probe is tuned to the plasma electron density following photodetachment of oxygen negative ions. The laser flux is kept constant a value of 2000 J/m^2.

When the hairpin is placed at some radial distance outside the path of the beam, the electron density dynamics are governed by negative ions diffusing in the electropositive plasma region. This response is rather slow compared with the observed dynamics at the centre of the beam. Therefore the rate of increase and the rate of decrease of the electron density outside the beam are correspondingly slow. This allows the probe to respond in accordance with the time-varying density, hence both the resonance peaks during the rising and decaying phase are pronounced and symmetric as shown in figure 5.4 (data is taken in an oxygen ICP discharge discussed in the section 5.4). Again at a background

frequency of 2.12 GHz there is a dip due to the photoelectron population shifting the probe and plasma off resonance. As shown in figure 5.4, although the background electron density is the same as that obtained at the centre of the laser beam, the negative ion density is now decreased to 1.4×10^{15} m^{-3}. This is because the electrons diffusing outward (at a faster rate) from the laser beam are governed by negative ions diffusing (at a slower rate) in to the laser channel.

5.3.4 Tuning of the laser intensity and calibration technique

The dependence of the detachment fraction of negative ions is a function of the laser energy density as given by the expression [Bacal, 2000]:

$$\frac{n_-^{detached}}{n_-} = 1 - \exp\left(\frac{-\sigma}{h\nu}\frac{E}{A}\right) \qquad (5.2)$$

Where E is the energy of the laser pulse, σ is the photo-detachment cross section, ν is the laser frequency and A is the beam cross section area. By varying E and A, the laser flux can be adjusted to ensure saturation level for the experiment.

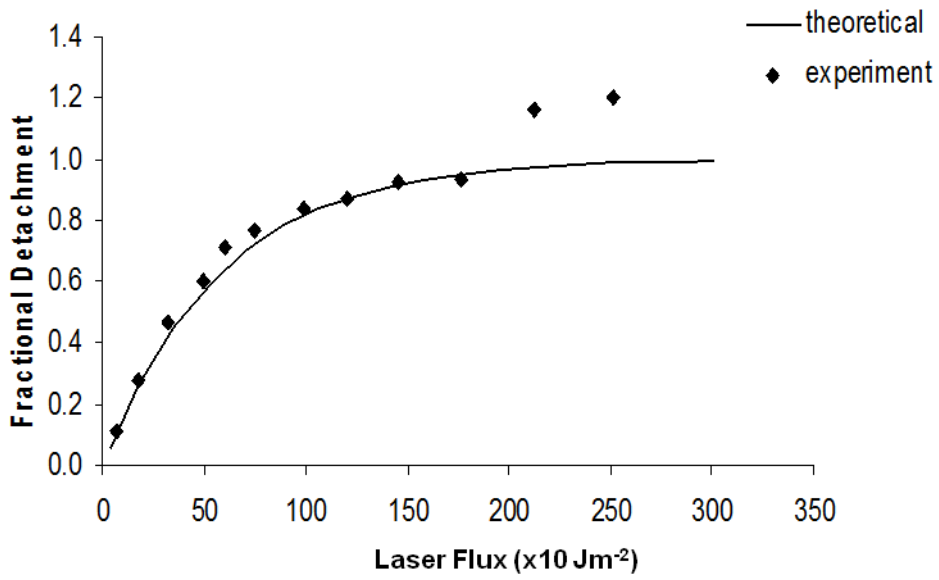

Figure 5.5: Plot of photodetachment fraction as a function of laser energy density with the probe placed inside the laser beam. The operating conditions of the plasma are 30 mTorr and 200 W rf power.

As shown in figure 5.5, the fractional detachment (LHS of equation (5.2)) of negative ions in the laser illuminated region reaches saturation with increasing laser flux. This is observed to follow a similar trend to that expected from equation (5.2). However

deviation from the theoretical plot is observed above 2000 J/m^2. This deviation is thought to be due to ablation from the probe. Ablation phenomena have been reported in the case of Langmuir probes [Kajita, 2004] due to thermionic electron emission from the probe surface which leads to spurious electron current signal. Since we reached a photodetachment fraction of nearly 90% for 2000 J/m^2, we have restricted the laser flux to this value.

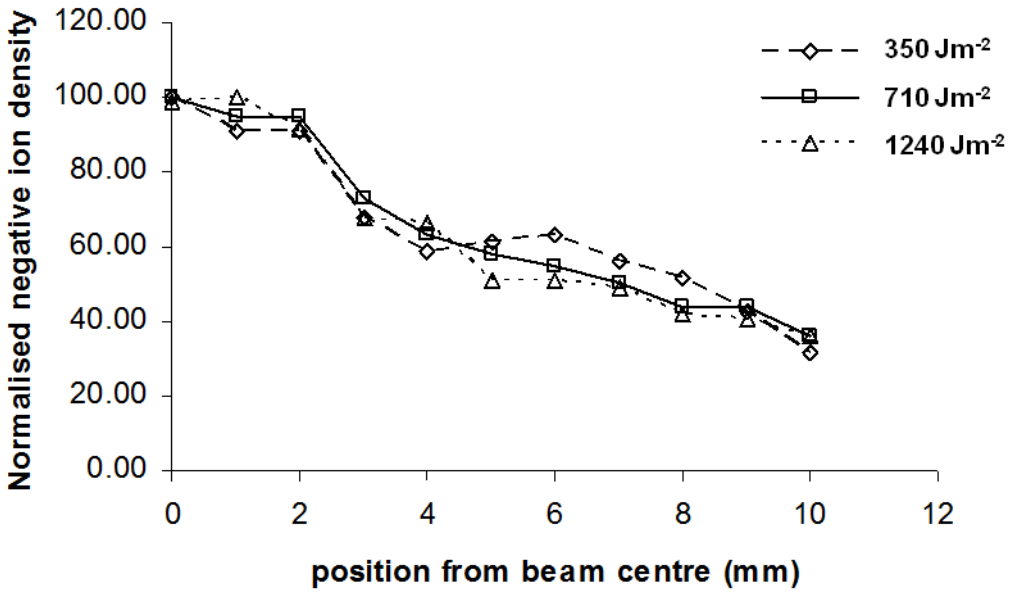

Figure 5.6: Hairpin probe data recorded at various positions moving from the beam centre outwards. The operating conditions of the plasma are 30 mTorr and 200 W rf power.

The interaction between the laser and the probe can be completely avoided by placing the pins outside the path of the beam. This was also applied earlier for Langmuir probes [Nishiura, 1999]. Because the probe pins are at a certain distance from the electropositive channel, the electron density dynamics cannot be seen unless negative ions begin to move into the detachment region. As the local negative ions move inwards, the electrons from the electropositive region occupy the position of the negative ions. This will happen on the time scale when the negative ions move at the characteristic thermal speed. Therefore the probe situated outside the electropositive signal will under-estimate the value of the negative ion density compared with the probe directly placed in the electropositive region. This is because we are only observing the secondary effect associated with the fractional amount of negative ions diffusing inwards. Therefore the negative ions estimated by locating the probe at different radial

distances from the centre fall off with distance. However the trend is found to be independent of the laser flux, as shown in figure 5.6. These measurements were performed at reduced laser powers to avoid ablation effects. The data is normalized to 100 for each laser power.

At a distance of 3.0 mm from the centre the density drops by approximately 65 % of the peak density at the centre. After this distance, the density signal remains fairly constant as the probe is moved to 6.0 mm. The profile of the spatial variation of the electron density remains the same irrespective of the laser power used for photodetachment. This suggests that one can estimate n_{-0} without having the probe placed in the line of sight of the beam. Once a calibration curve is obtained, the negative ion density can be measured by positioning the probe outside the path of the laser beam. The laser can be operated at much higher powers without any interference of the probe. This is evident from figure 5.7, which shows that no probe assisted interference was caused compared with figure 5.5 when the probe was placed 4 mm from the center of the beam as the laser power was pushed up to 3000 J/m^2.

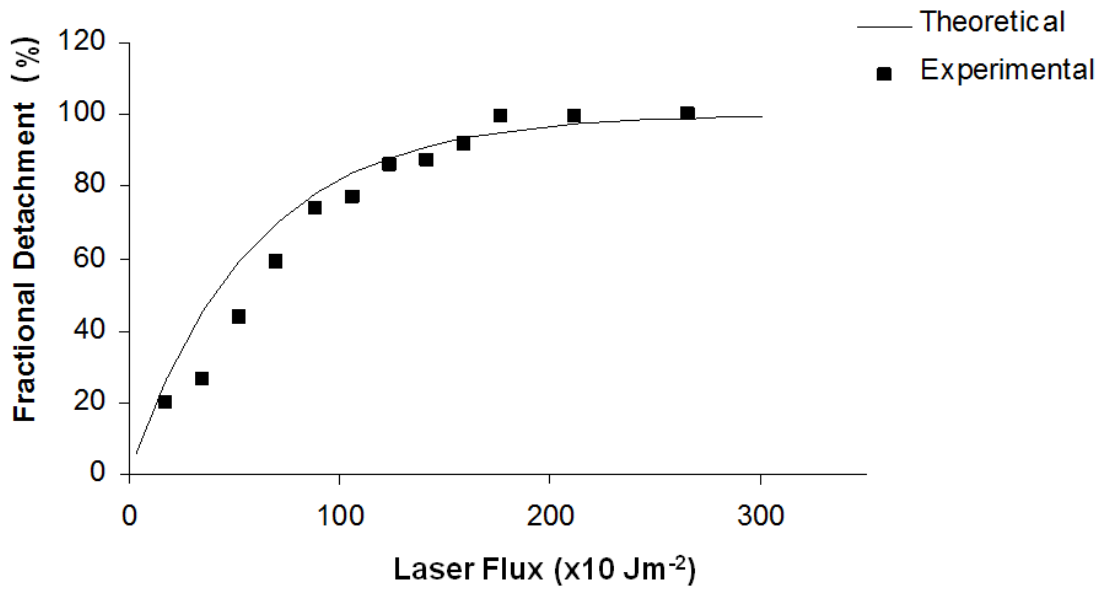

Figure 5.7: Plot of photodetachment fraction as a function of laser energy density with the probe placed outside the laser beam. The operating conditions of the plasma are 30 mTorr and 200 W rf power

5.4 Negative ion density in oxygen ICP discharge

In this section we investigate the negative ion density using the above technique in an oxygen ICP discharge. The absolute negative ion density is obtained for a range of powers and pressures and the results are discussed.

5.4.1 Experimental setup

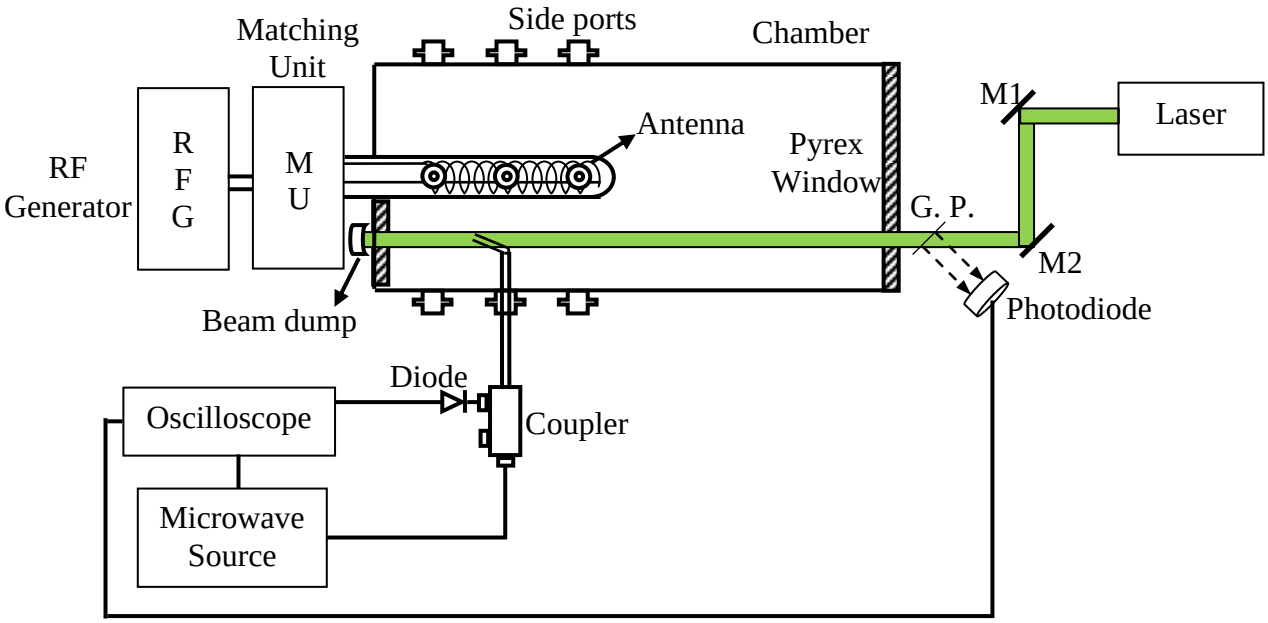

Figure 5.8**:** Schematic diagram of the experimental setup (top view) to detect the negative ion density using laser photodetachment with a floating hairpin probe. M1 and M2 - steering mirrors, G.P. - glass plate.

The experiment was carried out in the experimental setup called BARIS (BAsic Radiofrequency Ion Source) at DCU. The setup shown in figure 5.8 is a stainless steel cylindrical chamber 800 mm long with an internal radius of 100 mm. Gas is introduced into the chamber using a STEC SEC-4000 series mass flow controller and the chamber is pumped using a pfeiffer balzars turbomolecular pump which is backed by an edwards rotary pump. An 11 turn helicon antenna of diameter 30 mm made from 1/8 inch diameter gold plated copper tubing is mounted into the chamber region through one of the chamber end walls along the chamber axis. The antenna is isolated from the vacuum chamber by a Quartz tube (i.e. re-entrant configuration). The antenna is driven by a 13.56 MHz ENI ACG10B signal generator via a standard ‘L’ RFPP AM20 impedance

matching unit. Water cooling of the antenna and discharge chamber allows the discharge to be operated at power levels as high as 1 kW.

To allow access to the chamber for detachment experiments, a number of viewports are present in the chamber. A 20 mm thick by 60 mm wide Pyrex viewport is fitted into the antenna endwall of the chamber. This viewport extends radially from the edge of the antenna out towards the flange edge. This window is mounted at the Brewster angle to minimise laser light reflections back into the chamber. The opposite end of the chamber is sealed with a 15mm thick Pyrex viewport allowing the laser beam to enter the chamber at any position. The laser enters the chamber through the front viewport and exits the chamber via the Brewster window beside the antenna. A hairpin probe is inserted through one of the radial ports in the path of the laser beam as shown in figure 5.8, such that the position of the probe is at a distance of 40 mm from the quartz tube covering the coil. The oscilloscope is triggered by a photodiode signal obtained via reflection from the glass plate placed in the path of the laser beam just before entering the reactor. The microwave source is operated in the CW mode to produce a single frequency output which is feed to the hairpin probe via a 50 Ohm coaxial cable and a loop. The technique of measuring the absolute negative ion density is based on finding the frequency that corresponds to the maximum amplitude of the reflected signal following photodetachment (as discussed in section 5.3.2).

5.4.2 Electronegativity as a function of applied power and pressure

Effect of RF power

Figures 5.9 and 5.10, present a characterization of the electron density and the negative oxygen ion density over a wide range of RF powers varied between 50 W and 500 W by keeping a constant pressure of 30 mTorr with a flow rate of 100 sccm.

The electron density is found to increase almost linearly with increasing RF power above 100 W. The linear relationship between the applied power and density suggests the electron density n_o is below the critical limit at which absorbed power scales as, $P_{abs} \propto n_o I_{rf}^2$ or $n_o = \frac{P_{abs}}{eu_B A_{eff} E_T}$ [Lieberman and Lichtenberg, 2005]. The negative ions are primarily generated by dissociative attachment: $e + O_2 \rightarrow (O_2)^* \rightarrow O^- + O$. This is consistent with the experimental results plotted in figure 5.10 that shows that the negative ion density rises linearly with electron density, hence we can confirm that

dissociative attachment is the dominant process for the production of negative oxygen ions in the reactor. At low operating powers below 75W, the negative ion density is found to be higher than the electron density, with a negative ion fraction $\alpha = n_{-0}/n_{e0} =$ 1.5 as seen in figure 5.11. Whereas α drops significantly to about 0.3 with increasing rf power. This is consistent with the fact that the electron density increases at a higher rate than the negative ion density with increasing rf power. This suggests that negative ion destruction mechanisms become increasingly prominent as the rf power increases up to 150W. The main destruction channels for negative ions are electron detachment and ion-ion neutralization via the reactions $e + O^- \rightarrow O+2e$ and $O^- + O_2^+ \rightarrow O + O_2$. From figure 5.9 the electron density in the plasma increases with rf power which would result in an increased rate of destruction of negative ions, consistent with our finding. Above 150W α remains essentially constant indicating that equilibrium is reached between the production and destruction rate of the negative ions as the electron density further increases with rf power, provided the electron temperature remains constant. As the measurements were performed at constant pressure, the electron temperature remains essentially constant over the rf power range, and has been measured for the system to be ~4eV using a Langmuir probe.

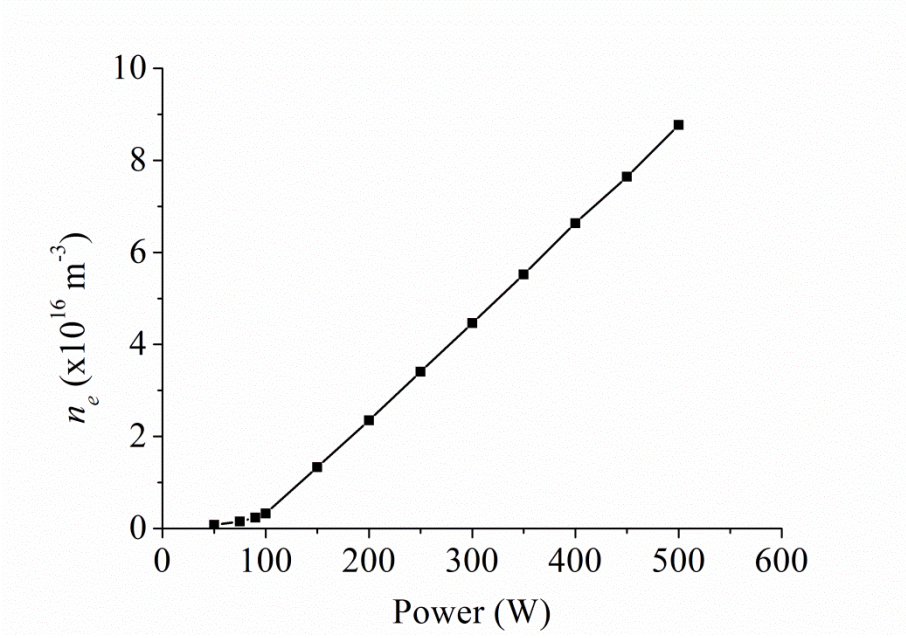

Figure 5.9: Variation in electron density verses rf power (on beam) in an oxygen plasma operating at 30 mTorr and 200 sccm.

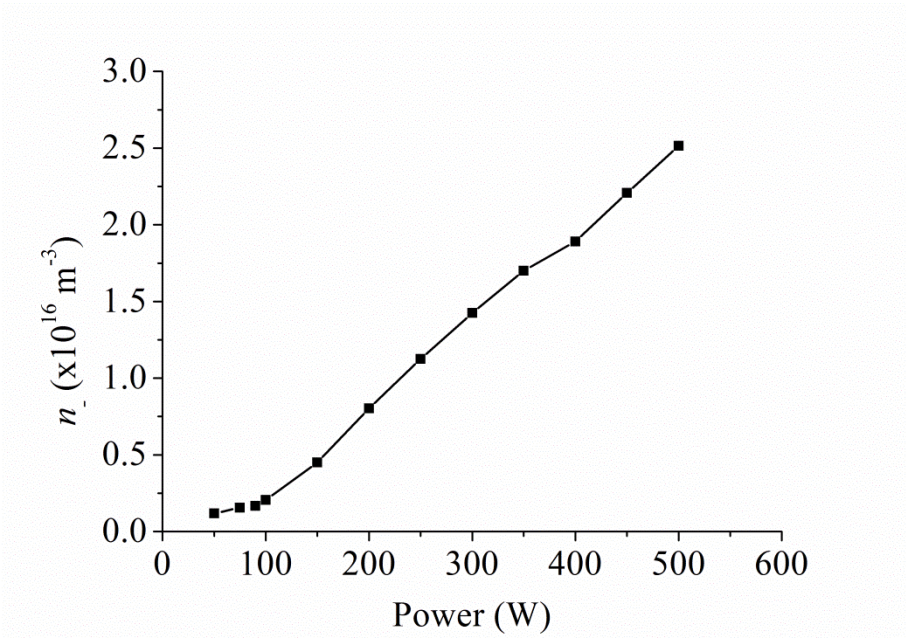

Figure 5.10: Variation in negative ion density verses rf power (on beam) in an oxygen plasma operating at 30 mTorr and 200 sccm.

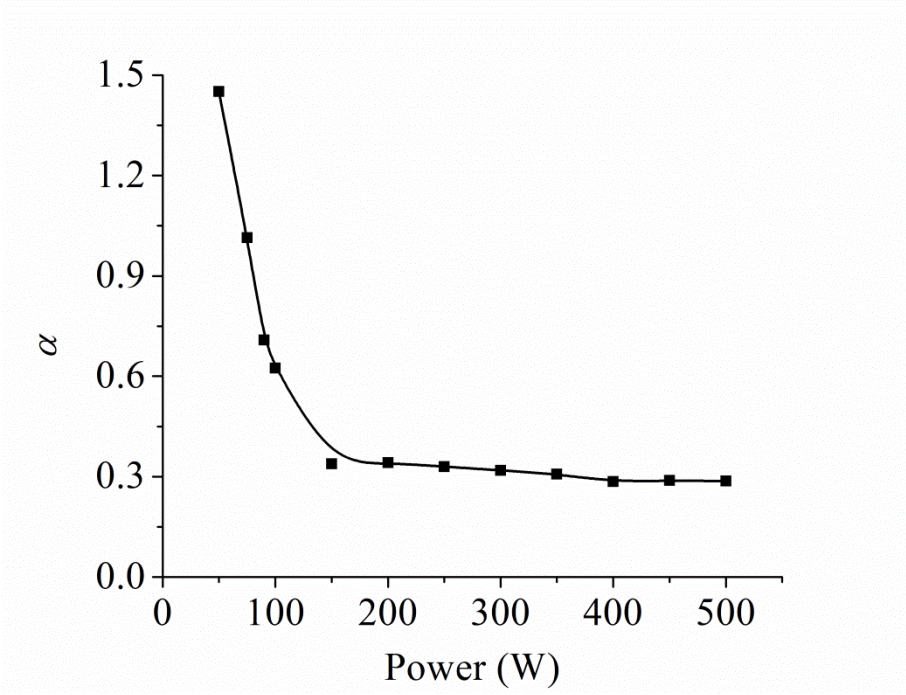

Figure 5.11: Plot of the ratio of negative ion density to electron density verses rf power (on-beam) in an oxygen plasma operating at 30 mTorr and 200 sccm.

Effect of pressure

The effect of background pressure on the electronegativity is presented in figure 5.12(a). The pressure was varied between 10.0 mTorr and 70.0 mTorr for a constant

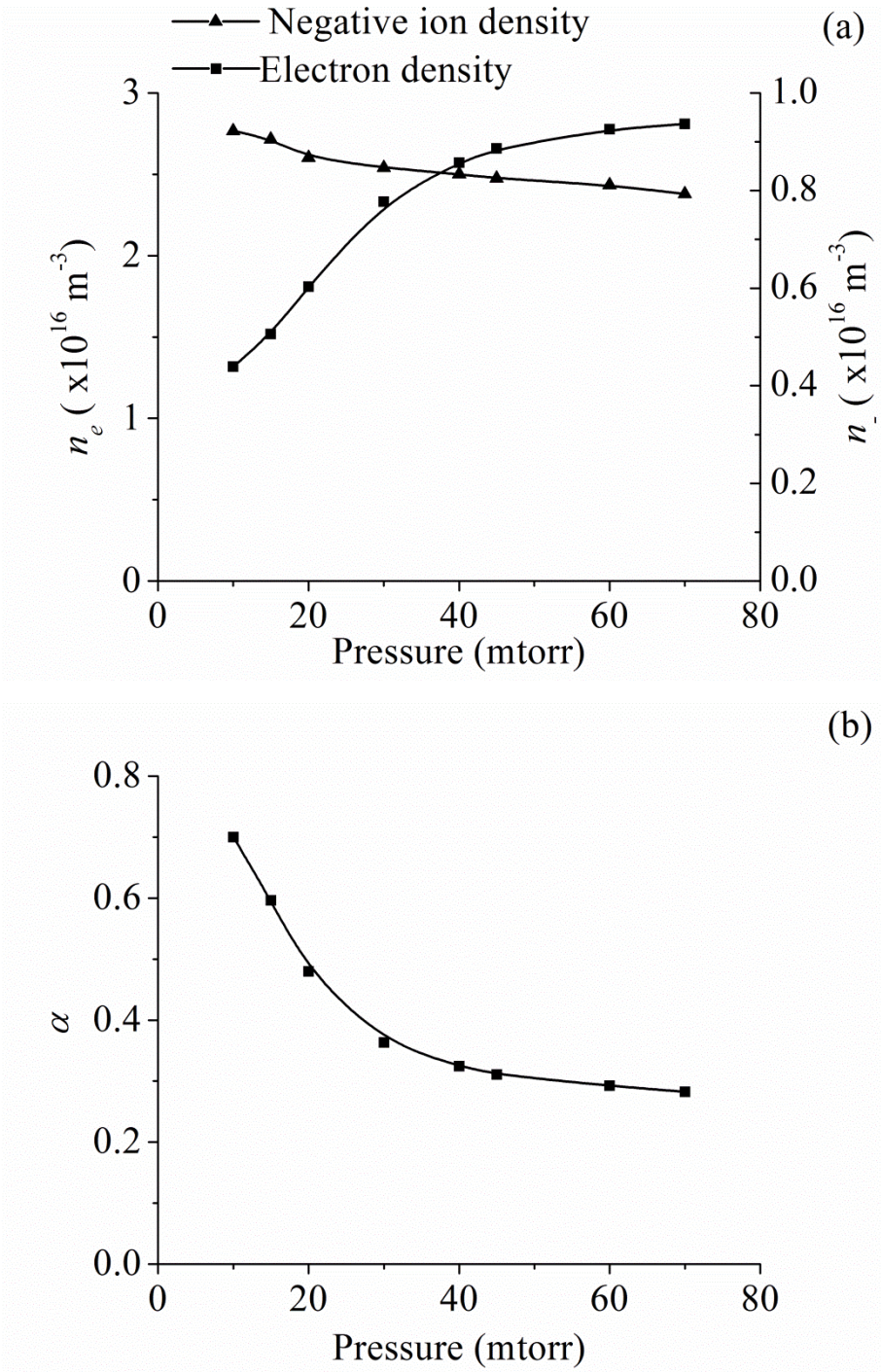

Figure 5.12: Plot of (a) absolute total negative ion density (right abscissa) and, electron density (left abscissa) and (b) $\alpha = (n-/ne)$ verses total pressure. The radio frequency power was set at 200 W.

flow rate of 100.0 sccm while keeping the RF power constant at 200 W. The graph shows the electron density increases almost linearly and tends to saturate at higher pressures. However the absolute value of the negative ion density decreases to within 20 % of the maximum density as the pressure is increased [c.f. 10 mTorr and 50 mTorr

data]. The plots of electronegativity α in figure 5.12(b) shows a consistent trend; that α reaches a saturation with increasing background neutral density (pressure).

The observed decay of the negative ion density can be understood by considering the following mechanism. The negative ions are formed by two competing processes, one is the electron attachment ($O_2 + e \rightarrow O^- + O$; rate constant = 3.5×10^{-17} m^3s^{-1}), competing with constant losses by destruction of negative ions mainly via ion-ion recombination ($O^- + O_2^+ \rightarrow$ Neutrals; rate constant = 1.0×10^{-13} m^3s^{-1}), and associative detachment via reactions; Rate $O^- + O \rightarrow O_2 + e$; rate constant = 1.4×10^{-16} m^3s^{-1} [Stoffels, 1995]. At sufficiently low pressures the dominant mechanism is the dissociative attachment and ion-ion recombination. However as the pressure increases, associative detachment also starts dominating and the discharge mainly becomes detachment dominated. Therefore the negative ion density tends to decrease as the pressure is increased. Similar behaviour has also been reported by previous authors in rf capacitively coupled oxygen discharges [Stoffels, 1995]. The maximum value of α for these operating parameters is found to be ~ 0.7, at a background pressure of 10 mTorr.

5.4.3 Summary and conclusions

In this section we presented the application of the floating hairpin probe, in conjunction with laser photodetachment, to the characterization of the absolute negative ion density in an oxygen ICP discharge. The absolute value of the negative ion density is obtained directly. Ablation effects are found to be negligible unlike the case where Langmuir probes are used, as the probe is fully floating and does not draw a net current from the plasma. However the effects can be enhanced in the case of depositing plasmas where the ejected neutrals could become ionized. In this condition the probe can be placed outside the beam and the negative ion density is still obtained provided that the underestimation should be evaluated first at low laser power.

Using this technique the negative ion density is recorded as a function of rf power and found to increase in a manner determined by the increase in electron density. The electronegativity of the plasma is found to drop significantly with increasing power as the rate of increase of n_- is smaller than the rate of increase of n_e. However we observed no significant difference in the absolute negative ion density with operating pressure at constant RF power. The difference is less than 20% for the pressure range of 10-50 mTorr. The electronegativity drops significantly with operating pressure, revealing that the discharge is detachment dominated at high pressures.

5.5 Time resolved negative ion density: Comparison between the Hairpin probe and Langmuir probe assisted photodetachment

This section is devoted to the measurement of the time resolved electron and negative ion densities in an argon-oxygen pulsed discharge. The motivation behind this experiment is to compare the electron and negative ion densities obtained by hairpin probe assisted laser photodetachment with those obtained by Langmuir probe assisted photodetachment. The detailed description of the experimental setup and the comparison of results are presented in the following sections.

5.5.1 Description of the experimental setup

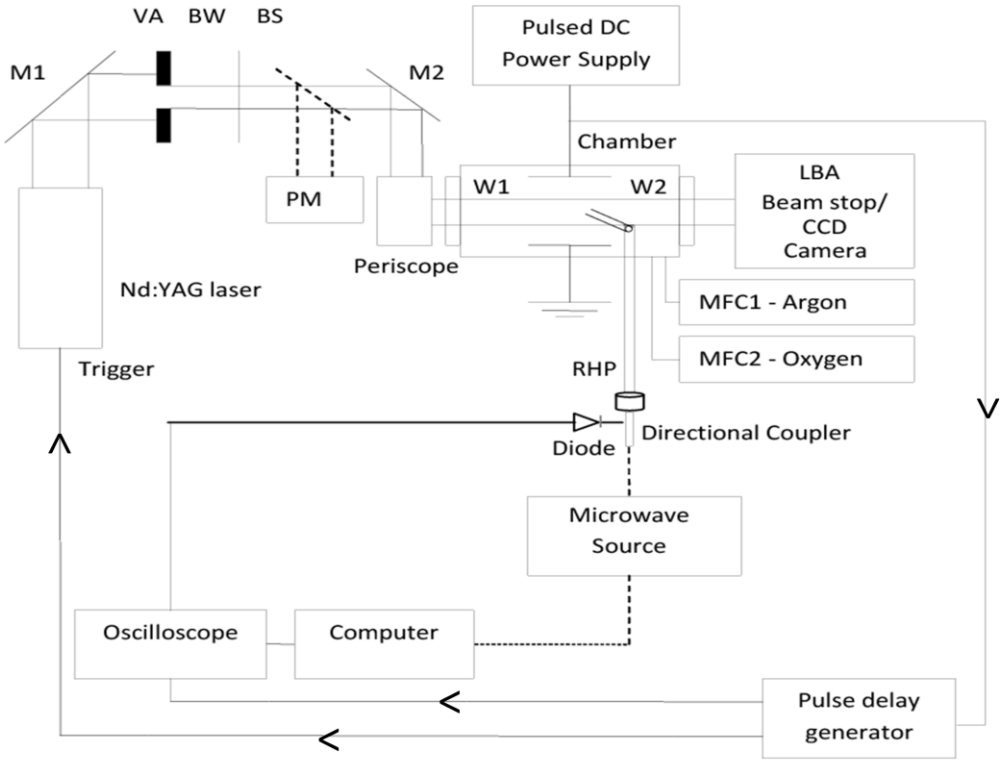

Figure 5.13: Magnetron sputtering and photodetachment systems for resonance hairpin probe (RHP) assisted photodetachment. For the Langmuir probe (LP) measurements, the microwave source and acquisition unit are replaced with the detection and acquisition circuitry described in reference [You, 2010].

A schematic diagram of the magnetron discharge, together with the hairpin probe setup, is shown in figure 5.13. A VTech 150 series unbalanced magnetron (Gencoa Ltd, UK)

was mounted vertically and positioned 120 mm from a grounded electrode in a 10 litre aluminum vacuum chamber. The water cooled magnetron head had a 150 mm diameter titanium target surrounded by a ground shield. Regulated pulsed dc power was supplied to the target using an electrical chopper unit made in-house and powered by a Pinnacle Plus power supply (Advanced Energy Inc.) operating in dc mode. The magnetic field configuration and field strengths are shown in figure 5.14, together with the position of the resonance hairpin probe and laser beam when situated 100 mm from the target.

The target current and voltage waveforms were measured by a P5100 voltage probe and TCP202 current probe (Tektronik) respectively. A base pressure of less than 1×10^{-6} Torr was achieved with a turbo molecular pump (Pfeifer TMU 071P) backed by a rotary pump (Edwards E1M40). Argon and oxygen gases (> 99.99 % purity) were fed into the chamber via two 20 sccm MKS mass flow controllers (MFC). The chamber pressure was measured by a Baratron gauge (MKS Type 627) and was used in conjunction with a MFC controller box (MKS Type 146) to regulate the MFCs. In this manner the desired total and partial pressures could be regulated in the range 0.26 to 3.2 Pa (at flow rates of 2 – 43 sccm).

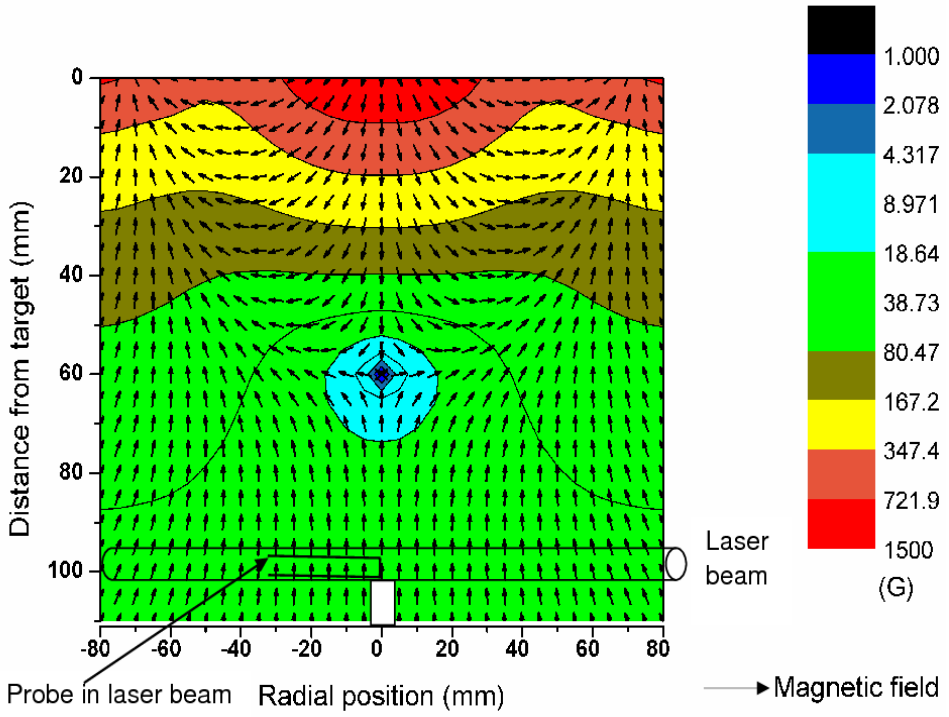

Figure5.14: Magnetic field configuration relative to the cathode target position (0 mm). The laser-beam line-of-sight and position of the RHP tips at 100 mm from the target are shown.

The resonance hairpin probe (RHP) was placed on the centerline in the downstream plasma at a position of 100 mm from the target, and the alignment with the laser is the same as discussed in section 5.3.1. This is the position close to the open field lines. The RHP, due to its length, occupied a radial distance of 32 mm from the discharge axis. The Langmuir probe was placed only at one position, a distance of 100 mm from the target (on the discharge centre line) occupying 3.5 mm of radial distance.

The laser used in this experiment is a frequency-doubled pulsed Q-switched Nd: YAG laser (Quantel Brilliant B) with wavelength 532 nm. The laser repetition rate was 10 Hz with a 5 - 6 ns pulse width and a beam divergence of 0.5 mrads. By using variable aperture (VA in figure 5.13) the beam diameter could be varied. A power meter (PM) monitored a known fraction of the average laser beam power via a beam splitter (BS). Optical access to the chamber was provided by two windows (W1 and W2) made of synthetic fused silica 10 mm thick. To minimize film deposition on the windows, which may cause reflections or reduce the optical transmission, they were positioned 10 cm from the chamber axis. The beam entered the chamber through the window W1 after being directed by the turning mirrors (M1 and M2) and a periscope arrangement. The laser beam exited the chamber through window W2 and its diameter and intensity profile were measured by a laser beam analyser (LBA – US Beam Pro Photon Inc. CMOS profiler). This was also used to ensure that the laser beam was co-axial with the probe and blocking wire in case of eclipsed photodetachment. In these experiments the laser beam diameter was set at 4 mm with a pulse energy of 30 mJ, giving an energy density of 2400 J/m^2.

5.5.2 Experimental results

In this study the pressure was fixed at ~10mTorr and the discharge was operated at a power of 50W in 70% argon and 30% oxygen gas mixtures. Figure 5.15 shows a plot of the measured temporal profile of the electron density n_e and negative ion density n_- during the pulse cycle by both the RHP and LP techniques, 100 mm from the cathode target. The two techniques were not done simultaneously, but carried out during different experimental runs. In the on-phase of the pulse, the Langmuir probe values of n_e are larger than those determined by the RHP (up to about 50 %), however in the off–time the values are in very close agreement. A similar discrepancy is obtained in the temporal profile of the negative ion density. Compared to the hairpin probe, the Langmuir probe measures a higher negative ion density in the on-phase, but gives

excellent agreement in the off-phase of the pulse. The highest value of n_- determined at this position was 1.5 x 10^{15} m^{-3} measured at the end of the off-time using the Langmuir probe. It seems unlikely that the Langmuir probe can produce an overestimate of the negative ion density, since we cannot detect more photoelectrons than exist in the beam, and the results indicate that the RHP in this particular configuration is marginally less sensitive in detecting the rise in electron density than the LP.

The discrepancy in electron density and negative ion density in the driven phase of the discharge may be a result of the plasma being spatially inhomogeneous, with the probes sampling different volumes of plasma due to the different extensions. The RHP is 32 mm in length and radially samples 32 mm of plasma, cutting across the magnetic flux lines. This is compared to only a 3.5 mm radial extension of the Langmuir probe (with a length of typically 7 mm) from the axis, situated in a relatively field-free region. In the off-time as the plasma decays and the electric fields collapses, the plasma may become more evenly distributed, with smaller spatial gradients, and therefore the probes will give more consistent results. Also, the LP measured electron currents may not give a true measure of the local electron density, due to perturbation of the plasma, since for the measurement of photoelectrons, the probe is always biased 20 V more positive than the space potential. It is not straightforward to predict if the drawn electron current would increase or decrease in such a case without a detailed study.

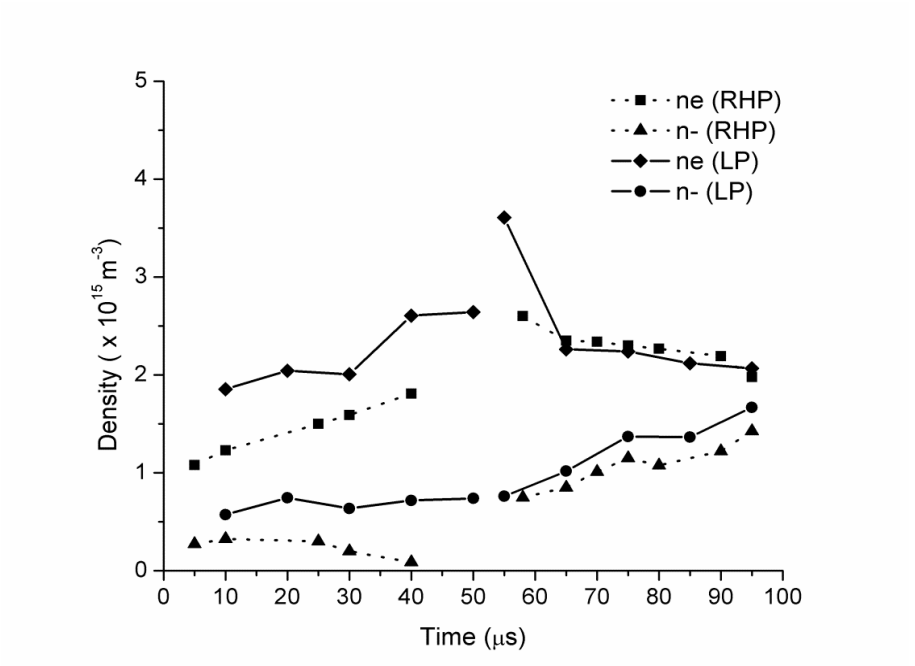

Figure 5.15: Negative ion (n_-) and native electron (n_e) densities for times during the pulse (10 KHz frequency) measured by both the RHP and LP at 100 mm from the target.

The discharge behaviour for both the RHP and LP techniques show higher values of n_- in the off-time compared to the on-time, and that n_- clearly rises during the off-time. This would indicate that oxygen plasma chemistry is taking place in the afterglow, giving rise to the production of new O^- ions. In the afterglow when T_e falls rapidly, the conditions are more favourable for the formation of negative ions (O^-) through dissociative electron attachment of highly-excited oxygen matastables, which themselves are created in the pulse on-time [Dodd, 2010]. The cross-section for this reaction increases with decreasing electron temperature and this is consistent with conditions in the afterglow where the electrons cool to temperatures of about 0.5 eV [You, 2010], For greatly extended off-times, the negative ion density can grow further followed eventually by a decay which happens at a rate determined by the ambipolar diffusion of the charged species to the wall [Dodd, 2010].

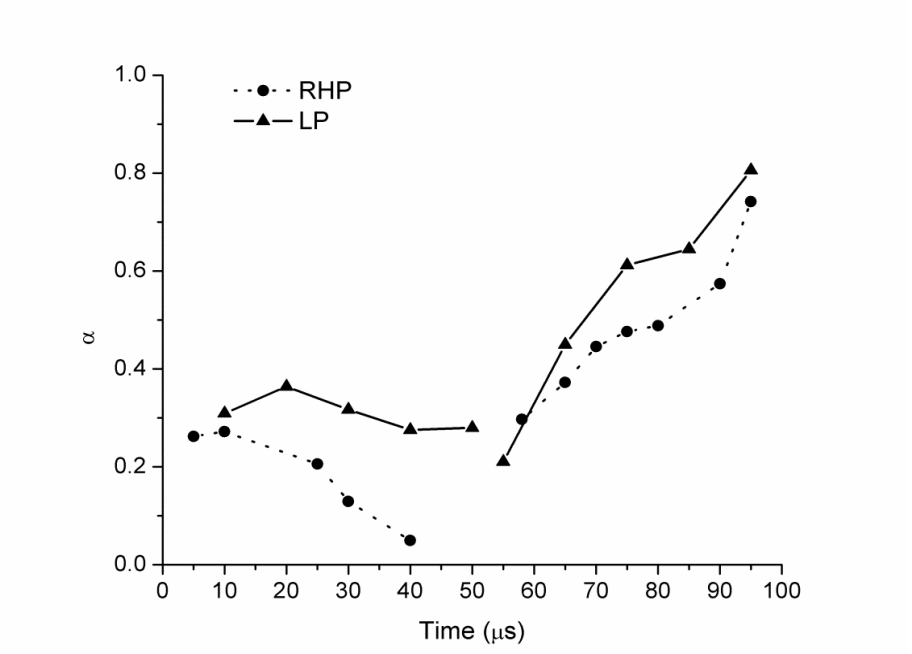

Figure 5.16: Negative ion-to-native electron density ratio $\alpha = n_-/n_e$ measured by both the RHP and LP techniques at 100 mm from the target.

Figure 5.16 shows a comparison of measured values of α determined by both techniques at a distance of 10 cm from the target. The trends in time during the pulse cycle are in generally good agreement. Both techniques clearly show larger and increasing α values in the off time and lower and decreasing values in the on-time. The worst agreement between the different probes occurs at t = 40 μs, with a discrepancy in excess of 500%. As alluded to above, the difference in n_-, and therefore α, may stem

from the fact that the RHP has a larger radial extension than the LP, and therefore detects photoelectrons originating from a larger plasma volume than the LP. In this particular magnetic geometry, the O^- densities may be largest on the axis, and therefore the RHP, which is sampling a radial plasma, would show inherently lower n_- values than the Langmuir probe.

5.5.3 Summary and conclusions

A hairpin probe with laser photodetachment is successfully applied to the time resolved measurement of the negative ion density in a pulsed dc magnetron discharge. A comparison of the resonance hairpin probe technique with the more conventional Langmuir probe assisted laser photodetachment generally shows very good agreement in both n_- and α, particularly in the afterglow phase of the pulse cycle. In the on-time however, the Langmuir probe typically gives higher values for both parameters by factors in excess of 2 as the discharge current builds-up. The discrepancy in the on-phase of the pulse is thought to be because of the spatial inhomogenity of the plasma. Using this technique, the absolute O^- densities and negative ion-to-electron density ratios α have been obtained during the pulse on and off-times. The results show the highest O^- densities occur in the afterglow with n_- reaching 1.5×10^{15} m^{-3} at the end of the off-time at a position 100 mm from the target, with degree of electronegativity of up to 0.6.

5.6 Measurement of negative ion temperature

The hairpin probe can also be used for measuring negative ion temperatures based on the temporal evolution of the electron density following photodetachment [Conway 2010]. The underlying principle is based on identifying the recovery time of the transient electron density signal. A similar technique was used earlier by [Bacal, 2000], where the electron saturation current was monitored with a Langmuir probe. However we find that the negative ion temperature obtained from the density evolution is overestimated compared with the negative ion temperatures obtained if we consider the plasma potential evolution. It will be shown that the latter technique is more accurate compared with the temperature obtained from the recovery time of the electron density.

5.6.1 Underlying concept

As is well known from the literature, the negative ion temperature can be obtained from the recovery time of the electron density [Devynck, 1989] when using probe assisted laser photodetachment. Another technique demonstrated by Bacal et al [Stern, 1990] involves using two successive photodetachments in which a second laser is fired after a certain delay. This photodetachment signal, corresponding to the second laser peak, quantifies those negative ions which are refilling the electropositive channel from the ambient plasma.

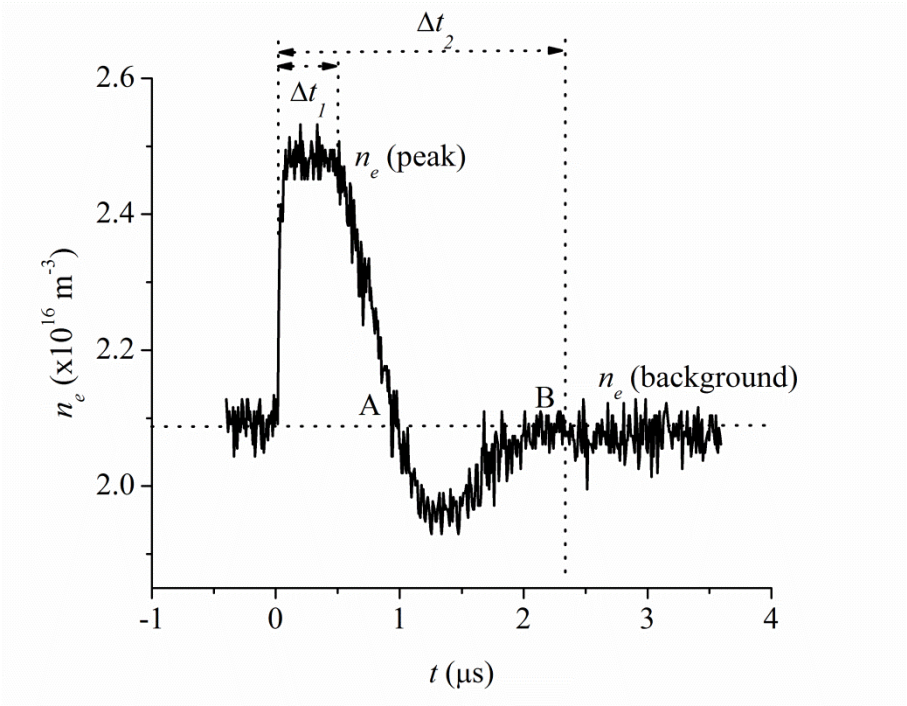

Figure 5.17: Temporal evolution of electron density at the centre of the laser beam measured using the hairpin during laser photodetachment.

Briefly, according to the electron density recovery theory, the electron departure from the laser illuminated region is because of the arrival of negative ions from the surrounding plasma. Thus there is a range of negative ion thermal speeds which correspond to two characteristic time scales; namely Δt_1 and Δt_2 [Devynck, 1989] as shown in figure 5.17. The first time period Δt_1 corresponds to the arrival of the fastest negative ions. This is characterized with a rapidly decreasing electron density, followed by a second time scale Δt_2 which corresponds to the arrival of slower negative ions, recovering gradually to the background density. Using Δt_1 and Δt_2 it is possible to estimate the range of negative ion temperatures, as discussed in reference [Devynck, 1989].

In the two laser photodetachment measurement, the curves of the negative ion density recovery are obtained by the use of two lasers, one of which destroys all negative ions and the other is delayed in time and is used for searching for the recovering negative ions. In order to deduce the negative ion temperature, the experimental curves of the negative ion density recovery are usually fitted with a theoretical curve, i.e. the following equation is derived from the ballistic kinetic theory (BKT) for negative ions [Stern, 1990]:

$$n_{-}(r=0,t)=n_{-0}\exp\left(-\left(R/v_{th}^{-}t\right)^{2}\right) \tag{5.3}$$

Here $n_{-}(t)$ is the negative ion density at a time t after firing the laser shot, n_{-0} is the initial negative ion density, R is the laser beam radius, and v_{th}^{-} is the thermal velocity of negative ions.

The equation is derived using a kinetic approach by considering the set of coupled Boltzmann and Poisson equations [Stern, 1990] for times small compare to the collisional time. However there is one limitation associated with both techniques; the ambipolar electric field in the laser illuminated region is neglected. The creation of an ambipolar electric field between the electropositive plasma channel and the surrounding negative ion plasma is because the thermal energy of the electrons exceeds the positive as well as the negative ion temperature by several orders of magnitude. The typical thermalization time of photodetached electrons is of the order of few 100 ns. The hot electrons tend to escape from the electropositive channel leaving behind a slight excess of positive charges which creates a reverse electric field stopping the freely escaping electrons from the electropositive channel. This ambipolar electric field, if sustained for some time, it will tend to accelerate the negative ions because of the potential difference created by the energetic electrons. Thus if we neglect the ambipolar field, it can lead to an overestimation of the negative ion temperature. The formation of an ambipolar electric field is well known theoretically but has never experimentally quantified. In the following sections we apply a floating emissive probe for the first time to measuring the relative variation in the plasma potential following photodetachment of electrons from negative ions. Finally the negative ion temperature deduced by the electron density evolution is compared with that obtained by the plasma potential evolution.

5.6.2: Measurement of the plasma potential by an emissive probe

The emissive probe is a well known technique for measuring the plasma potential [Kemp, 1966]. In this technique if the amount of electron flux received from the plasma

is compensated for by an equal number of electrons released from the surface of the probe then net potential difference between the probe and the plasma is zero. Therefore the probe potential ideally reaches the plasma potential.

The probe can be made to thermionically emit electrons by heating a small filament with an AC or DC current, until the filament is visually white hot. In some experiments a small probe tip was irradiated with a laser beam [Schrittwieser, 2008] in order to avoid interference caused to the plasma due to the probe heating power supply. In the literature we find three basic methods of using emissive probes for measuring the plasma potential [Sheehan and Hershkowitz, 2011],

- The saturated floating probe method is the one in which the voltage at zero probe current is identified as the plasma potential.
- In the divergence point method, the point of divergence between the hot and cold probe characteristics is taken as the space potential.
- The space potential is identified with the inflection point in the hot probe current-voltage characteristic.

In our case we are interested in measuring the dynamic variation in the plasma potential. Therefore it is simpler to use the floating point method. The probe in our case is a small loop of tungsten wire which is heated by passing 2.0 – 3.0A DC current, which lifts the potential of the probe close to the plasma potential as the probe becomes visually white hot. The tip of the filament stays in the path of the laser beam. This method is simpler but comes with a small compromise because the floating potential saturates on the order of T_e/e due to space charge around the probe [Sheehan and Hershkowitz, 2011]. If the temperature is small and constant, this effect will merely give the plasma potential measurements a small and constant offset [Sheehan and Hershkowitz, 2011]. For our present application we are interested in the relative change in plasma potential before and after the laser pulse rather than its absolute value. Therefore the constant off-set can be eliminated by subtracting from the background potential (i.e with and without photodetachment).

5.6.3: Experimental setup for the emissive probe

A schematic diagram of the emissive probe is shown in figure 5.18. The probe comes with a thin 0.03 mm ‘tungsten filament in the shape of inverted ‘V’. The filament is tightly inserted into a double-bore ceramic tube which contains beaded copper wires. The filament makes very good surface contact with the copper and is compressed against the inner bore of the ceramic tubing. The end of the copper tube is soldered to a

vacuum compatible electric feedthrough. The tungsten filament gets heated by passing 2.0A of current through a regulated constant current power supply. The potential is measured across the centre point of two 20 kΩ resistors connected across the two ends of the filaments. The potential measured is directly displayed on the oscilloscope. Using this method, a time resolution of the order of < 20 ns [Karkari, 2003] can be achieved.

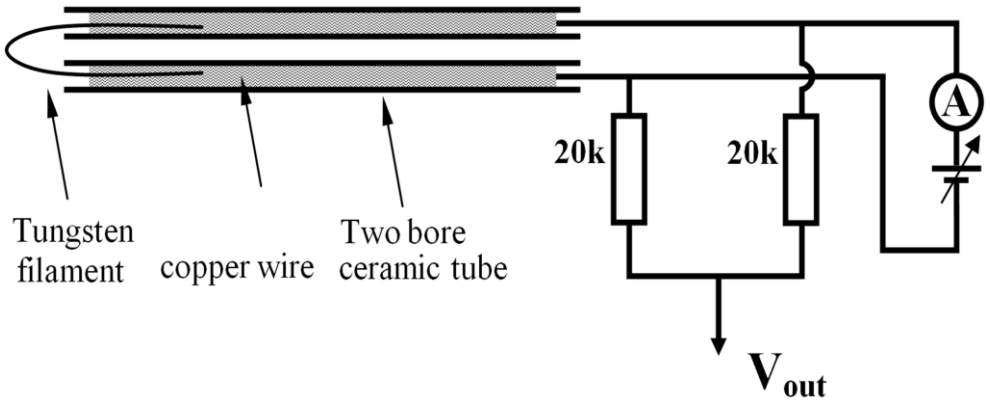

Figure 5.18: Schematic of the construction of the emissive probe and its electronic circuit.

The experimental setup for observing the temporal evolution of the space potential following photodetachment is the same as that shown in figure 5.8, in which we have replaced the hairpin probe with an emissive probe such that the tip of the filament is placed at the centre of the laser beam. However the interaction of the laser with the two bore ceramic tube is avoided by placing it outside of the laser beam. The discharge is produced in oxygen at different pressures controlled by turbo molecular pump.

5.6.4: Experimental results: Space potential variation data

In figure 5.19 we present the temporal evolution of the relative change in plasma potential ΔV_p with respect to the unperturbed state. Three different pressures 10 mTorr, 25 mTorr and 50 mTorr are considered. The sharp rise in V_p is observed at the instant $t = 0$ *s* when a pulse laser of duration 6 ns is fired into the plasma. We observed and recorded a systematic delay in the rise of V_p. for example 1.04, 1.2 and 1.44 μs as we varied the pressures 10, 25 and 50 mTorr respectively.

The observation of the plasma potential going higher than its equilibrium value following complete annihilation of negative ions suggests that space charge neutrality may not be absolute in the electropositive plasma channel. The relative difference in the

mobility of electrons compared with negative and positive ions is the factor which can lead to a transient departure from quasineutrality. As the electrons tend to diffuse faster from the photodetached zone, negative ions from the surrounding plasma cannot compete with the escaping electrons from the photodetached region due to differences in the thermal velocities. Therefore a local electric field is created between the electropositive channel and the surrounding plasma which will enhance the inward flux of negative particles into the laser illuminated region. The mobility of electrons and negative ions is affected by the operating pressure and thus it is reflected in the delay of rise in the plasma potential. In the following sections we find that the ratio of electron temperature to negative ion temperature for this pressure range is increased by 80%.

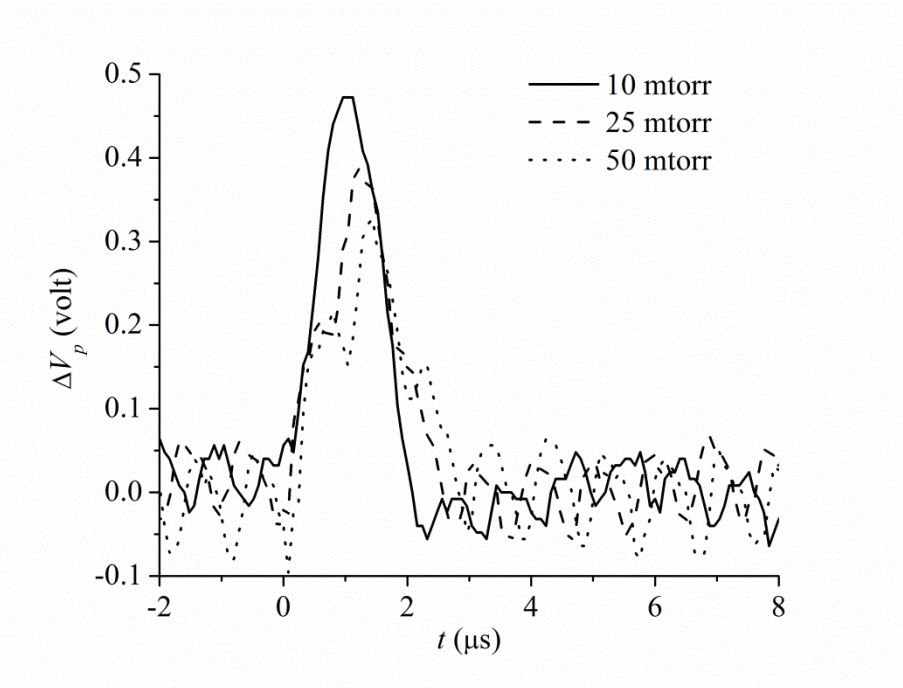

Figure 5.19: Temporal evolution of the change in plasma potential during pulsed laser photo detachment at different operating pressures. The laser energy density is set to 2000 J/m^2 at 532 nm. The rf power for this experiment is set at 200 W.

5.6.5: Discussion of various features and time scales

To gain more insight, the plasma potential evolution is compared with the electron density evolution measured by the hairpin probe. Figure 5.20 present a comparison between the electron density and space potential evolution during photodetachment of electrons from the negative ions. The measurements were independently done at the same location by inserting the emissive and the hairpin probes one after the other using a manually operated differentially pumped gate valve.

The gate valve placed in the path of the probes feedthrough allowed the probes to be taken out without disrupting the vacuum in the main plasma chamber. The experimental conditions such as power, pressure (via gas flow rate) and the pumping speed was maintained constant throughout the experiment.

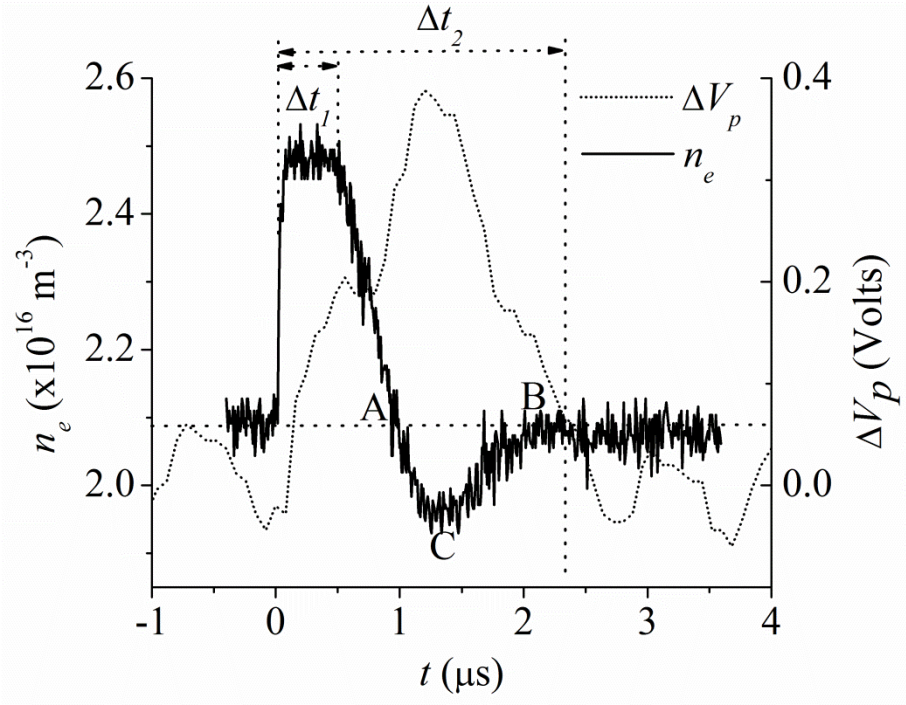

Figure 5.20: Comparison of the temporal evolution of the change in plasma potential and electron density during pulsed laser photo detachment of negative ions. The laser energy density is set to 2000 J/m^2 at 532 nm. The rf power for this experiment is set to 200 W at 25 mTorr operating pressure. The laser is injected at time t = 0 s.

Looking at figure 5.20 we observe a clear delay between the rise and fall times of the electron density and the plasma potential. For discussing different phases, we label the specific electron density profile by A, B and C. The points A & B on the density plot correspond to the unperturbed electron density during $t < 0$ s. Between points A and B we observe the electron density to drop below the equilibrium value and exhibit a minimum at C. The minimum electron density value at C coincides with the peak in ΔV_p.

Coincidence between the density minimum and peak plasma potential observed in figure 5.20 confirms the idea that the potential maximum is created because of an excess loss of electrons from the electropositive plasma channel. The local electric field created between the electropositive channel and the surrounding plasma tends to enhance the inward flux of negative ions into the laser illuminated region. Therefore the

peak in ΔVp may be considered as the demarcation point between the thermal diffusion of negative ions and the fast negative ions due to the creation of the ambipolar electric field.

5.6.6 Estimation of the negative ion temperature from the space potential evolution

Before proceeding to the comparison between the negative ion thermal speed obtained by two techniques (namely electron density evolution and plasma potential evolution), it is necessary to model how the plasma potential evolution is related to the negative ion thermal speed. The rise in plasma potential buildup in the initial phase results in accelerating negative ions towards the centre of the electropositive plasma. After starting from their thermal speed, these negative ions eventually reach some equilibrium speed because of ΔV_p.

In the simplest case, when assuming no collisions, we can express the kinetic energy gained by the negative ions at the expense of $e\Delta V_p$. Hence,

$$\frac{1}{2} m_{-} v_{-}^2 - \frac{1}{2} m_{-} v_{th-}^2 = e\Delta V_p \tag{5.4}$$

Where v_{-} is the velocity of the negative ions due to the potential difference ΔV_p created between the illuminated region and the background after detachment, whereas v_{th-} is the actual thermal velocity of negative ions of mass m_{-}. Thus rearranging equation (5.4),

$$\frac{v_{th-}}{v_{-}} = \left(1 - \frac{2e\Delta V_p}{M v_{-}^2}\right)^{\frac{1}{2}} \tag{5.5}$$

From the above equation, one can estimate the actual value of the negative ion thermal speed v_{th-} by substituting ΔV_p obtained using the emissive probe. On the other hand, v_{-} can be estimated from the time taken for the plasma potential to decay from its peak to its equilibrium value by ions situated at a distance 3.0 mm just outside the beam radius.

5.6.7 Negative ion temperature: Space potential verses density evolution

A comparison of the negative ion thermal speed obtained independently via the electron density evolution and the plasma potential evolution (equation (5.5)) is shown in figure 5.21. The thermal speed of negative ions obtained using the electron density evolution in figure 5.17 is calculated by considering Δt_2 which corresponds to the minimum speed of the negative ions. Figure 5.21 shows that the thermal speed is

consistently lower when evaluated using the time scale determined from the plasma potential variation as based on discussions in previous sections.

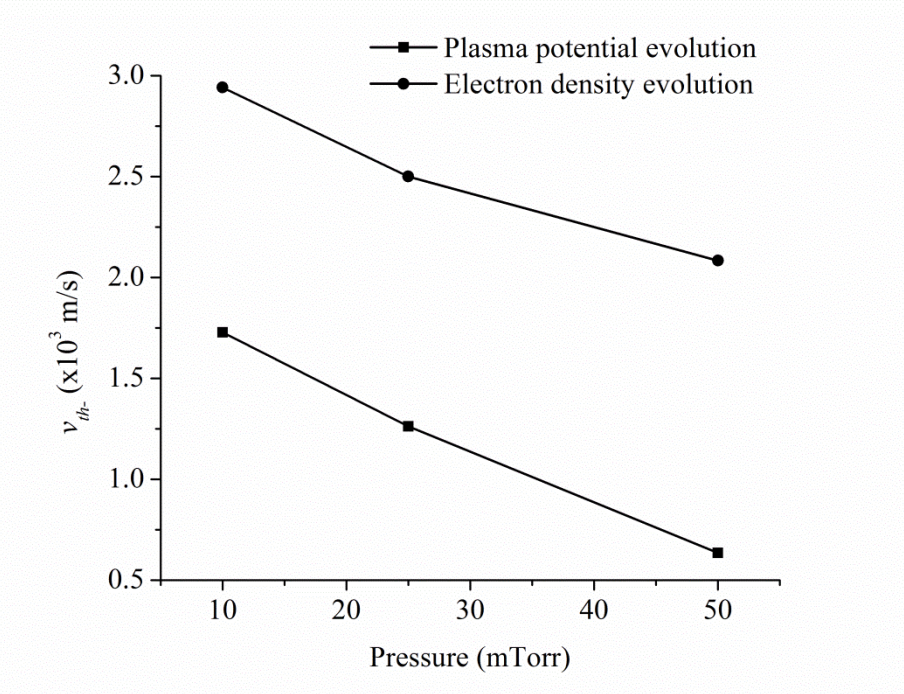

Figure 5.21: Plot of the thermal speed of negative ions obtained by the electron density and the plasma potential evolution verses operating pressure. The laser energy density is set to 2000 J/m^2 at 532 nm. The rf power for this experiment is set to be 200 W

Assuming O^- as the dominant negative ion in the plasma, which is valid for RF oxygen discharges [Stoffels 1995], the negative ion temperature and electron temperature are plotted in figure 5.22 (a) and (b) respectively. The electron temperature is obtained from the emissive probe prior to detachment. The main highlights of figure 5.22 are that both negative ion and electron temperature decrease with pressure [Lieberman and Lichtenberg, 2005] giving a ratio $\gamma = T_e/T_-$ of nearly 20 and 100 at 10mTorr and 50mTorr respectively.

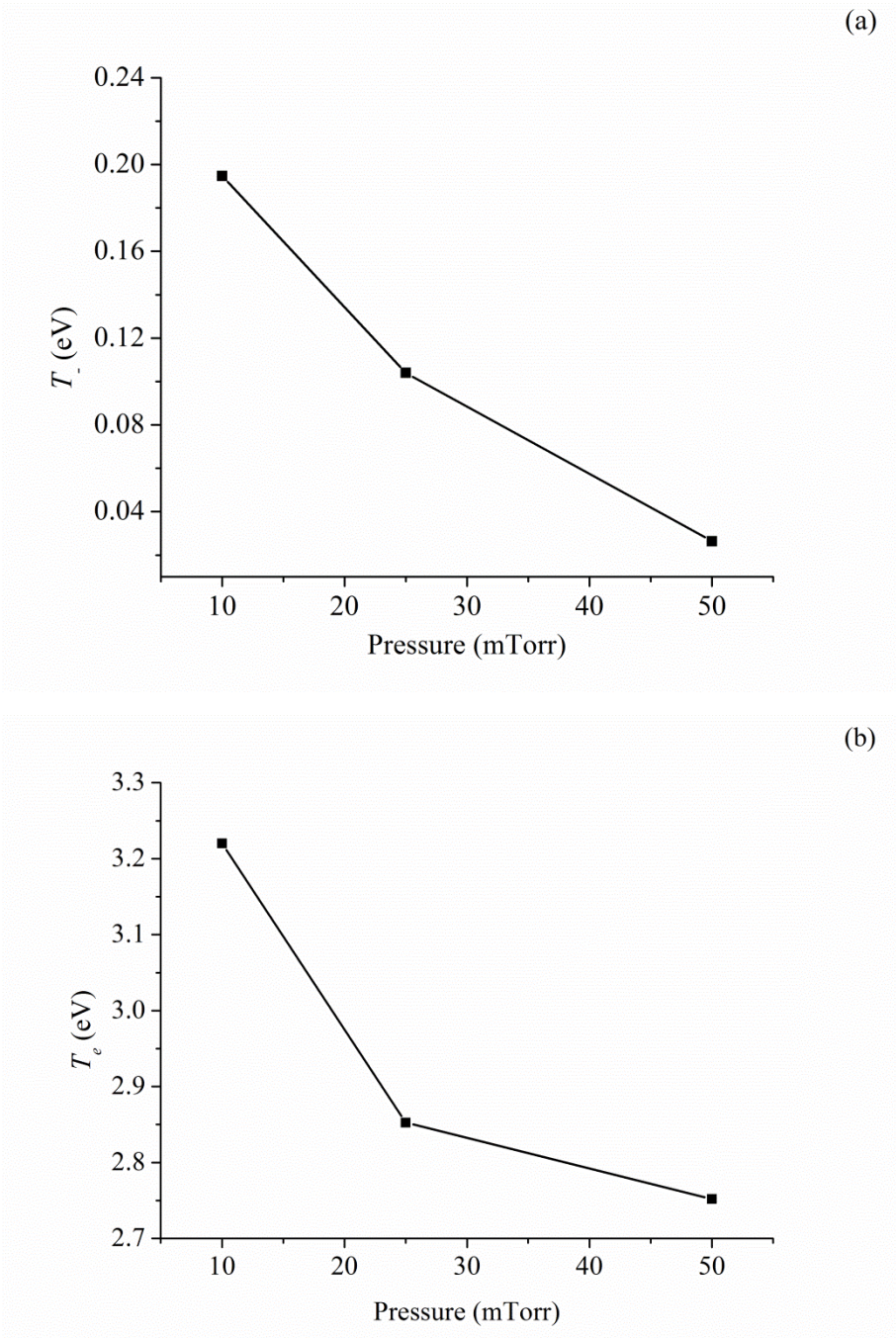

Figure 5.22: Plot of (a) the negative ion temperature (O^-) (b) the electron temperature verses operating pressure. Laser energy density is set to 2000 J/m^2 at 532 nm. The rf power for this experiment is set to 200 W.

Finally, figure 5.23 shows a comparison between the electronegativity and the maximum change in the plasma potential. It is clear from the graph that the maximum change in the plasma potential in the illuminated region increases with increases in the electronegativity α. This is true because a higher electronegativity produces a high number of photodetached electrons in the laser illuminated region, and hence a higher plasma potential is needed to confine them. Therefore for high electronegativities if one

neglects the ambipolar potential, a significant error in estimating the negative ion thermal speed can occur. Using particle-in-cell simulation with a one-dimensional slab model [Mizuno, 2007] it has been shown that for $\alpha > 0.1$ ambipolar electric fields cannot be neglected when estimating the negative ion thermal speed using the electron density recovery or by two laser photodetachment. Thus we propose the use of the emissive probe to measure the negative ion thermal speed.

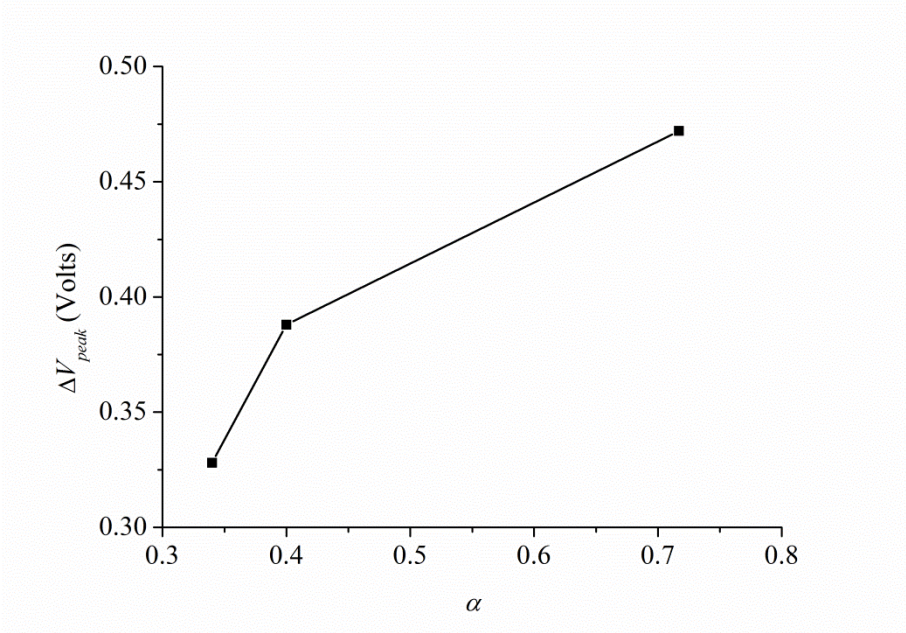

Figure 5.23: Plot of the maximum change in the plasma potential and electronegativity verses operating pressure. Laser energy density is set to 2000 J/m^2 at 532 nm. The rf power for this experiment is set to 200 W.

5.7 Summary and Conclusions

In this chapter we systematically investigated the hairpin probe to measuring the negative ion density and its temperature with laser photodetachment. Although the photodetachment technique is a well known technique routinely applied in conjunction with a biased Langmuir probe, it has certain limitations when applied to magnetized plasmas. It is shown for the first time that the hairpin probe can be used in conjunction with pulsed photodetachment for obtaining the electronegativity in steady state as well as time-resolved as in the case of a pulsed dc magnetron plasma.

However, we also discussed certain issues related to the application of the hairpin when applied in conjunction with laser photodetachment. The primary problem

is related to the physical size of the probe as the alignment is tricky. In this study we addressed this problem by aligning the pins off-line of sight to the beam. This has the advantage that ablation from the probe surface can be avoided. We presented a systematic study of the electron density dynamics at different radial distances from the region of detachment. It is understood that the electrons created by photodetachment along the beam will diffuse outwards at a characteristic time-scale determined by the temperature of the negative ions. In principle one can determine the negative ion temperature. This technique was primarily applied by Bacal [Bacal 2000] with the help of a Langmuir probe. However the ambipolar electric field created at the axis of the laser beam during photodetachment has been completely neglected until now, which can cause an overestimation in the measured negative ion temperature by this technique.

In order to highlight the above limitations we performed a plasma potential measurement using an emissive probe. The plasma potential is clearly seen to be rising with the photodetachment of electrons from negative ions. This is an indication that the electrons are quickly thermalized, which then tends to escape from the electropositive plasma channel. The estimated thermal speed of negative ions from the plasma potential evolution is found to be lower than those obtained from the electron density evolution. The potential evolution clearly show the presence of an ambipolar electric field which was ignored earlier. Thus we propose to use the temporal evolution of the plasma potential to measure the negative ion thermal speed when the electronegativity is high. However, for low electronegativities (α < 0.1) the ambipolar electric field can be neglected and the hairpin probe can be used to measure the negative ion temperatures as well with laser photodetachment.

Based on the above technique we presented systematic study of negative ion parameters in the case of a steady state oxygen plasma in an ICP reactor. The temporal evolution of the electronegativity is also presented in the case of a pulsed dc magnetron discharge. The results are found to be in good agreement with the expected behavior of electronegativity, and were found to be consistent with the power and pressure variations present within the literature.

Chapter 6

Stimulated hairpin probe for electronegative plasma diagnostic

Pulsed induced laser photodetachment discussed in the previous chapter involved sophisticated optical alignment for focussing the laser beam into the plasma. Direct exposure of the intense laser onto the probe placed in the path of the laser beam can ablate material from the probe's surface and thereby unwanted impurities may be introduced into the plasma. Deposition on optical windows can also affect the performance of photodetachment due to scattering of the beam.

In this chapter we present a novel method of using the hairpin probe independently for measuring the negative ion parameters. The technique is based on stimulating the hairpin by repetitive pulsed bias of the hairpin to large negative potentials. The negative ion parameters are obtained from the dynamic measurement of the temporal electron density profiles. The details are presented in the following sections.

6.1 Basic principle

Plasma always tends to remain quasineutral. Any disturbance created via an electrically biased object leads to the break in the quasineutrality locally around the object. The perturbation can be several Debye lengths depending on the applied negative potential. In the negative ion plasmas, the positive charge density is balanced by the negative ion density and the electron density. Because of the vast disparity between mobility of the electrons and negative ions, the response of charged particles to shield the opposing charge lags with significant time delays.

Based on the above argument a large negative potential is applied to the hairpin that displaces the negative ions and electrons from the vicinity of the probe. This is in contrast to the laser photodetachment technique where the pulsed laser annihilates negative ions. The region around the probe is mainly dominated by the positive ion sheath with negligible negative charge particles if a sufficient bias has been applied. This is in contrast to the electron-positive ion plasma region created by the application of pulsed laser photodetachment. When the pulsed potential is removed swiftly at a time

scale $(\omega_{pe})^{-1} < \tau_{period}$, the electrons are the only species which will immediately respond to shield the negative potential. This will result in the observation of a peak in electron density compared with the steady-state as the electrons will immediately respond to shield the positive space charge around the probe. Hence the peak electron density is a measure of the positive ion density based on the assumption that the plasma is quasineutral. Once the background positive ion density is obtained, subtracting the equilibrium electron density from it gives the measure of the negative ion density.

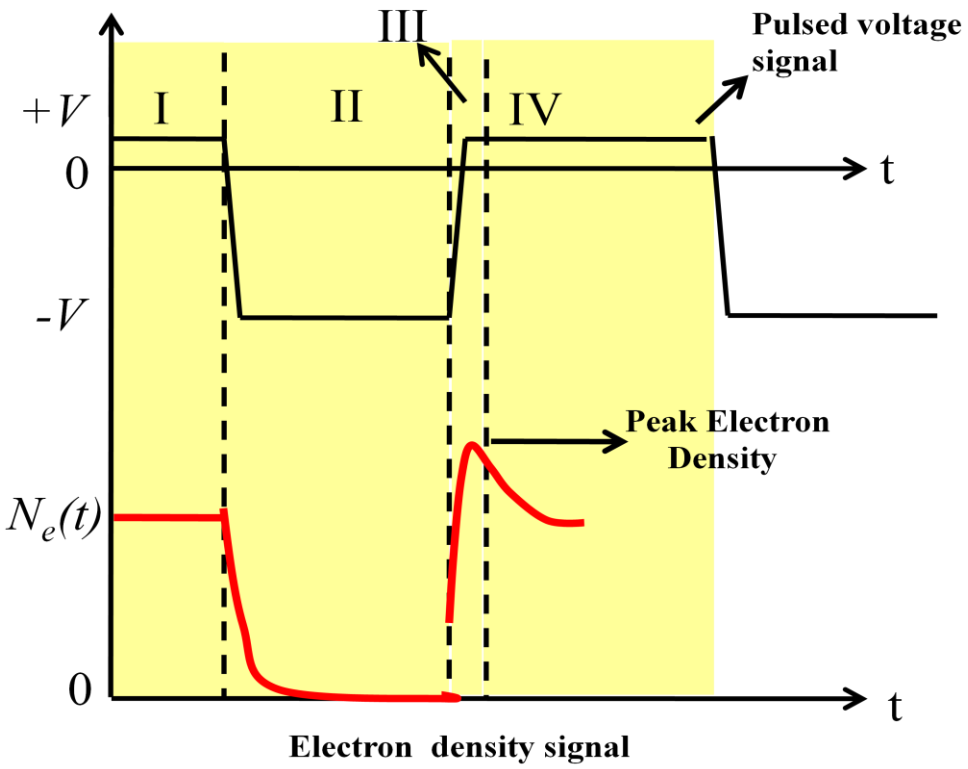

Figure 6.1: Pulsed voltage signal and the expected change in the electron density during each phase of the pulse applied to the hairpin probe.

In figure 6.1 a sequence of negative voltage pulses is applied while the instantaneous electron density feature is shown schematically. The different phases of the voltage waveform are marked as Phase I, II, III and IV.

The phase I of the pulse is the positive potential phase when the sheath around the hairpin is almost zero. Therefore the electron density corresponding to this phase is the background electron density in the plasma in equilibrium with the positive ions and negative ions. i.e.

$n_{+0} = n_{-0} + n_{e0}$

In phase II, the potential falls sharply to certain negative values. All the negative charged species including the negative ions and the electrons are removed leading to the observed drop in the electron density.

The overshoot in the electron density, as discussed earlier, corresponds to the phase III conjunction with the removal of the negative potential. The peak electron density is the measure of the positive ion density as the electrons are mainly responsible for shielding the positive ions i.e.

$(n_e)_{peak} = n_{+0}$

In the off-phase, the negative ions move towards the probe after $\tau_{off} >> (\omega_n)^{-1}$ while the peak in the electron density gradually reaches the equilibrium background electron density.

Hence the negative ion density is obtained by subtracting the background electron density from the peak electron density

$n_{-0} = (n_e)_{peak} - n_{e0}$

The decay in the electron density also contains information about the negative ion thermal velocity as in the case of photodetachment. As discussed before, the decay of peak electron is mainly due to the diffusion of the negative ions from the surrounding volume. Hence by taking diffusion time the thermal velocity of the negative ions can be estimated as,

$$v_{th-} = \frac{h}{t_{diff}} \tag{6.1}$$

Where h is the half width of the hairpin probe and t_{diff} is the time of diffusion of peak electron density to background electron density. Collisions between the particles are completely neglected in the above calculation.

6.2 Experimental setup

For validating the above concept, the pulsed negative potential is applied to the hairpin immersed in an inductive discharge setup described in section 3.3.3. One time the hairpin was subjected to a pure electropositive argon discharge while the same experiment was repeated for an electronegative O_2 plasma.

The hairpin probe was comprised of a mechanism for electrically biasing the probe tip in the plasma. An Agilent 33250A arbitrary waveform generator was used for producing a pulsed waveform of a few KHz frequencies and variable duty cycle. The output is connected to the high voltage amplifier (WMA-280) which gives a

corresponding amplified voltage output to ±100 Volts. An L-shape hairpin probe of length 26 mm and width 3 mm is inserted through one of the radial ports of the chamber. For time resolved electron density measurements we have used the automated technique. This technique incorporates a LabVIEW program for incrementing the output frequency of a commercial microwave oscillator (HP8350B). The software helps to increment the applied microwave frequency in steps of prescribed value, $\Delta f = (f_e - f_i)/n$, where $f_i < f_0 < f_r < f_e$ and where n is the number of steps; and register the reflected signal amplitude which is converted into a dc signal corresponding to each frequency. For increasing signal to noise ratio the dc level at each frequency is subtracted from the signal.

6.3 Results and discussions

Before performing experiments it is important to understand and fix the applied pulse parameters. A pulsed voltage waveform is mainly described by its basic parameters namely the rise time, duty cycle, pulse period and its amplitude. A square waveform is used in this experiment because of its symmetrical behaviour and easily determined phase and antiphase boundary. The rise time of the pulse is another important parameter which is chosen in such a way that it can resolve the thermal motion of the electrons and negative ions when the negative pulse voltage is removed from the hairpin probe. The response time of the electrons is typically of the order of a nanosecond for laboratory plasmas whereas the negative ions respond on microsecond time scales (as experimentally found in previous chapters). Thus pulse rise time is fixed for a few nanoseconds to distinguish between the thermal motion of electrons and negative ions.

The choice of the pulse width defines the depletion of the negative charged species from the vicinity of the hairpin probe. The duration of the pulse must be greater than the time scale at which the sheath is fully established. Typically the pulse width chosen was 0.5ms; many orders greater than the typical collision rate. The choice of 0.5ms will give sufficient time for the negative ions to be displaced from the region around the probe. Last, and the most important pulse parameter, is its magnitude. The magnitude of the pulse voltage defines the sheath dimension around the hairpin prongs. As discussed in chapter 4 the sheath width is large for larger biases and decreases with increases in the electronegativity of the plasma.

Figure 6.2 shows the measurement of the time-resolved resonance frequency of the hairpin probe during an applied negative pulse voltage on the hairpin probe in an oxygen discharge. Operating conditions for the oxygen discharge were 35mTorr operating pressure at 400Watt ICP power. The amplitude of the pulsed voltage is set to be -80 volts while the rest of the parameters are the same as discussed above. The corresponding electron density plot for oxygen and argon is shown in figure 6.3. The argon discharge is produced at 35 mTorr operating pressure and 200Watt ICP power. As expected no overshoot in electron density was observed on removal of the applied negative pulse for the electropositive argon plasma while a distinct peak is observed in the case of the electronegative oxygen plasma confirming the principle behind the technique. From the electron density overshoot, the negative ion density was calculated and found to be approximately $2.68*10^{15}$ m^{-3}. Whereas the positive ions are measured to be $5.498*10^{16}$ m^{-3} and the corresponding electron density is $5.230*10^{16}$ m^{-3}. However these densities are not absolute because the basic principle behind this technique says that the electron density should go to zero (figure 6.1) which is not the case in this experiment (figure 6.3). One of the possible reasons is partially formed sheath around the resonator prongs and discussed later in this chapter.

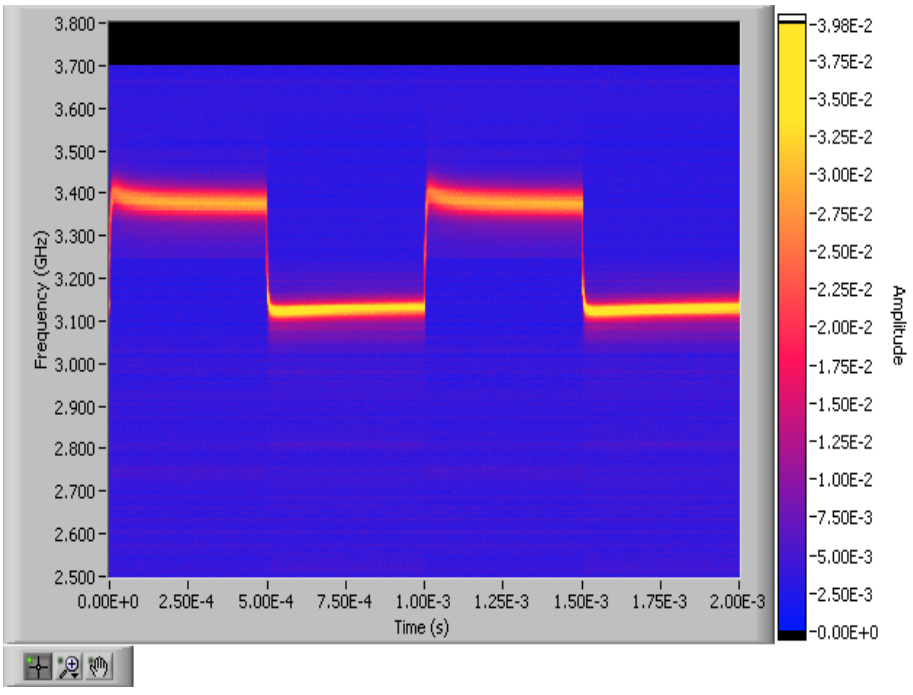

Figure 6.2: Time resolved resonance frequency of the hairpin probe during an applied negative pulse voltage in oxygen plasmas. Pulsed voltage applied to the hairpin probe is -80 volts with a frequency of 1 KHz.

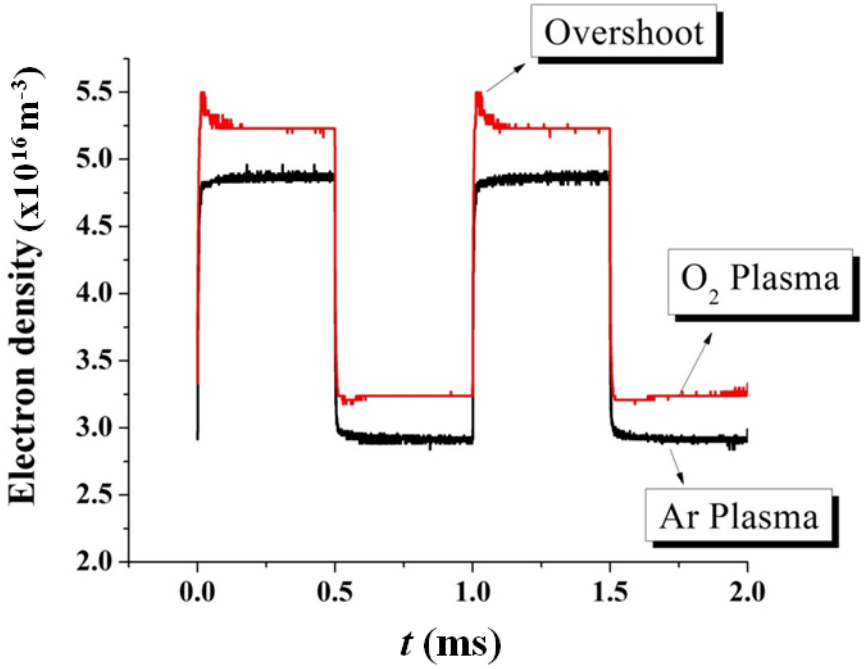

Figure 6.3: Time resolved electron density in argon and oxygen plasmas. Pulsed voltage applied to the hairpin probe is -80 Volts having a frequency of 1 KHz. Operating conditions for O_2 plasma and Ar plasma are 35mT/400W and 35mT/200W respectively.

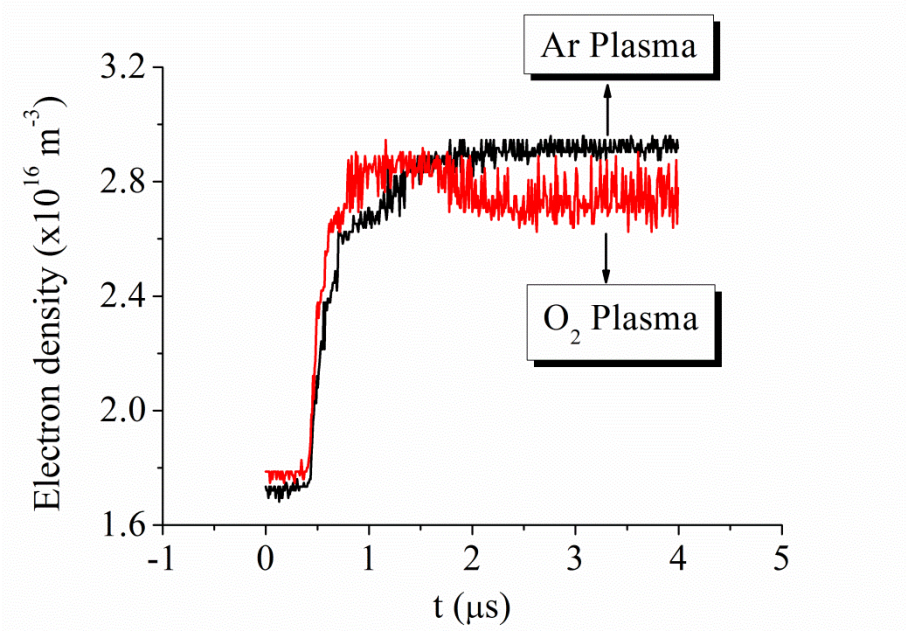

Figure 6.4: Time resolved electron density in argon and oxygen plasmas. Pulsed voltage applied to hairpin probe is -80 Volts having a frequency of 1 KHz. Operating conditions for the O_2 plasma and Ar plasma are 30mT/300W and 30mT/100W respectively.

To confirm further the validity of the technique, the same experiment is repeated with a slight change in the operating conditions of the discharge. The measurement was mainly focused during the starting phase of the pulse. Figure 6.4 shows the comparison of the time resolved electron density measurement by the hairpin probe in oxygen and argon discharges produced at 300W/30mT and 100W/30mT respectively. The experimental result at this operating condition consistently shows an electron density overshoot at the instant of removal of the negative potential from the hairpin probe. The characteristic overshoot in electron density resembles in some form with the photodetached electron density obtained in the laser photodetachment experiment in chapter 6. By hypothesis the positive ion density corresponds to the electron density peak obtained to be $2.8637*10^{16}$ m^{-3} while the steady state electron density in the long off phase is $2.7243*10^{16}$ m^{-3}. The difference gives the negative ion density of the order of $1.394*10^{15}$ m^{-3}.

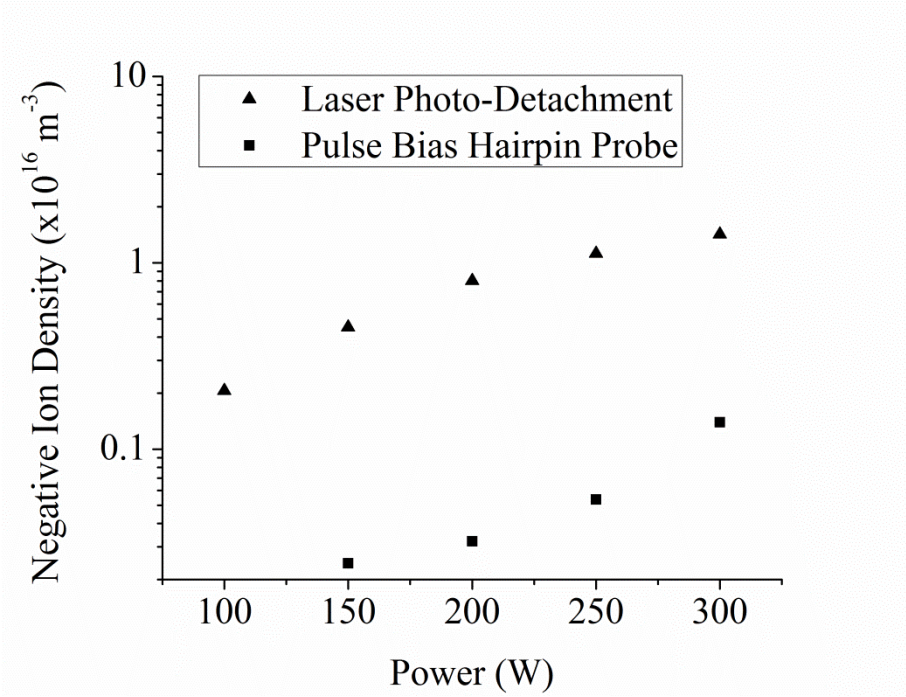

Figure 6.5: Negative ion density measured by pulse biased hairpin probe and hairpin probe assisted laser photodetachment as a function of ICP power in O_2 plasma operating at 30mT. Pulsed voltage applied to the hairpin probe is -80 Volts with a frequency of 1 KHz.

Using the above method, systematic experiments with the pulsed hairpin probe was carried out for various ICP powers and the results compared with those obtained

using pulsed laser photodetachment in conjunction with the hairpin probe. The negative ion density can be varied by changing the ICP power at fixed pressure (figure 5.10) whereas at fixed ICP power changing the pressure from 5-90mTorr the negative ion density change is very small (figure 5.12a). Thus the operating pressure was kept constant at 30mTorr corresponding to maximum negative ion production.

Figure 6.5 shows the comparison of the absolute negative ion density measured by the two independent techniques involving the pulse biased hairpin probe and laser photodetachment under identical operating condition. As observed in figure 6.5, both techniques show an increase in the negative ion density with ICP power. Increases in the electron density with ICP power increases the dissociative attachment therefore increasing the negative ion density. However the negative ion density obtained with the pulse bias technique underestimates the density by a factor of 10 less than those obtained by the photodetachment method. Despite this, both laser photodetachment and pulse bias hairpin probe shows a ~80% change in the negative ion density with rf power varied from 150 W to 300W.

The reason for the observed underestimated negative ion density can be explained on the basis of a partial or fully formed sheath around the hairpin. For the experiment described the maximum applied voltage was - 80Volts. The sheath thickness (figure 4.8) obtained from the theoretical model for cylindrical probes in chapter 4 require values of α and γ. These values can be taken from the photodetachment experiment. For example at 200 watt ICP power and 30 mTorr operating pressure the values of α and γ are 0.34 and 30 respectively (see figure 5.11, 5.22a and 5.22b). Using these values the model equation governing the sheath surrounding the cylindrical probes can be solved [c.f. chapter 4]. It gives the sheath thickness of near about 0.7mm. Thus at 200W ICP power and 30mTorr operating pressure the sheath thickness on each limb of the hairpin probe is 0.7mm. This is nearly half the width of the hairpin probe (~1.5mm) used in this experiment. However the basic principle assumes that the sheaths around the hairpin must be completely overlapping. Therefore one should reduce the separation between the pins to a reasonable distance for the technique to work precisely, or increase the magnitude of the bias voltage.

The thermal speed of negative ions is obtained from the time scale of the decay in electron density peak. At 30mTorr the decay time for the electron density to reach the background electron density is 0.6μs and found to be constant with ICP power. Considering the half width of the hairpin probe (~1.5mm), the thermal speed of negative ions is estimated to be ~2.5×10^3 m/s. The magnitude of the thermal speed of negative

ions obtained by the above technique at this operating pressure is somewhat higher than the one measured by the plasma potential evolution (~$1.2x10^3$ m/s) as shown in figure 5.21. However considering negative ions responding to the probe surface from the distance equivalent to the typical sheath width of approximately 0.7mm we obtained reasonably good agreement as the thermal speed of negative ions increased to ~$1.6x10^3$ m/s comparable to those obtained from the plasma potential evolution (figure 5.21) discussed in chapter-5. Thus in equation 6.1 the half width should be replaced by the sheath thickness obtained in our conditions i.e. 0.7 mm.

6.4 Summary and Conclusions

In conclusion we presented a novel use of pulsed bias hairpin for the diagnostic of negative ions in an electronegative discharge. Preliminary results comparing the time resolved electron density in the electronegative plasma with that of the electropositive plasma confirmed that the overshoot is due to the presence of negative ions in the plasma. With this method the electron density, negative ion density, positive ion density and negative ion temperature can be obtained in electronegative plasmas. This is an independent diagnostic technique as it does not require expensive and cumbersome laser photodetachment equipment. The negative potential is easy to apply also in the case of dielectric shielded probes by means of capacitive coupling with a 1 MHz signal in short transient bursts as typically also applied for ion-flux probes [Braithwaite 1996]. The perturbation to the plasma is also small as compared with positive biased probes. The technique is simple as the density is calculated using quasineutral approximations. Despite many advantages, this technique has some drawbacks. One of the limitations of this technique is that it is not species selective when multiple negative ions are present. As in the case of photodetachment experiments, it is possible by tuning the laser frequency corresponding to the detachment energy of selected negative ions.

The negative ion density measured in an O_2 discharge shows an increase in the negative ion density with ICP power. However the values were underestimated when compared with the hairpin probe assisted laser photodetachment. By evaluating the sheath dimension it is validated that the underestimation in the measured negative ion density is mainly due to low bias potential. Although the results were limited to low bias potential it suggests that the pulse bias hairpin probe can be used for relative measurements of negative ion density in electronegative plasmas. Thus it can be used to characterize the electronegative plasma discharges with using a laser. However for

absolute measurements, one should be careful about the magnitude of the sheath potential. The negative ion thermal velocity is also estimated and found to be higher than the one calculated by the plasma potential evolution. However when the correct sheath dimension is used it gives reasonably good agreement with that obtained using the photodetachment method.

Chapter7

Summary, conclusions and future prospects

7.1 Summary and conclusions

In this thesis we presented practical applications of resonance hairpin probes for characterizing electronegative discharges. The key parameters, namely the negative ion density and its characteristic temperature, are obtained in a steady state inductively coupled oxygen discharge. Time resolved negative ion parameters were obtained in a pulsed dc magnetron source at the University of Liverpool. The principal technique investigated is the use of resonance hairpin probes in conjunction with pulsed laser photodetachment. The hairpin probe provided the principle role for measuring spatial and temporal electron density evolution in the photodetached channel. As compared to the use of conventional Langmuir probes, the hairpin has the following advantages. Firstly, one can directly obtain the temporal value of the absolute electron density. Another advantage is that one can apply it in depositing plasmas and also in plasma systems where the reference electrode is unavailable or poorly conducting. For avoiding ablation from the probes surface we have systematically investigated the electron density measured outside the photodetached region and related it to the density measured in the illuminated column. It is found that if one can perform a certain calibration, it is possible to relate the negative ion density from the electron density response at some distance outside the photodetached region. These results are discussed in chapter 5.

The use of laser photodetachment and Langmuir probes has been extensively used for the measurement of the negative ion temperature. Here for the first time we have applied a hairpin to the measurement of the negative ion temperature in an oxygen discharge. One of the important facts revealed from the systematic experiment is that the negative ions are being accelerated because of a potential difference created between the electropositive plasma channel and background electronegative plasma measured by a floating emissive probe. The experimental results show the peak plasma potential coinciding with the dip in the electron density. A positive potential is required for stopping the loss of fast electrons from the electropositive plasma channel. We have also discussed the use of emissive probes for obtaining the negative ion temperature and compared these results with those obtained from the temporal evolution of the electron density using the hairpin probe. The negative ion temperature obtained from the decay

in the electron density peak was found to be higher (~40%) than those obtained from the temporal evolution of the plasma potential. These results are presented in chapter 5. The final chapter of the thesis describes the basic principle and application of a pulsed bias hairpin probe for characterizing negative ion parameters. In this technique we have applied a sequence of strong negative dc biases to the hairpin, strong enough to remove negative ions from the vicinity of the hairpins. On removal of the external bias, one expects the quasineutrality condition to be quickly established, first primarily by electrons and then followed by negative ions. With the help of time-resolved measurement of the electron density, we can identify the presence of negative ions by subtracting the background electron density from the electron density obtained on removal of the external bias. The same technique also allows the determination of the negative ion temperature from the state at which the electron density returns to equilibrium. We have validated the underlying principle based on preliminary experiments performed in an oxygen ICP discharge. Because of limitations of the power rating of the pulsing negative biasing supply, the applied negative bias was limited to -80 V. Therefore absolute measurements were not possible but the relative measurements are found to be in reasonably better agreement as compared with those obtained from laser photodetachment.

The thesis also addressed some key issues concerning accuracy of the electron density measurement over a wide range. As found at low density (below 10^{16} m^{-3}), the sheath sizes can be comparable with the separation between the pins. This limitation was addressed by Peijak et al [Piejak 2004] who proposed an analytical expression for sheath correction. This analytical expression is based on finding the sheath width using a theoretical sheath model (step front sheath model as proposed by Piejak) and thus requires information of the electron density and electron temperature. A technique based on a negative dc biased hairpin probe is investigated to overcome this limitation. In this technique the sheath width is estimated by the well know Child-Langmuir sheath model from the measured current and voltage. The sheath correction in the raw densities obtained by the negative dc biased hairpin probe is compared with those obtained by the step front sheath model and gives reasonably good agreement. On the other hand the sheaths can be purposely created around the resonator pins by a negative dc bias in order to stretch the higher orders of the measured density with the available limited range of the frequency from the hairpin microwave generator. Thus the technique of measuring a high plasma density (>10^{18} m^{-3}) is proposed.

7.2 Future prospects

In this thesis we have addressed some important applications of the resonance hairpin probe for electronegative plasmas. Amongst different techniques discussed in the thesis are the use of dc and pulsed dc biasing techniques where the hairpin was externally biased with respect to the reference electrode. However for broader applicability one needs to address the technique in depositing plasmas when the electrode surface is poorly conducting. Similarly under the influence of large rf oscillation in plasma potential as in the case of symmetric capacitively coupled radio frequency discharges one has to appropriately treat the sheaths around the hairpin. One of the important applications of the pulsed bias hairpin is in the filter field region of negative ion source. The effect of strong magnetic field on electron density dynamics towards the hairpin on removal of high voltage pulse needs further investigation. Furthermore, the role of external magnetic field on the sheath structure, anisotropy in plasma permittivity because of the presence of magnetic field needs systematic investigation and requires 3d simulation of the electric field structure around the hairpin.

The pulsed dc biasing technique shows good agreement with laser photodetachment. However variation in absolute densities by a factor of 10 lower than those obtained (shown in figure (6.5)) by pulsed photodetachment. This is attributed due to partially formed sheath around the hairpin resonator. This is confirmed by estimating the sheath width using the theoretical sheath model (discussed in chapter 4). This limitation can be overcome by increasing the magnitude of the pulsed voltage or by decreasing the width of the resonator. The extent to which this can be done considering practical applications is the subject of future research. The effect of pulse parameters like pulse width, width of the hairpin probe on sheath structure needs further investigation for explaining the diffusion of charged particles in case of multi-component negative ion species . However an important question needs to be addressed is whether it is possible to achieve zero electron density with negative dc bias or not?

The technique described for the sheath correction (in chapter 3) is based on the simultaneous measurement of resonance frequency and positive ion current with different probe bias. The positive ion current and resonance frequency is a function of the electron density, electron temperature and plasma potential. Once the corrected electron density is obtained it is also possible to estimate the average electron

temperature and plasma potential from the measured value of the ion current and resonance frequency. Thus the future work shall aim in modelling positive ion current and resonance frequency as a function of these parameters.

Bibliography

Allen J E, *A note on the Bohm criterion for electronegative gases*, Plasma sources sci. Technol. Vol. **13**: 48, 2004.

Amemiya H, Annartone B M and Allen J E, *The collection of positive ions by spherical and cylindrical probes in electronegative plasma*, Plasma sources sci. Technol. Vol. **8**: 179, 1999.

Amemiya H, *Plasmas with negative ions-probe measurements and charge equilibrium,* J. Phys. D: Appl. Phys. Vol. **23**: 999, 1990.

Bacal M, *Photo-detachment diagnostic techniques for measuring negative ion densities and temperatures in plasmas*, Rev. Sci. Instrum. Vol. **71**: 3981, 2000.

Boilson D et al., Fusion Engineering and Design Vol. **74**: 295, 2005.

Booth J P, Corr C S, Curley G A, Jolly J, Guillon J and Földes T, *Fluorine negative ion density measurement in a dual-frequency capacitive plasma etch reactor by cavity ring-down spectroscopy,* Appl. Phys. Lett. Vol. **88**: 151502, 2006.

Braithwaite N St J and Allen J E, *Boundaries and probes in electronegative plasmas*, J. Phys. D: Appl. Phys. Vol. **21**: 1733, 1988.

Braithwaite N St J, Booth J P and Cunge G, *A novel electrostatic probe method for ion flux measurements*, Plasma Sources Sci. Technol. Vol. **5**: 677, 1996.

Chabert P, *Electronegative plasma moto*r, US2008/0271430 A1, 2007.

Chabert P and Braithwaite N St J, *Physics of radio-frequency plasmas*, Cambridge university press, 2011.

Chabert P, Plihon N, Corr C S, Raimbault J-L, and Lichtenberg A J, *Equilibrium model for two low-pressure electronegative plasmas connected by a double layer*, Physics of Plasmas Vol. **13**: 093504, 2006.

Chabert P, Sheridan T E, Boswell R W and Perrin J, *Electrostatic probe measurement of the negative ion fraction in an SF6 helicon discharge*, Plasma Sources Sci. Technol. Vol. **8**: 561, 1999.

Chung T H, *Sheath structure for cylindrical probe in low-pressure electronegative discharges*, Phys. Plasmas Vol. 13: 024501, 2006.

Conway J, Sirse N, Karkari S K and Turner M M, *Using the resonance hairpin probe and pulsed photo-detachment technique as a diagnostic for negative ions in oxygen plasma,* Plasma Sources Sci. Technol. Vol. **19**: 065002, 2010.

Crespo R M, Palop J I F, Hernandez M A, Pino S B D, Diaz-Cabrera J M and Ballesteros J, *Floating potential and sheath thickness for cylindrical and spherical probes in electronegative plasmas*, J. Appl. Phys. Vol. **99**: 053303, 2006.

Curley G A, *The dynamics of charged particles in a dual frequency capacitively coupled dielectric etch reactor*, PhD thesis, Ecole Polytechnique France, 2008.

Curley G A, Gatilova L, Guilet S, Bouchoule S, Booth J P, Gogna G S, Sirse N and Karkari S K, *Surface loss rates of H and Cl atoms in an inductively coupled plasma etcher using time-resolved electron density and optical emission measurements*, J. Vac. Sci. Tech. A Vol. **28:** 360, 2010.

Devynck P, Auvray J, Bacal M, Berlemont P, Brunetueau J, Leroy R and Stern R A, *Photodetachment technique for measuring H^- velocities in a hydrogen plasma*, Rev. Sci. Instrum. Vol. **60**: 2873, 1989.

Dodd R, You S D and Bradley J W, *O^- density measurements in the pulsed-dc reactive magnetron sputtering of titanium*, Thin solid films Vol. **519**:1705, 2010.

Franklin R N, *The equations for electronegative plasmas are not singular at the plasma centre at low pressures*, J. Phys. D: Appl. Phys. Vol. **38**: 2790, 2005.

Franklin R N, *The plasma-wall boundary region in negative-ion-dominated plasmas at low pressures*, Plasma sources sci. Technol. Vol. **9**: 191, 2000.

Franklin R N and Snell J, *Are the oscillations found in electronegative plasmas at low pressure an artefact?* , J. Phys. D: Appl. Phys. Vol. **33**: 1990, 2000.

Flamm D L, *Mechanisms of silicon etching in fluorine- and chlorine-containing plasmas*, Report UCB/ERL M90/41, College of Engineering, University of California, Berkeley, 1990.

Gogna G S and Karkari S K, *Microwave resonances of a hairpin probe in a magnetized plasma*, Appl. Phys. Lett. Vol. **96**: 151503, 2010.

Grabowski C, Gahl J M and Schamiloglu E, *Initial Plasma-Filled Backward-Wave Oscillator Experiments Using a Cathode-Mounted Plasma Prefill Source***,** IEEE Trans. Plasma Sci. Vol. **26**: 653–68, 1998.

Haas F A, AL-Kuzee J and Braithwaite N St J, *Electron and ion sheath effects on a microwave "hairpin" probe*, Appl. Phys. Lett. Vol. **87**: 201503, 2005.

Heald M A and Wharton C B, *Plasma Diagnostics with Microwaves*; New York: Krieger Publishing, 1978.

Hebner G A and Abraham I C, *Characterization of electron and negative ion densities in fluorocarbon containing inductively driven plasmas*, J. Appl. Phys., Vol. **90**: 4929, 2001.

Howling A A, Sansonnens L, Dorier J L, and Hollenstein Ch., *Time-resolved measurements of highly polymerized negative ions in radio frequency silane plasma deposition experiments***,** J. Appl. Phys., Vol. **75**: 1340, 1994.

Kajita S, Kado S, Shikama T, Xiao B and Tanaka S, *Effect of probe surface ablation on laser photodetachment signals*, Contrib. Plasma Phys. Vol. 44: 607, 2004.

Karkari S K and Ellingboe A R, *Effect of radio-frequency power levels on electron density in a confined two-frequency capacitively-coupled plasma processing tool*, Appl. Phys. Lett. Vol. **88**: 101501, 2006.

Karkari S K, Ellingboe A R, Gaman C, Swindells I and Bradley J W, *A floating hairpin resonance probe technique for measuring time-resolved electron density in pulse discharge*, Meas. Sci. and Technol. Vol. **18:** 2649, 2007.

Karkari S K, Law V J and Ellingboe A R, *Design and performance of a floating hairpin resonance probe for measuring plasma density in radio-frequency discharges*, 27th ICPIG (Eindhoven, The Netherlands) Abstract No 08-168, 2005.

Karkari S K, Vetushka A and Bradley J W, *Measurement of the plasma potential adjacent to the substrate in a midfrequency bipolar pulsed magnetron*, J. Vac. Sci. Technol. A Vol. **21**: L28, 2003.

Kemp R F and Sellen J M, *Plasma Potential Measurements by Electron Emissive Probes*, Rev. Sci. Instrum. Vol. **37**: 455, 1966.

Kim J, Schamiloglu E, Martinez-Tovar B and Jungling K C, *Temporal measurement of plasma density variations above a semiconductor bridge (SCB)*, IEEE Trans. Instrum. Meas. vol. **44:** 843, 1995.

Kono A, *Intrinsic sheath edge conditions for sheath instability in low-pressure electronegative plasmas*, J. Phys. D: Appl. Phys. Vol. **36**: 465, 2003.

Kono A, *Complex sheath formation around a spherical electrode in electronegative plasmas: a comparison between a fluid model and a particle simulation*, J. Phys. D: Appl. Phys. Vol. **34**: 1083, 2001.

Lampe M, Manheimer W M, Fernsler R F, Slinker S P and Joyce G, *The physical and mathematical basis of stratification in electronegative plasmas*, Plasma Sources Sci. Technol. Vol. **13**: 15, 2004.

Lampe M, Manheimer W M, Fernsler R F, Slinker S P and Joyce G, *Comment on 'The equations for electronegative plasmas are not singular at the plasma centre at low pressures' by R N Franklin*, J. Phys. D: Appl. Phys. Vol. **39**: 3919, 2006.

Langmuir I and Blodgett K B, *Currents between coaxial cylinders*, Phys. Rev. Vol. **22**: 347, 1923.

Langmuir I and Mott-Smith H M, *Studies of Electric Discharges in Gases at Low pressures*, Gen. Elec. Rev. Vol. **27**: 449, 1924.

Lieberman M A and Lichtenberg A J, *Principles of Plasma Discharges and Materials Processing*, New York: Wiley, 2005.

Mizuno T, Hatayama A and Bacal M, *One-dimensional analysis of the effect of the ambipolar potential on the H^- ion density recovery after a laser photodetachment in the high density regime*, J. Phys. D: Appl. Phys. Vol. **40**: 168, 2007.

Mujawar M A, Karkari S K and Turner M M, *Properties of a differentially pumped constricted hollow anode plasma source*, Plasma Sources Sci. Technol. Vol. **20**: 015024, 2011.

Nishiura M, Sasao M, Wada M and Bacal M, *Plasma perturbation induced by laser photodetachment*, EPS conference on Contr. Fusion and Plasma Physics (Maastricht), ECA Vol. **23J**: 1369, 1999.

Piejak R B, *A dc biased hairpin resonator probes*, Gaseous Electronics Conf. (Shannon) **ES2.011**, 2004 a.

Piejak R B, Al-Kuzee J and Braithwaite N St J, *Hairpin resonator probe measurements in RF plasmas*, Plasma Sources Sci. Technol. Vol. **14**: 734, 2005.

Piejak R B, Godyak V A, Garner R, Alexandrovich B M and Sternberg N, *The hairpin resonator: A plasma density measuring technique revisited*, J. Appl. Phys. Vol. **95**: 3785, 2004.

Samukawa S, *Ultimate top-down etching processes for future nanoscale devices: Advanced neutral-beam etching*, Japanese Journal of Applied Physics Part-1 Regular Papers and Brief Communications and Review Paper Vol. **45** (4A): 2395, 2006.

Sands B L, Siefert N S and Ganguly B N, *Design and measurement considerations of hairpin resonator probes for determining electron number density in collisional plasmas*, Plasma Sources Sci. Technol. Vol. **16**: 716, 2007.

Sheehan J P and Hershkowitz N, *Emissive probes*, Plasma Sources Sci. Technol. Vol. **20**: 063001, 2011.

Sheridan T E, Chabert P and Boswell R W, *Positive ion flux from a low-pressure electronegative discharge*, Plasma sources sci. Technol. Vol. **8**: 457, 1999.

Shibata M, Nakano N and Makabe T, *The effect of laser-induced photodetachment in O_2 rf discharges*, J. Phys. D: Appl. Phys. Vol. **30**: 1219, 1997.

Shindo M, Uchino S, Ichiki R, Yoshimura S and Kawai Y, *Measurements of the negative ion density in SF_6/Ar plasma using a plane electrostatic probe*, Rev. Sci. Instrum. Vol. **72**: 2288, 2001.

Sirse N, Conway J, Karkari S K and Turner M M, Hairpin *probe in conjunction with laser photo-detachment technique for negative ion density measurement*, Proceedings

37th EPS conference on plasma physics (Dublin) Vol. **34A**: ISBN 2-914771-62-2, June-2010.

Spencer-Smith J L, *Negative ions of iodine- Part I Probe measurements,* Philosophical magazine Vol. **19:** 806, 1935.

Spencer-Smith J L, *Negative ions of iodine- Part II Ion beams,* Philosophical magazine Vol.
19: 1016, 1935.

Stenzel R L and Gould R W, *Upper-hybrid resonance absorption, emission, and heating of an afterglow plasma column,* J. Appl. Phys. vol. 42: 4225, 1971.

Stenzel R L, *Microwave resonator probe for localized density measurements in weakly magnetized plasmas,* Rev. Sci. Instrum., vol. **47**: 603, 1976.

Stern R A, Devynck P, Bacal M, Berlemont P and Hillion F, *Nonresonant optical tagging and "monopolar" transport in negative-ion plasmas,* Phys. Rev. A Vol. **41**: 3307, 1990.

Stoffels E, Stoffels W W, Vender D, Kando M, Kroesen G M W and de Hoog F J, *Negative ions in a radio-frequency oxygen plasma,* Phys. Rev. E Vol. **51**: 2425, 1995.

Schrittwieser R, Ionita C, Balan P, Gstrein R, Grulke O, Windisch T, Brandt C, Klinger T, Madani R, Amarandei G and Sarma A K, *Laser-heated emissive plasma probe,* Rev. Sci. Instrum., vol. **79**: 083508, 2008.

Tonks L and Langmuir I, Phys. Rev. Vol. **33:** 195, 1929.

Werner P W and Schamiloglu E, *Two-photon ionization of trimethylamine using KrF laser radiation***,** J. Appl. Phys. Vol. **79**: 2728, 1996.

Wickens L M and Allen J E, Jour. Plasma Physics Vol. 22: 167, 1978.

Xu J, Nakamura K, Zhang Q and Sugai H, *Simulation of resistive microwave resonator probe for high-pressure plasma diagnostics*, Plasma Sources Sci. Technol. Vol. **18**: 045009, 2009.

You S D, Dodd R, Edwards A and Bradley J W, *A study of the plasma electronegativity in an argon-oxygen pulsed-DC sputter magnetron***,** J. Phys. D: Appl. Phys. Vol. **43**: 505205, 2010.

Publications

(As of 1st November 2011)

Peer reviewed journals:

1. **N. Sirse**, S. K. Karkari, M. A. Mujawar, J. Conway and M. M. Turner, "The temporal evolution in plasma potential during laser photo-detachment", *Plasma Sources Sci. and Technol. (2011)* **20** 055003.
2. J. W. Bradley, R. Dodd, S - D. You, **N. Sirse** and S. K. Karkari, "Resonance hairpin and Langmuir probe assisted laser photo-detachment measurements of the negative ion density in a pulsed dc magnetron discharge", *J. Vac. Sci. Tech. A **29** (2011) 031305.*
3. J. Conway, **N. Sirse**, S. K. Karkari and M. M. Turner, "Using the resonance hairpin probe and pulsed photo-detachment technique as a diagnostic for negative ions in oxygen plasma", *Plasma Sources Sci. and Technol. (2010)* **19** 065002.
4. G. A. Curley, L. Gatilova, S. Guilet, S. Bouchoule, G. S. Gogna, **N. Sirse**, S.K. Karkari and J. P. Booth, "Surface loss rates of H and Cl atoms in an inductively coupled plasma etcher using time-resolved electron density and optical emission measurements", *J. Vac. Sci. Tech. A **28** (2010) 360.*

Conference proceedings

5. **N. Sirse**, J. P. Booth, Y. Azamoum and P. Chabert, "Electron density comparison between experiments and simulations in chlorine based ICP discharge", *Proceedings XXX International Conference on Phenomena in Ionized Gases (ICPIG 2011), UK,* D13-292.
6. J. P. Booth, **N. Sirse**, Y. Azamoum and P. Chabert, "Absolute atomic chlorine densities in a Cl2 ICP determined by TALIF with a new calibration method", *Proceedings XXX International Conference on Phenomena in Ionized Gases (ICPIG 2011), UK,* B6-376.
7. J. P. Booth, **N. Sirse**, P. Chabert, Y. Azamoum and M. Zaka-Ul-Islam "Recombination coefficient of Cl atom on Al2O3 walls determined by Two-Photon Laser-Induced Fluorescence", *Proceedings XXX International Conference on Phenomena in Ionized Gases (ICPIG 2011), UK,* B6-158.
8. **N. Sirse**, M. A. Mujawar, J. Conway, S. K. Karkari and M. M. Turner, "Negative ion temperature from the temporal evolution of plasma potential during laser photo-detachment", *Proceedings XXX International Conference on Phenomena in Ionized Gases (ICPIG 2011), UK,* B6-230.
9. **N. Sirse**, J. Conway, S. K. Karkari and M. M. Turner, "Hairpin probe in conjunction with laser photo-detachment technique for negative ion density measurement", *37th EPS Conference on Plasma Physics, June 21-25. 2010, Dublin, Ireland.*

Oral/Posters

10. **N. Sirse**, S. K. Karkari and M. M. Turner, "Sheath boundary of a cylindrical probe immersed in electronegative plasma", *2nd Workshop on RF Discharges, May 17-20, 2009, La Badine, France.*

11. **N. Sirse**, S. K. Karkari and M. M. Turner, "Sheath Boundary of Cylindrical Probe in Weakly Collisional Electronegative Plasma", *3rd ITER International Summer School on "Plasma Surface Interaction in Controlled Fusion Devices", June 22-26, 2009, Aix en Provence, France.*

12. **N. Sirse** and S. K. Karkari, "Practical applications of hairpin resonator probe for electron density measurement in low temperature plasmas", *37th EPS Conference on Plasma Physics, June 21-25, 2010, Dublin, Ireland.*

13. **N. Sirse**, G. S. Gogna, S. Karkari, G. A. Curley, L. Gatilova, S. Guilet, S. Bouchoule and J. P. Booth, "Diagnostics of Cl2-based inductively coupled plasmas used for the etching of III-V materials", *BOC Gases Poster Competition, Dublin City University, Dublin, 24th September 2010.*

14. **N. Sirse**, M. A. Mujawar, J. Conway, M. M. Turner and S. K. Karkari, "Spatial and temporal evolution of electron density and plasma potential by resonance hairpin probe and emissive probe during pulsed laser photo-detachment of negative ions", *63rd Annual Gaseous Electronics Conference, October 4-8, 2010, Paris, France.*

15. **N. Sirse**, S. K. Karkari**,** R. Dodd, S-D. You and J. W. Bradley, "Resonance hair pin probe and laser photo-detachment technique for measuring time resolve negative ion density in pulsed dc magnetron discharge", *63rd Annual Gaseous Electronics Conference, October 4-8, 2010, Paris, France.*

16. **N. Sirse** and S. K. Karkari, "Resonance hairpin probe for low temperature plasma diagnostics", *European Summer School, Bad Honnef, Germany, 9-16th October 2010.*